UNIVERSITY OF CALIFORNIA
RIVERSIDE

Multi-scale Characterization of Collagen-based Material and its Correlation to the Neuronal Differentiation of Embryonic Stem Cell

A Dissertation submitted in partial satisfaction
of the requirements for the degree of

Doctor of Philosophy

in

Cell, Molecular, and Developmental Biology

by

Yu-Jer Hwang

September 2012

Dissertation Committee:

Dr. Julia G. Lyubovitsky, Chairperson
Dr. Manuela Martins-Green
Dr. Christopher J. Bardeen
Dr. David Kisailus

The Dissertation of Yu-Jer Hwang is approved:

_____

_____

_____

_____

Committee Chairperson

University of California, Riverside

ACKNOWLEDGEMENTS

I would like to extend my sincere gratitude to Prof. Julia G. Lyubovitsky for her continual guidance and encouragements during my Ph.D study. I would also like to thank Prof. Manuela Martins-Green, Prof. Christopher J. Bardeen and Prof. David Kisailus as my thesis committee for their support and helpful discussions.

I would also like to acknowledge all professors and colleagues at University of California, Riverside for sharing their knowledge and technical wisdoms with me. Prof. Victor Rodgers for access to the UV-Vis spectrometer, Prof. Jiayu Liao for access to the FlexStation fluorescence microplate reader (Molecular Devices), Yong Song for the technical expertise and initial assistance with FlexStation, Dr Hong Xu for access to the incubator, Dr. Krassimir N. Bozhilov and Stephen McDaniel for the technical expertise and initial assistance with transmission electron microscopy, Dr. Dan Borchardt (Analytical Chemistry Instrumentation Facility) for the initial assistance with Dilor XY Laser Raman, Dr. David Carter for the technical expertise and initial assistance with fluorescence recovery after photobleaching experiment, Dr. Duncan Liew for providing the induced pluripotent stem cell line, Joseph Granelli for help with preparation of second harmonic generation images.

I would also like to thank professors and colleagues at University of California, Irvine for sharing their knowledge and technical wisdoms with me. Prof. Bruce J. Tromberg for access to a Zeiss LSM 510 NLO Meta microscopy system, Dr. Tatiana Krasieva for the initial assistance on the microscopy, and Dr Chung-Ho Sun for the technical expertise on cell culture.

I would also like to acknowledge the journals for giving the permission to use my entire published materials in my thesis. Reproduced by permission of The Royal Society of Chemistry. http://pubs.rsc.org/en/Content/ArticleLanding/2011/AY/C0AY00381F; reprinted with permission from Hwang, Y.; Granelli, J.; Lyubovitsky, J.G. Anal. Chem. 2010, 83, 1, 200-206. Copyright (2010) American Chemical Society; reprinted with permission from Hwang, Y.; Granelli, J.; Lyubovitsky, J.G. Appl. Mater. Interfaces. 2011, 4, 261-267. Copyright (2011) American Chemical Society; reprinted with permission from Hwang, Y.; Larsen, J.; Krasieva, T.B.; Lyubovitsky, J.G. ACS Appl. Mater. Interfaces. 2011, 3, 2579-2584. Copyright (2011) American Chemical Society.

ABSTRACT OF THE DISSERTATION

Multi-scale Characterization of Collagen-based Material and its Correlation to the Neuronal Differentiation of Embryonic Stem Cell

by

Yu-Jer Hwang

Doctor of Philosophy, Graduate Program in Cell, Molecular and Developmental Biology
University of California, Riverside, September 2012
Dr. Julia G. Lyubovitsky, Chairperson

The ultimate goal of regenerative medicine is to create functional engineered biomaterial to repair or replace the damaged tissues. My work firstly was to perform multi-scale characterization on the collagen hydrogels used as scaffolds. Different initial collagen concentrations and incubation temperatures were identified to affect the properties of collagen hydrogels, such as the microstructure obtained with second harmonic generation imaging (SHG), nanostructure imaged with transmission electron microscopy (TEM) and molecular structures detected with Raman spectroscopy. Compared to the real tissues, the drawback of collagen hydrogels is the lack of mechanical strength. Cross-linking has been known to increase the mechanical strength. I then characterized the effect of different cross-linking reagents including glycation reagents, genipin and 1-Ethyl-3 (3dimethylaminopropyl) carbodiimide (EDC) on the collagen hydrogel. SHG imaging showed that glycation reagents and genipin modify the microstructure within collagen

hydrogel but EDC has no effect on the microstructure. TEM images revealed that glycation reagents and genipin also remove the native-like striation pattern in nanostructure but EDC has no effect on it. Raman spectroscopy showed that glycation reagents and EDC affect the molecular information of collagen hydrogels. Lastly, two different types of stem cell, mouse embryonic stem cells (ES cells) and induced pluripotent stem cells (iPS cells) were seeded to the collagen hydrogels and was examined the effect of different structure of collagen hydrogel on the neuronal differentiation of stem cells. The behaviors of G-Olig2 ES cells and a7wt iPS cells were compared during early differentiation with retinoic acid into a neural lineage employing separately the encapsulated or topographic 3D collagen hydrogel models. For the encapsulated model, the differentiation of ES cells and iPS cells was slower for the cells encapsulated within 4 g/l collagen hydrogels as compared to the cells in 2 g/l hydrogels. The differentiation process of both cell types seeded on top of the 3D collagen hydrogels was affected by cross-linking. For example, the differentiation rate of ES cells was slower on the cross-linked hydrogels but the differentiation rate of iPS cells was faster on the cross-linked hydrogels.

TABLE OF CONTENTS

LIST OF FIGURES

Chapter 2: Collagen-based materials: multi-scale and multi-modality characterization

LIST OF TABLES

CHAPTER 1

THESIS OVERVIEW

Introduction

Tissue transplantation has been the final solution to the patients who suffer from dysfunctional tissue or organs; however due to lack of donor and issues with immune rejection, transplantation can't cure many patients. The emerging and promising field of regenerative medicine could be the future routine procedure to treat these patients.

The aim of regenerative medicine is to repair the damaged tissues or organs which are previously untreatable by using a combination of stem cells, engineered materials and suitable biochemical factors. My thesis work provides a fundamental understanding on how to manipulate the structure within materials and how the manipulated structure can control the behaviors of stem cells.

Biologically derived materials are increasingly becoming a major research focus in tissue engineering. Many of these materials are made of proteins that are components of extracellular matrix (ECM) which is composed of proteins, glycoproteins, and proteoglycans assembled in a distinctive, tissue-specific 3D structure[1]. Among natural polymers and their synthetic analogues employed as biomaterials, collagen, a well-known protein, has been widely used in biomedical applications due to its ability to form and maintain the structural integrity of tissues and organs [2]. Collagens are also important for the cellular integrity. They are involved in cellular signaling and define adhesion, differentiation, growth and survival of cells [3-5]. Compared to other natural polymers, collagens display better biodegradability, weaker antigenecity and superior

biocompatibility [6]. Because of these advantages, collagen-based biomaterials have been employed in the development of tissue/organ substitutes, such as bone [4], peripheral nerve [7] and skin [8].

In regenerative medicine, cells are often seeded onto an appropriate material which is an artificial structure capable of supporting 3D tissue formation. These 3D materials have distinct biological properties and architectures under different assembly parameters. The cells interact differently with materials having diverse compositions. It is important to pick the appropriate assembly parameters so the morphology, chemistry, and signaling environment of natural ECM can be better represented. In Chapter 2, the collagen-based materials assembled under different parameters are characterized at the molecular, nano and micro-scale levels. Because one disadvantage of collagen-based materials is their lack of mechanical properties, cross-linking reagents have been used to increase the strength of materials. In Chapter 3, 4, 5 and 6, different cross-linking reagents are applied to the collagen-based materials and their effects on the materials are characterized from molecular, nano and micro-scale level.

After engineering materials are designed, stem cells can be seeded onto them with suitable growth factors and cytokines to form bio-artificial tissues or organs. Characterizing the interaction between stem cells and ECM materials can increase our understanding of *in-vivo* stem cells environments and create physiological stem cell settings. This knowledge can further enhance the development of engineered human organs and tissues to resemble and replace natural ones at a reduced medical cost. In

Chapter 7, multiphoton microscopy is utilized to investigate the interaction between the collagen-based materials that I characterized and the embryonic and induced pluripotent stem cells.

References

(1) Song, E.; Kim, S. Y.; Chun, T.; Byun, H.; Lee, Y. M. *Biomaterials* **2006**, *27*.

(2) Hubert, T.; Grimal, S.; Carroll. P.; A., F.-C. *Cell. Mol. Life Sci.* **2009**, *66*, 1223-1238.

(3) Kaufman, L. J.; Brangwynne, C. P.; Kasza, K. E.; Filippidi, E.; Gordon, V. D.; Deisboeck, T. S.; Weitz, D. A. *Biophys. J.* **2005**, *89*.

(4) Behring, J.; Junker, R.; Walboomers, X. F. *Odontology* **2008**, *2008*, 1-11.

(5) Gelse, K.; Poschl, E.; Aigner, T. *Drug. Deliver. Rev.* **2003**, *55*, 1531-1546.

(6) Lee, C. H.; Singla, A.; Lee, Y. *Int. J. Pharm.* **2001**, *221*, 1-22.

(7) Chamberlain, L. J.; Yannas, I. V.; Hsu, H.-P.; Strichartz, G.; Jung, W. K. *Exp. Neurol.* **1998**, *154*, 315-329.

(8) Yannas, I. V.; Lee, E.; Orgill, D. P.; Skrabut, E. M.; Murphy, G. F. *Proc. Natl. Acad. Sci.* **1989**, *86*, 933-937.

CHAPTER 2

COLLAGEN HYDROGEL CHARACTERIZATION: MULTI-SCALE AND MULTI-MODALITY APPROACH

Abstract

The complex supramolecular architecture of collagen biopolymer plays an important role in tissue development and integrity. Developing methods to report on collagen structures assembled *in vitro* would accelerate the pace of utilizing them in biomedical applications. Employing imaging techniques and turbidity measurements, we mapped the light scattering properties of 3D collagen hydrogels formed at initial concentrations of 1 mg/ml to about 5 mg/ml and several incubation temperatures. The transmission electron microscopy (TEM) images show that collagen scattering features consist of both native-like fibrils and filamentous structures that do not have the characteristic fibrillar striation observed in this protein. Spindle-shaped fibrils appear at the concentrations of 1, 2, 2.5 and 4 mg/ml and the spiral-shaped fibrils are formed at the concentrations of 2 and 2.5 mg/ml. The multiphoton microscopy (MPM) images reveal that in the 3D collagen hydrogels a unified relationship between second harmonic generation (SHG) signal directionality and fibril morphology and/or sizes is not likely. The MPM images, however, showed important micro-structural details. The Raman spectroscopy detects the molecular information on the collagen hydrogels. These details lead us to conclude that the dependence of SHG signals on the number of interfaces created upon assembly of 3D collagen hydrogels can account for the strength of the detected backscattered signals.

Introduction

Biologically derived materials that mimic the *in vivo* cellular environment are at the vanguard of new approaches in tissue engineering because they have the advantage of biocompatibility and are able to signal fundamental cellular processes. To identify the structures within these biomaterials that would benefit the rational construction of engineered tissues, there is a growing need to systematically characterize them.[2]

Collagen is one of the most extensively utilized biomaterials in scaffold construction in tissue engineering applications. When biopolymers made of fibrillar collagen are used *in-situ* to form matrices to support 3D scaffolds, the arrangement of higher order structures such as tertiary (fibrils) and quaternary (fibers) inside these matrices is often not known.

The complex process of collagen assembly involves formation of structural elements that range from angstroms to microns and larger dimensions. Structures on a smaller scale such as molecular dimensions are best studied with techniques that utilize electrons. Higher order assemblies present in the engineered tissues and composed of fibrils and fibers can be effectively investigated using non-destructive laser-scanning optical multiphoton microscopy (MPM) method.[3, 4]

MPM is a non-linear optical method that utilizes femto-second pulses of near-infrared (NIR) laser light. It has the ability to perform high resolution and three-dimension imaging of biological samples. Its advantages include reduced scattering because NIR wavelengths are employed, no out-of focus excitation, very small sample volumes and deeper tissue penetration compared to confocal microscopy.[5] Empowered by the

spectroscopic contrast, MPM is ideally suited to study morphology and physiology of engineered tissues. [6]

The interaction between fibrillar collagen and NIR pulsed, femto-second laser light of MPM results in second harmonic generation (SHG) and two-photon excited fluorescence (TPF)[7, 8] signals. SHG is produced when photons interacting with fibrillar collagen are combined to form new photons with exactly twice energy.[9] It gained recognition in tissue imaging [7, 8, 10-17] because this source of contrast resists photo-bleaching and had been used to successfully image structural proteins in various non-animal and animal sources[6] with strong enhancement suitable for biomedical assessment of tissue structure.[11] It is believed that the interaction between laser pulses and collagen's non-centrosymmetric, triple helix structure in addition to molecular packing within collagen materials leads to scattering from the tertiary (fibrils),[11] and quaternary (fibers)[9] levels of organization thus producing SHG.[18]

Raman spectroscopy, used widely to examine variety of complex biomolecules and biological tissues[1, 19-27] is a powerful tool for studying molecular properties based on the vibrational changes.[28-30] When compared to other techniques, which are used to study molecules, Raman spectroscopy has the advantages of being label-free, non-destructive and capable of providing real-time structural as well as molecular analysis.[31] It can furnish information to potentially determine the crystallinity, conformation, density, monomer content, degradation, stress-strain distribution and other properties relevant to supramolecular order of structures composed from collagen proteins.

The goal of this work was to develop and to demonstrate the multi-scale and multi-modality approach to systematically examine the 'fiber-like' structures formed within collagen hydrogels assembled under different initial collagen concentrations and incubation temperatures. We evaluated the assembly kinetics of collagen hydrogels by examining the turbidity of solutions undergoing fibrillogenesis and applied transmission electron microscopy (TEM) to observe reconstituted nano-structures. The turbidity measurements and TEM observations reinforced and validated the SHG imaging and quantification of these signals. Raman spectroscopy is employed to obtain the molecular information. The approach and knowledge obtained can be applied to rationally tissue engineer extra-cellular matrices (ECMs) that use collagen as a substrate material.

Experimental Section

Supramolecular assembly kinetics

9.37mg/ml stock rat-tail type I collagen (BD Biosciences) was in 0.02N acetic acid solution. The purity of the stock was confirmed with 4%-20% Tris-HCl gels (Bio-Rad) following standard procedure. The stock was diluted with 0.02 N acetic acid to obtain the 2× collagen aliquots. 2× fibrillogenesis initiation buffers were prepared from NaCl and phosphate buffer. The concentration of mono-and dibasic phosphate in the buffer at pH=7.4 were calculated using Henderson-Hasselbalch equation. The pH was adjusted drop-wise with 1N NaOH or HCl. Specifically, the 2× fibrillogenesis initiation buffer selected for the kinetic studies had the following components: 6.40 mg/ml K_2HPO_4; 3.16 mg/ml KH_2PO_4; 38.55 mg/ml NaCl (ionic strength = 0.6 M). After the pH was adjusted

to a desired value, the solvents were filtered with 0.22 μm, 25 mm syringe filter (Fisher) and stored at 4℃. Prior to the beginning of fibrillogenesis, both 2× collagen stock and 2× initiation buffer were de-airated by placing them in a 1.5 L desiccator (Fisher) and applying house vacuum for 2 hrs. Fibrillogenesis was initiated by mixing on ice 2× collagen aliquot with 2× fibrillogenesis initiation buffer at 1:1 ratio, adjusting the pH to 7.4±0.1 and incubating at experimental temperatures (4℃, 14℃, 27℃ and 37℃).

To study the effect of different initial collagen concentration, 1:1 mixture was transferred into semi-micro spectrophotometer quartz cell (1 mm light path) in a UV-VIS spectrophotometer (UV-1201, Shimadzu). The optical density at 450 nm was recorded at 30 s intervals until it reached the plateau. In this work, optical density values represent a quantitative measure of turbidity induced within collagen solutions as a result of polymerization. The lag time (T_{lag}) was defined as the time prior to the optical density value increasing from zero to a positive one. The time for complete fibril assembly (T_p) was defined as the time when the optical density value became constant.

Transmission Electron Microscopy (TEM) imaging

After 20 hours of incubation, entire portion of incubated sample was retrieved. A drop of sample containing polymerized material was added on a formvar film coated with a layer of carbon supported on a 300-mesh copper grid (Carbon type A, Ted Pella, Inc.). Excess liquid was drained with filter paper after 30 s. A drop of double de-ionized water was added for 1 s to remove the excess, and was drained slowly with filter paper. This procedure was repeated twice. A drop of same-day-prepared 1 mg/ml sodium

phosphotungstate (Sigma), pH=7.4 was added on top of the sample on the grid. After 10 min, the grid was drained slowly with filter paper and air-dried for about 15 minutes. The grids were examined immediately in a Tecnail 12 electron microscope operated at 120 kV.

Fibril diameters were estimated using a free image-processing software ImageJ (version 1.41). They were measured at the intact regions of the fibrils where the features were discernable. Fibril diameter histograms were constructed by sampling only fibrils that had striation around 67 nm as observed in TEM images. Average fibril diameters were found by dividing the sum of all multiples (number of fibrils × fibril diameter) by total number of fibrils measured; range of fibril diameters was estimated by adding the smallest fibril diameter and the largest fibril diameter and as such represents a variation in the fibril diameters. The number of fibrils measured for each initial collagen concentration incubated 27 ℃ was 67 fibrils (0.1 mg/ml), 15 fibrils (1 mg/ml), 84 fibrils (1.8 mg/ml), 28 fibrils (2 mg/ml), 13 fibrils (2.5 mg/ml), 18 fibrils (3 g/), 21 fibrils (4 mg/ml), 47 fibrils (4.68 mg/ml). The number of fibrils measured for each initial collagen concentration incubated 37 ℃ was 9 fibrils (0.1 mg/ml), 50 fibrils (1 mg/ml), 38 fibrils (1.8 mg/ml), 45 fibrils (2 mg/ml), 68 fibrils (2.5 mg/ml), 60 fibrils (3 g/), 30 fibrils (4 mg/ml), 35 fibrils (4.68 mg/ml).

In-situ multiphoton photon microscopy (MPM) imaging

The inverted Zeiss LSM 510 NLO Meta laser scanning microscopy system (Carl Zeiss MicroImaging, Incorporated, Thornwood, New York) was used in this work. It was based

on the Axiovert 200M inverted microscope equipped with standard illumination systems for transmitted light and epi-fluorescence detection and equipped with an NLO interface for a femto-second Titanium:Sapphire laser excitation source (Chameleon-Ultra, Coherent, Incorporated, Santa Clara, California) for multi-photon excitation. The Chameleon laser provided femto-second pulses at a repetition rate of about 80 MHz, with the center frequency tunable from 690 to 1040 nm. A Long working distance objective (Zeiss, 40X water, N.A. 0.8) was used to acquire images shown in this work. The two-photon signals from the sample are epi-collected and discriminated by the short pass 650 nm dichroic beamsplitter. The SHG images were collected with the 390-465 nm band pass filter (excitation wavelength = 800 nm). Each image presented in this work is 12 bit, 512 × 512 pixels representing 225 μm × 225 μm field of view. All the images were successfully reproduced on separate days, using up to three independent samples on each day and examining about five field of views per sample. The imaging samples were prepared following the same fibrillogenesis procedure used in supramolecular assembly kinetics except adding the mixed solutions into eight-chambered coverglass (MP Biomedicals) prior to the incubation at 27 ℃ or 37 ℃. To quantify the amounts of SHG signal backscattered from each sample, we first collected the images at depth intervals of 2 μm from the surface of the samples to a maximum depth corresponding to the working distance of the objective. Subsequently, within each image we quantified SHG signal by calculating average intensity. We then constructed depth decay curves of the SHG signal and determined the area under the curves. To analyze and to compare the amount of backscattered SHG signal from different collagen hydrogels, we normalized the areas

obtained as $\frac{Area(x_i) - Area(\infty)}{Area(0) - Area(\infty)}$, where *Area* ($x_i$) is area at the concentration of interest, *Area* (∞) is maximum and *Area* (0) is minimum area identified.

Raman Microspectroscopy

Raman spectra were recorded directly on the control and cross-linked collagen gels with a DILOR XY microspectrometer. The samples were placed on a microstage and signals were collected with a Minolta 50mm/F1.7 lens in a backscattering manner. The 532 nm radiation from a diode-pumped solid state laser (Aixiz, USA) was used for excitation. The laser power at the sample was about 110 mW, and other experimental parameters were as following: grating 1800 gr/mm; 30 acquisitions of 30 s each. These parameters gave spectra that were measured at a spectral resolution of 2 cm^{-1}. The conditions were kept constant for all the measurements. Raman data were recorded in the 800–3000 cm^{-1} spectral range. All spectra were repeated on the separate days and at least 3 times, baseline corrected with Origin 8 software. No further spectral processing (smoothing, etc.) was performed.

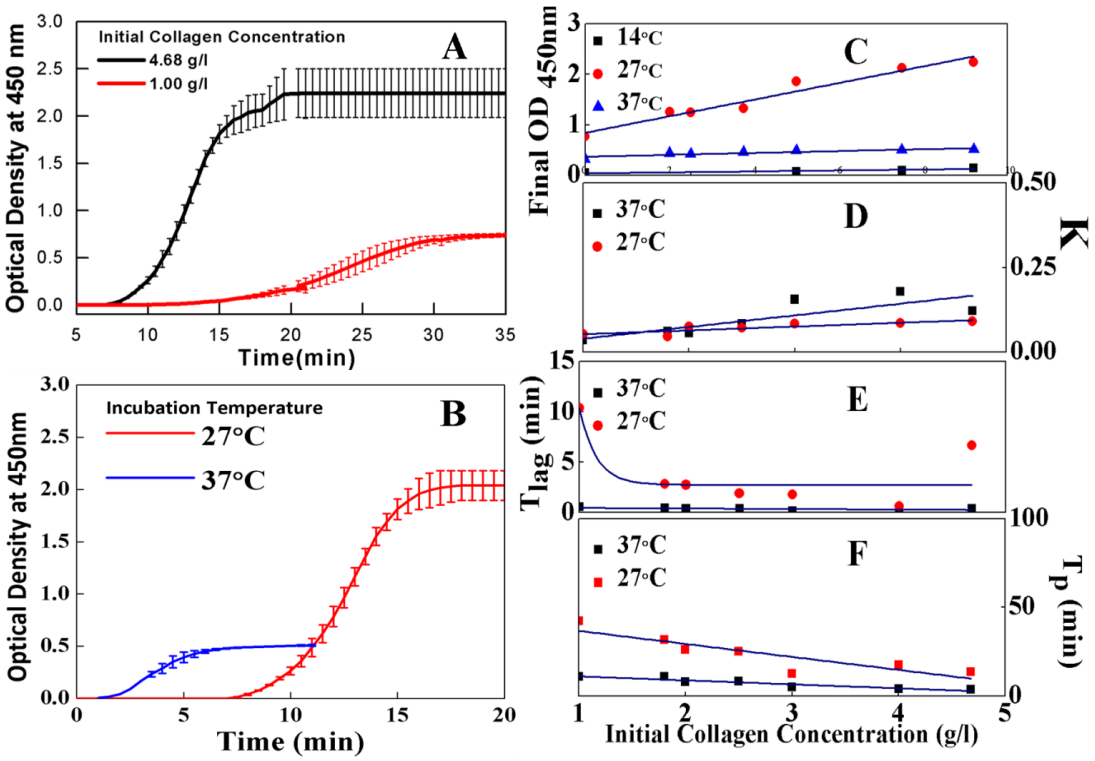

Figure 1. The effect of initial collagen concentrations and incubation temperatures on turbidity and kinetic parameters. Polymerization conditions: pH 7.4, 30 mM phosphate buffer of 0.3 M ionic strength. (A) Typical turbidity-time curves and corresponding standard deviations of the mean during collagen self-assembly from different initial concentrations of protein incubated at 27°C. (B) Typical turbidity-time curves and corresponding standard deviations of the mean during collagen self-assembly at different incubation temperatures and 4.68 g/l initial collagen concentration. (C) The observed final optical densities. Line is the best fit. (D) The rate constants (K) of collagen self-assembly evaluated by fitting the slopes of turbidity curves like those shown in Figure 1A and 1B. Lines are best fits. (E) The times to the beginning of collagen self-assembly. Lines are best fits. (F) The times to the completion of collagen self-assembly. Lines are best fits. Left to right: 0.1, 1, 1.8, 2, 2.5, 3, 4, and 4.68 g/l initial collagen concentrations.

Results and Discussion

Polymerization turbidity assays.

The turbidity measured as a change in optical density in solutions that undergo polymerization (Figure 1A and 1B) indicates formation of collagen fibrils and/or other large collagen aggregates that scatter light. We evaluate turbidity at 450 nm, because at

this wavelength, there is a minimal effect due to collagen absorption. Note that we not only studied polymerization kinetics of acid soluble collagen at dilute initial concentrations (0.1 mg/ml, data not shown) as previously employed in biochemical studies but at higher concentrations (1 mg/ml to ~ 5 mg/ml) used in contemporary biomedical and tissue engineering research. We separately employed 4 ℃, 14 ℃, 27 ℃, and 37 ℃ incubation temperatures as well.

The fibrillogenesis initiation buffer induced changes in optical density are consistent with cooperative polymerization mechanism to form collagen supramolecular structures. However, we find that the slopes obtained by fitting the sigmoid portion or growth period of the curves like those shown in Figure 1 vary for different initial collagen concentrations. The final optical density (Figure 1C) and slope K corresponding to the rate of fibrillogenesis (Figure 1D) both increase as the initial concentration of acid-soluble collagen I is raised. Increasing the initial collagen concentration decreased the T_{lag} and T_p (Figure 1E and 1F).

Different incubation temperatures used during polymerization also affect fibrillogenesis kinetics. The fibrillogenesis that occurs at 27 ℃ produces higher final optical density values (Figure 1C) and in a few cases slightly lower values for the rate constants (Figure 1D) compared to fibrillogenesis at 37℃. The values of lag period (T_{lag}), time to a complete fibril assembly (T_p) and final optical density are all higher when fibrillogenesis occurs at 27 ℃ compared to 37 ℃ (Figure 1E and 1F). No fibrillogenesis occurs at 4 ℃, and only marginal fibrils are assembled at 14 ℃.

Initial collagen I concentration (mg/ml)	Striated fibrils		Nonstriated filaments		Observations	
	27°C	37° C	27° C	37°C	27°C	37°C
0.1	X	X	X	X	Striated fibrils with smaller D value	Non-striated filaments
1	X	X	X	X	Long thin spindle-shaped striated fibrils	Spindle-shaped striated fibrils
1.8	X	X	X	X	Fibrils fuse together Fibrils are bent	Two or more fibrils/filaments are interweaved
2	X	X	X	X	Spiral-shaped, spindle-shaped striated fibrils	Spiral-shaped , spindle-shaped striated fibrils
2.5	X	X	X	X	Spiral-shaped, spindle-shaped striated fibrils	Spiral-shaped, spindle-shaped striated fibrils
3	X	X	X	X	Striated fibrils	Spindle-shaped fibrils Hair-like short filaments
4	X	X	X	X	Spindle-shaped striated fibrils	Spindle-shaped fibrils Hair-like short filaments
4.68	X	X	X	X	Striated super fibrils	No superfibrils Hair-like short filaments

Table 1. Summary of observed structures of reconstituted fibrils assembled at differet initial collagen concentrations and incubation temperatures observed with transmission electron microscopy.

In this work we examined fibrils formed from initial collagen concentrations in the range of 1 mg/ml to about 5 mg/ml that are utilized in contemporary biomedical and tissue engineering research.[32-36] Contrary to findings of Williams et al.[37] on dilute collagen solutions (0.1 to about 1 mg/ml), in our study, at both 27 ℃ and 37 ℃ assembly temperature, the self-assembly rate constants (slopes) increased upon increasing initial collagen concentration.

Transmission Electron Microscopy (TEM) experiments

Typically, different polymerization rates entail different assembly mechanisms potentially leading to different nanostructures; therefore, we used transmission electron microscopy to investigate them. The transmission electron micrographs showed that the

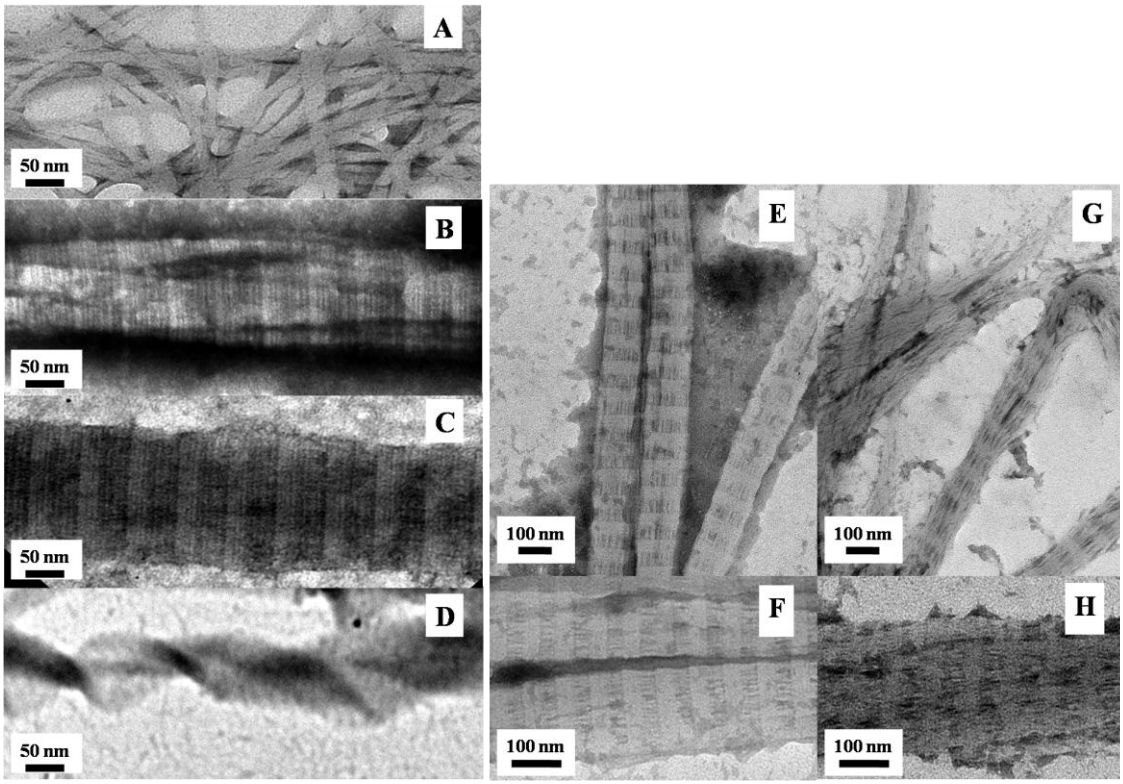

Figure 2. Transmission electron micrographs of negatively stained collagen fibrils assembled from different initial collagen concentrations at 27 ℃ (A-D) and assembled at different incubation temperatures with initial collagen concentration of 1.8 g/l (E-H). (A) Representation of a non-striated filament observed at all concentrations. (B) Smaller spindle-shaped fibrils organized into a larger fibril observed at 1.0 and 4.0 g/l. (C) Representation of a native-banded reconstituted fibril observed at all concentrations. (D) Spiral-shaped striated fibrils observed at 2.0 and 2.5 g/l. (E) Striated fibrils assembled at 27℃ observed at low magnification (F) Striated fibrils assembled at 37℃ observed at high magnification. (G) Striated fibrils assembled at 27℃ observed at low magnification. (H) Striated fibrils assembled at 37℃ observed at high magnification.

nanostructure of negatively stained reconstituted collagen fibrils varied greatly for different initial collagen concentrations and incubation temperatures (Table 1). Non-striated filaments (Figure 2A) as well as striated fibrils (Figure 2C) were present simultaneously at all concentrations. Other types of fibrillar nanostructures were also observed. When the initial collagen concentration was 2 or 2.5 mg/ml, the striated fibrils formed were spiral-shaped (Figure 2D). However, the spindle-shaped striated fibrils

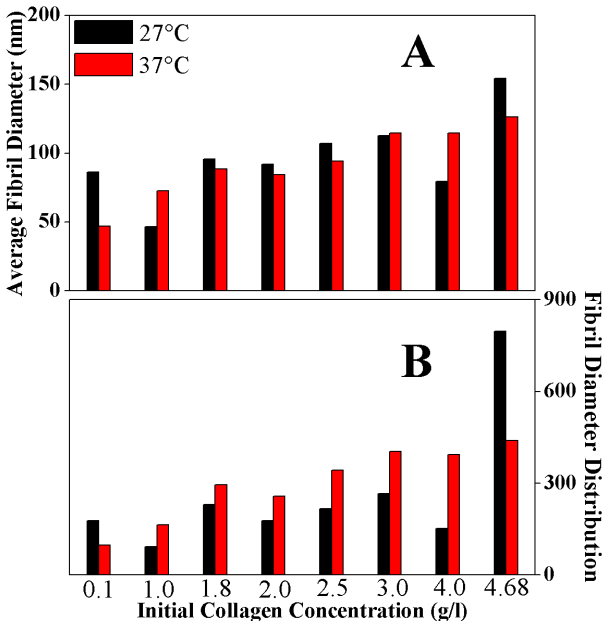

Figure 3. The effect of different initial collagen concentrations and incubation temperatures (27 ℃ or 37 ℃) on the average fibril diameter and on fibril diameter distribution. (A) Average fibril diameter. (B) Fibril diameter distribution. Left to right: 0.1, 1, 1.8, 2, 2.5, 3, 4, and 4.68 g/l initial collagen concentrations.

(Figure 2B) were prevalent for all initial collagen concentration except 0.1 and 4.68 mg/ml (data not shown). Despite the structural difference, all detected striated-fibrils had a D-period in the range of 62 to 67 nm, which is the major indication of the reconstitution of native fibrils.

The major difference observed between the fibrils assembled at 27 ℃ and 37 ℃ was that the fibrils assembled at 27 ℃ (Figure 2E) possessed a clear edge compared to those formed at 37 ℃ (Figure 2G). The D- period of fibrils assembled at both temperatures falls into the range of 62 to 67 nm (Figure 2F and 2H). Moreover, the histograms constructed from TEM image measurements demonstrate variations in the average fibril diameters (Figure 3A) and the fibril diameter distributions upon increase in the initial collagen concentration (Figure 3B).

The scattering structures formed within 3D collagen materials assembled under different initial collagen concentrations and incubation temperatures consist of both assembled fibrils that display a periodic banding pattern and filamentous structures that do not have

this characteristic collagen striation. In filaments, collagen molecules are not assembled in staggered alignment and the distance between them might be too close for the phosphotungstate stain to enter; hence, filaments do not exhibit banding patterns. The TEM detected morphologies of fibrils formed at different initial collagen concentrations also vary greatly.[38] The spindle-shaped fibrils are observed upon self-assembly from 1, 2, 2.5 and 4 mg/ml initial collagen concentrations. Similar types of spindle-shaped fibrils aggregating laterally to fibril bundles were observed in chicken tendons,[39] collagenous tissues of echinoderm[40] and collagen materials assembled at concentrations about 40 to 100 mg/ml.[41] Interestingly, at collagen concentration of 2 and 2.5 mg/ml, we observed the spiral-shaped fibrils. This type of fibril is thought to have evolved to constantly accommodate large and repetitive deformations and is commonly found in skin, cornea, some ligaments and interstitial connective tissues.[42, 43]

The different growth mechanisms of fibrils at different initial collagen concentrations could explain difference in the detected TEM structures. Collagen self-assembly is assumed to be a nucleation process that occurs in two successive steps, lag phase followed by the growth phase.[44] Aggregation of collagen molecules and linear growth of microfibrils mainly occur at lag phase. Based on several biochemical studies[37, 44-50] and the fibrils formed from dilute initial collagen concentrations, the growth phase is thought to be dominated by lateral assembly of microfibrils to fibrils. Different polymerization temperatures employed in fibrillogenesis further modulate these mechanisms.

Multi-photon microscopy (MPM) experiments

Besides TEM imaging of collagen nano-structures, direct observation of collagen-based materials by multiphoton microscopy (MPM) employing second harmonic generation (SHG) signals provides morphological details on the microscopic scale. The general utility of the method includes an ability to determine the sizes of collagen fibrils/fibers, their distribution and organization at depth within the scattering substrates such as collagen hydrogels examined in this work.

We are the first to apply SHG imaging to evaluate the microstructure of collagen hydrogels formed from different initial protein concentrations. The SHG images obtained in the x-y plane for the collagen microstructure formed at different incubation temperatures have been previously published.[9] We observe a wide diversity in the morphology of microscopic 'fiber-like' structures when collagen is assembled at different initial concentrations and incubation temperatures. Specifically, when different incubation temperatures are employed, the collagen materials show completely different microstructures (Figure 4). For example, 'fiber-like' looking structures formed at 37 °C (Figure 4E and 4F) are much shorter compared to those assembled at 27 ℃. They have uniform diameters around 1 μm even at the highest concentration of 4.68 mg/ml used in this work (Figure 4F). In this study, the SHG images obtained in x-z plane reveal the homogeneity throughout the materials assembled at 37 ℃ and collagen concentrations 3.0 mg/ml and 4.68 mg/ml (Figure 5E and 5F).

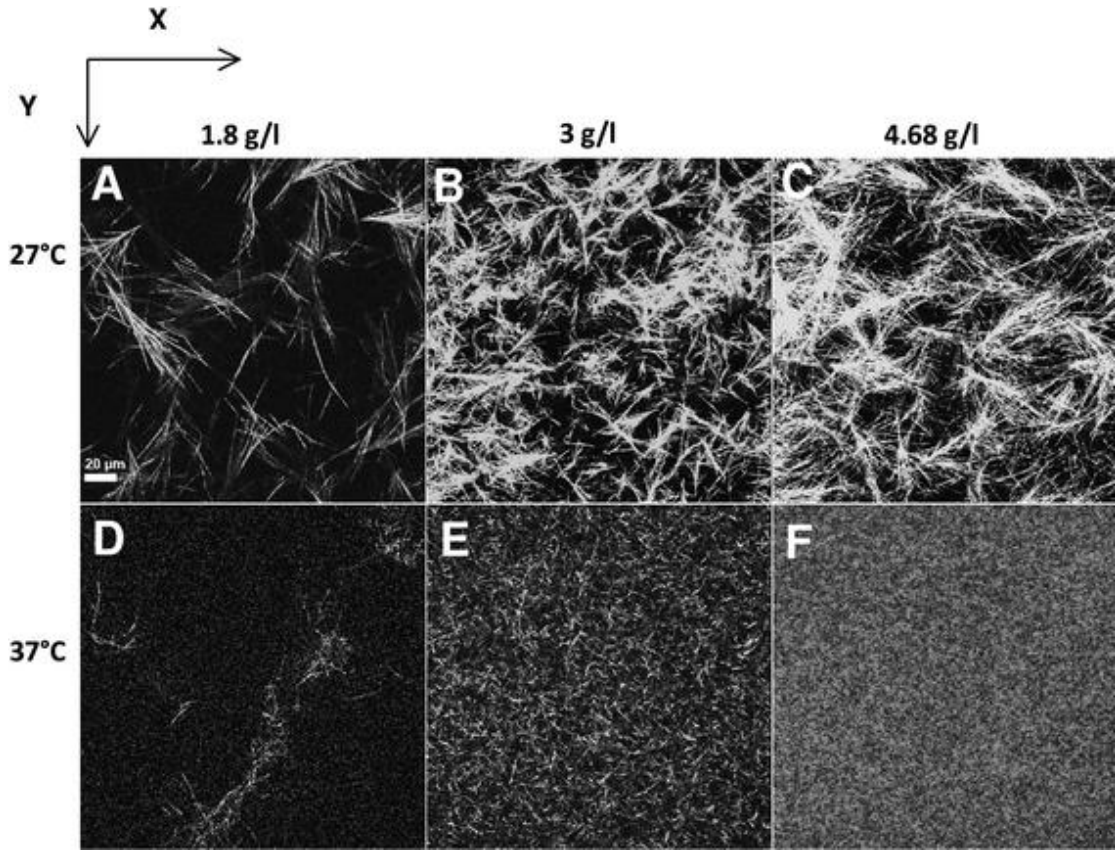

Figure 4. Backscattered second harmonic generation (SHG) images from collagen materials assembled at different initial collagen concentrations and incubation temperatures. The images obtained are 3D, however, only an X-Y plane representative of the sample is shown. (A) Rat-tail collagen assembled at 27℃ from the initial collagen concentration of 1.8 g/l. (B) Rat-tail collagen assembled at 27℃ from the initial collagen concentration of 3.0 g/l. (C) Rat-tail collagen assembled at 27℃ at initial collagen concentration of 4.68 g/l. (D) Rat-tail collagen assembled at 37℃ at initial collagen concentration of 1.8 g/l. (E) Rat-tail collagen assembled

We determined that all the materials formed at 27 ℃ display microscale heterogeneity in 3D with small diameter 'fiber-like' looking structures distributed near the top, and those with large diameters deposited preferentially at the bottom (Figure 5A, 5B, and 5C). Also, in all of the materials assembled at 27 ℃, most fibrils/fibers are situated flat in the x-y plane, however, with mixed orientations (Figure 4A, 4B and 4C). The majority of fibrillar clusters have lengths in the range of 40 to 60 µm, with a few fibrillar clusters that have lengths in the range of 80 to 90 µm.

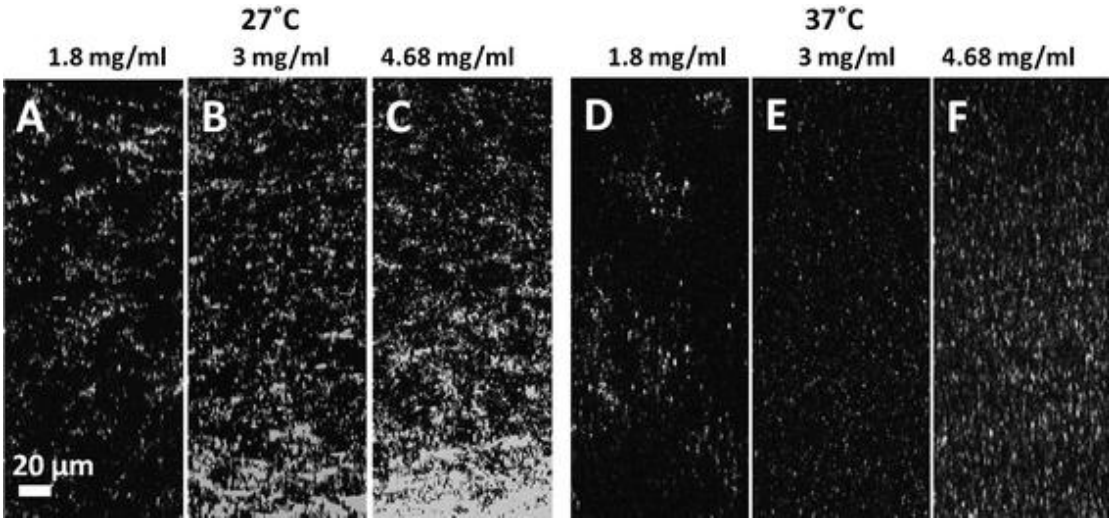

Figure 5. Backscattered second harmonic generation (SHG) images from collagen materials assembled at different initial collagen concentrations and incubation temperatures. The images were obtained in X-Z axis. (A) Rat-tail collagen assembled at 27℃ at initial collagen concentration of 1.8 g/l. (B) Rat-tail collagen assembled at 27℃ at initial collagen concentration of 3.0 g/l. (C) Rat-tail collagen assembled at 27℃ at initial collagen concentration of 4.68 g/l. (D) Rat-tail collagen assembled at 37℃ at initial collagen concentration of 1.8 g/l. (E) Rat-tail collagen assembled at 37℃ at initial collagen concentration of 3.0 g/l. (F) Rat-tail collagen assembled at 37℃ at initial collagen concentration of 4.68 g/l. All scale bars are 20 µm.

There is also a very strong dependence of the 'fiber-like' morphology within the assembled materials on the initial collagen concentration. For a 27 ℃ assembly initiated process, the main morphological difference is the number of 'fiber-like' clusters observed and the significant variations in their final diameters. When collagen is assembled at an initial concentration of 1.8 mg/ml (Figure 4A), the 'fiber-like' microstructures observed are thin and their numbers are few. When collagen concentration is raised to 2.0 mg/ml, fiber-like microstructures fuse and form a thicker 'fiber' with a larger diameter in the range of 1 to 3 µm (not shown). When the collagen concentration is increased to 2, 2.5 and 3 mg/ml (Figure 4B), the number of fibers again increases and their diameters

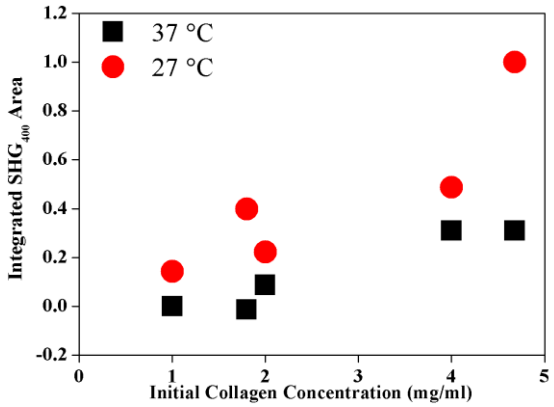

Figure 6. The amount of 800 nm backscattered second harmonic generation (SHG) signal obtained at different initial collagen concentrations (1.0, 1.8, 2.0, 4.0 and 4.68 g/l) and incubation temperatures (27℃ and 37℃).

became wider (3 µm to 5 µm). The morphology of microstructures visualized is again different when the initial collagen concentration is 4 mg/ml and 4.68 mg/ml (Figure 4C). Many smaller structures accumulate to form 'fiber-like' looking structures with diameters that can reach up to 9 or 10 µm. The initial collagen concentration does not have the same effect on the microstructure of materials assembled at 37 ℃ (Figure 4D, 4E, 4F). However, we observe the number of second harmonic generating 'fiber-like' one-micron-structures to increases as the initial collagen concentration is increased (Figure 4E and 4F).

Additionally, for both temperatures, the collagen materials assembled at the lower initial protein concentration (1 mg/ml) produce a reduced amount of backscattered second harmonic generation (SHG) signal compared to those assembled at higher once (Figure 6). Similarly to the final optical density trends obtained from turbidity measurements, the amount of backscattered second harmonic generation (SHG) signal detected is greater in collagen materials assembled at 27 ℃ than the once assembled at 37 ℃ (Figure 6).

Second harmonic generation images further revealed that 27 ℃ incubation temperature and high initial collagen concentrations produce fiber-like scattering structures with

larger diameters. This phenomena does not take place when the materials are formed at 37 ℃ because we believe the smaller fibrils formed as a result of faster initiation of nucleation undergo irreversible covalent cross-link formation between microfibrils. Cross-linked microfibrils might be more difficult to fuse to larger-sized 'fiber-like' structures seen in SHG images of the materials formed at 27 ℃.

The dependence of second harmonic generation (SHG) signals on the surface area or amount of interfaces created upon assembly of 3D collagen materials can account for the strength of the detected backscattered signals. Increasing collagen concentration generates a greater amount of "fiber-like" scattering features albeit interfaces within the materials concomitantly with an increase in the backscattered SHG signal strength averaged over a 3D optical volume imaged. The fusion of microscopic 'fiber-like' structures within the materials prepared upon incubation at 27 ℃ increases backscattered SHG signals compared to un-fused structures generated at 37 ℃. Our findings agree with previous indirect experiments aimed to disrupt the interfaces between collagen fibrils and collagen molecules, which showed reduction in the SHG intensity[51-53] upon introducing physical and chemical perturbations.

The present collective body of SHG examinations carried out to explain the relationship between collagen fibril sizes[11, 54] and SHG strength and/or aimed to create a unified relationship between collagen fibril morphology, fibril sizes and SHG directionality, showed that fibril orientations[11, 18, 55, 56] and polarization of laser[57, 58] strongly influenced the backscattered SHG. These studies determined that the mixture of various orientations

of fibrils in tendon and dermis reduce SHG signals. In our 3D materials, a uniform fibril orientation and a unified relationship between SHG directionality, collagen fibril morphology and sizes is not likely. The organization of reconstituted fibrils within our 3D materials is heterogeneous as seen in SHG and TEM images. The 3D SHG images show that fibrils don't have any preferred orientation in all tested conditions; moreover, higher collagen concentration leads to higher disorder of fibril orientations and large variations in the SHG signals in the proximity to the imaging surface. Increasing the initial collagen concentration increases the rate constant and indicates faster self-assembly. Faster self-assembly leads to more structural defects and therefore inconsistent backscatter from one sample to another. By the same token, although the incubation temperature has no effect on fibril morphology and periodic banding pattern, it affects the peripheral alignment of collagen molecules leading to unformed fibrillar edges seen in TEM images and reduced amount of SHG generated by materials formed at 37 ℃.

The methods traditionally employed to characterize collagen containing biological materials have been destructive and not readily applicable to the analyses of this structural protein *in situ.*[59, 60] The use of SHG imaging within the context of characterizing collagen hydrogels assembled from different initial conditions is novel and well timed. For example, recently Miron-Mendoza et al.[61] reported that the fibroblasts motile activity changes drastically over the collagen concentration range examined in our work. The differences in matrix stiffness determined by oscillation rheometry and porosity determined by scanning electron microscopy (SEM) were assumed to the causes for the observed changes. We suggest that the SHG imaging will shed a new light on the

cellular motility by examining cell-collagen biomaterial interactions[62] and evaluating the cell morphology after contact with collagen biomaterials prepared at different concentrations. The non-destructive, high resolution and contrast images that utilize SHG contrast are important in the field of tissue engineering as well. For example, Niklason. et al. [63] imaged the evolving distribution of collagen fibers in vessels during 8-week culture in the bioreactor. An application of SHG imaging to monitor pathology and wound healing additionally holds great promises.[53]

Raman spectroscopy

The position of all observed vibrational Raman bands and corresponding assignments are summarized in Table 2. They are compared to a comprehensive list of Raman line assignments for collagen from bovine Achilles tendon of Ref. [1]. In general, the intensities of the absorption bands in the Raman spectra that could be obtained for collagen hydrogels were weak.

The Raman spectra obtained after the collagen hydrogels assembled at different temperatures for 24 hour are shown in Figure 7. Within the region between 800 cm^{-1} to 1500 cm^{-1}, the intensity of several bands for collagen hydrogels assembled at 37° C are elevated compared to the one assembled at 27 ° C. 813 cm^{-1} represents the C-C stretch of protein backbone; 871 cm^{-1} and 921 cm^{-1} are assigned for the C-C stretch of proline and hydroxproline; 1078 cm^{-1} represents the C-N stretch. The increased intensity of these four peaks indicates the geometry of backbone of collagen molecules is differed within the hydrogels assembled at different incubation temperatures. The SHG images have shown

the collagen microstructure assembled at 37 ℃ is thin fiber-like structures and the one assembled at 27 ℃ is much thicker. The difference in microstructure suggests that the vibration of C-C stretch within thin fiber-like structures is interacted with photons in the larger cross-section than the C-C stretch in the thick fiber-like structures. As a result, the collagen hydrogels assembled at 37 ℃ generates stronger Raman signals than the one assembled at 27 ℃. In addition to the elevation of peak intensity, the position of all the peaks remains the same for the hydrogels assembled at both temperatures.

The Raman spectra obtained after the collagen hydrogels assembled at different initial collagen concentrations are shown in Figure 8. Within the region between 800 cm^{-1} to 1500 cm^{-1}, the collagen hydrogels assembled at 4 mg/ml has higher intensity in all the bands compared to the one assembled at 1.8 mg/ml. This suggests that the higher concentration of collagen molecules generate stronger molecular vibration. In addition, the position of all the peaks remains constant as shown in both spectra. Moreover, the spectrum obtained for the hydrogels assembled at 1.8 mg/ml, 27 ℃ also shows that the position of all peaks is the same (data not shown). This observation suggests that the concentration effect is only on the elevation of peak intensity which is independent of incubation temperature.

Collagen Hydrogel (cm^{-1}) assembled at 37°C , 4 mg/ml	Collagen Hydrogel assembled at 27°C , 4 mg/ml	Collagen Hydrogel assembled at 37°C , 1.8 mg/ml	Collagen from bovine Achilles tendon*	Assignment*
813	814	814	821	ν(C-C) backbone
846	853	853	856	ν(C-C) proline ring
871	868	875	876	ν(C-C) Hypro ring
		896		no assignment
921	921	921	921	ν(C-C) proline ring
936			938	ν(C-C) backbone/proline ring
983				no assignment
991	990	990		no assignment
	1001	1001	1006	tyrosine
1030	1032		1037	proline
1078	1081	1078	1087	ν(C-N)
1101	1101		1101	no assignment
1156	1160		1160	no assignment
1245	1245		1248	Amide III
1275	1275		1271	Amide III
1319	1319		1314	$\gamma_t(CH_3,CH_2)$
1346	1338		1343	$\gamma_w(CH_3,CH_2)$
1426	1426		1422	ν(COO-)
1453	1453	1453	1451	$\delta(CH_3,CH_2)$
1469			1464	$\delta(CH_3,CH_2)$
1554	1554	1554		no assignment
1604	1604			C=C Phe and Tyr
1636	1633	1635	1642	Amide I, H_2O
2063	2063	2066		no assignment

Table 2. The position of Raman spectral lines and their assignments in collagen hydrogels assembled at different incubation temperatures and initial collagen concentrations. The information in the columns with asterisk is from reference 1.

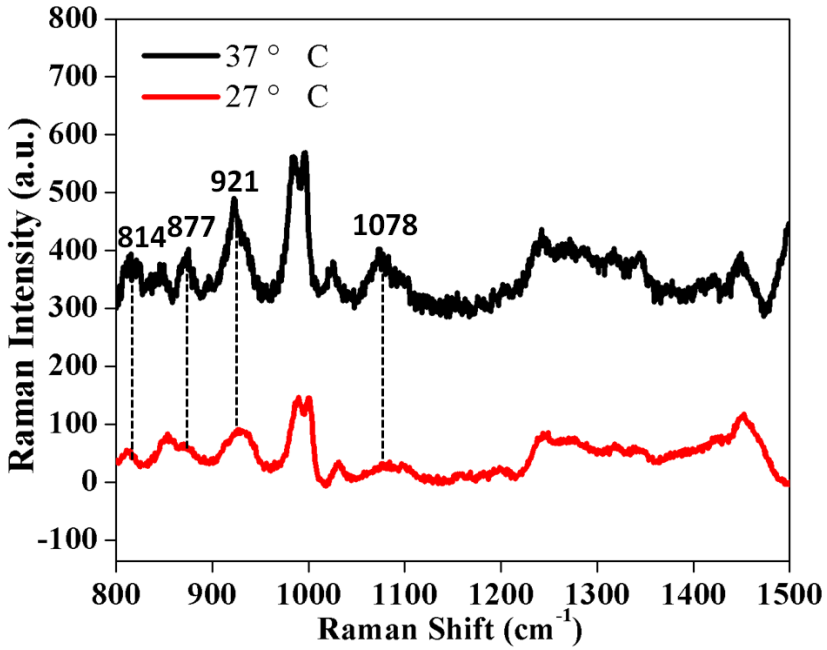

Figure 7. Raman spectra of the collagen hydrogels assembled at 27 ℃ and 37 ℃. The spectral range between 800 cm^{-1} to 1500 cm^{-1} is shown.

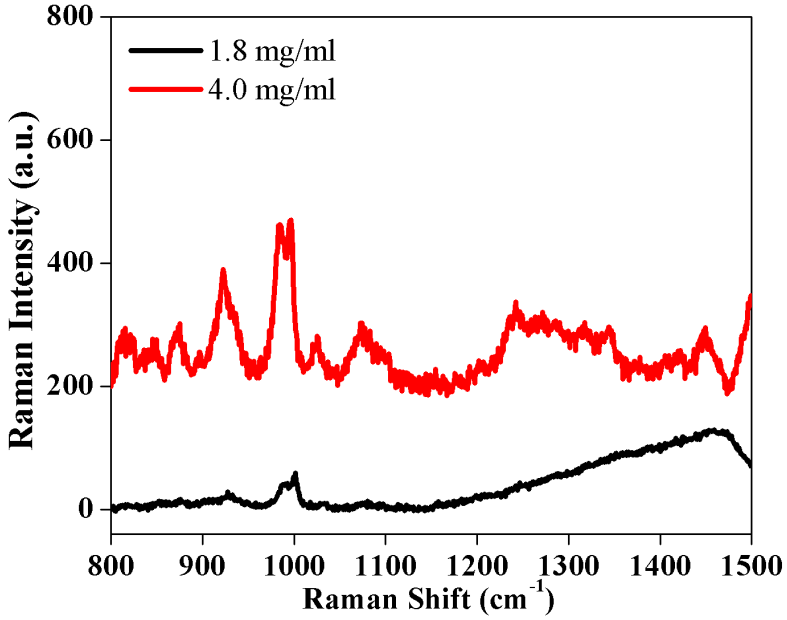

Figure 8. Raman spectra of the collagen hydrogels assembled at 1.8 mg/ml and 4.0 mg/ml at 37 ℃. The spectral range between 800 cm^{-1} to 1500 cm^{-1} is shown.

The SHG images have shown that collagen hydrogels assembled at different initial collagen concentrations and incubation temperatures have dramatic differences in microstructure. TEM images show that different initial collagen concentrations lead to the formation of different types of nanostructure but different incubation temperature only changes the roughness of the edge of nanostructure. However, Raman spectra show that these two assembly factors have minimal effect on the molecular information of collagen hydrogels. This observation suggests that the differecen in the micro- and nano-structure doesn't begin with the change in molecular conformation. For the concentration effect, the collagen molecules undergo different assembly mechansims to form different nano-structures and different nano-strucutres ultimatley affect the micro-structures. For the tempertaure effects, the collagen molecules might follow the similar assembly process to form the nano-structures. The assembly of nano-structures is influenced by the different incubation tempertures to form different micro-structures. Our data obtained from SHG, TEM and Raman imply that the structural level which could be most signifantly affected by external assembly factors might be the micro-strucutural level.

Conclusion

The scattering structures formed within 3D collagen materials assembled under different initial collagen concentrations and incubation temperatures consist of both assembled fibrils that display a periodic banding pattern and filamentous structures that do not have this characteristic collagen striation. Additionally, the transmission electron micrographs show variations in the collagen fibril nanostructure formed at different initial protein

concentrations and incubation temperatures. Spindle-shaped fibrils appear at the concentrations of 1, 2, 2.5 and 4 mg/ml and the spiral-shaped fibrils are formed at the concentrations of 2 and 2.5 mg/ml. Therefore, in the 3D collagen materials commonly employed in biomedical and tissue engineering research and examined in this work, a uniform fibril orientation and a unified relationship between second harmonic generation (SHG) directionality, collagen fibril morphology and fibril sizes is not likely. The dependence of SHG signals on the surface area or amount of interfaces created upon assembly of 3D collagen materials can account for the strength of the detected backscattered signals. The difference in initial collagen concentrations and incubation temperature also alters the molecular information of collagen hydrogels detected with Raman spectroscopy.

References

(1) Frushour, B. G.; Koenig, J. L. *Biopolymers* **1975**, *14*, 379-391.

(2) Abraham, L.; Zuena, E.; Perez-Ramirez, B.; Kaplan, D. L. *J Biomed Mater Res B Appl Biomater* **2008**, *87*, 264-285.

(3) Hanson, K. M.; Bardeen, C. J. *Photochem. Photobiol.* **2009**, *85*, 33-44.

(4) Yeh, A. T.; Nassif, N.; Zoumi, A.; Tromberg, B. J. *Optics Letters* **2002**, *27*, 2082-2084.

(5) Zipfel, W. R.; Williams, R. M.; Webb, W. W. *Nat. Biotechnol.* **2003**, *21*, 1369-1377.

(6) Legare, F.; Pfeffer, C.; Olsen, B. R. *Biophys. J.* **2007**, *93*, 1312-1320.

(7) Zipfel, W. R.; Williams, R. M.; Christie, R.; Nikitin, A. Y.; Hyman, B. T.; Webb, W. W. *Proc. Natl. Acad. Sci. USA.* **2003**, *100*, 7075-7080.

(8) Zoumi, A.; Yeh, A.; Tromberg, B. J. *Proc. Natl. Acad. Sci. USA* **2002**, *99*, 11014-11019.

(9) Raub, C. B.; Suresh, V.; Krasieva, T.; Lyubovitsky, J.; Mih, J. D.; Putnam, A. J.; Tormberg, B. J.; Geroge, S. C. *Biophys. J.* **2006**, *92*, 2212-2222.

(10) Campagnola, P. J.; Millard, A. C.; Terasaki, M.; Hoppe, P. E.; Malone, C. J.; Mohler, W. A. *Biophys. J.* **2002**, *82*, 493-508.

(11) Williams, R. M.; Zipfel, W. R.; Webb, W. W. *Biophys. J.* **2005**, *88*, 1377-1386.

(12) Guo, Y.; Savage, H. E.; Liu, F.; Schantz, S. P.; Ho, P. P.; Alfano, R. R. *Proc. Natl. Acad. Sci. USA* **1999**, *96*, 10854-10856.

(13) Moreaux, L.; Sandre, O.; Charpack, S.; Blanchard-Desce, M.; Mertz, J. *Biophys. J.* **2001**, *80*, 1568-1574.

(14) Schenke-Layland, K.; Riemann, I.; Damour, O.; Stock, U. A.; Konig, K. *Advance Drug Delivery Reviews* **2006**, *58*, 878-896.

(15) Raub, C. B.; Unruh, J.; Suresh, V.; Krasieva, T.; Lindmo, T.; Gratton, E.; Tromberg, B. J.; George, C. *Biophys. J.* **2008**, *94*, 2361-2373.

(16) Masters, B. R.; So, P. T. C. *Microsco. Res. Techniq.* **2004**, *63*, 3-11.

(17) Brown, E.; McKee, T.; DiTomaso, E.; Pluen, A.; Seed, B.; Boucher, Y. *Nat. Med.* **2003**, *9*, 796-801.

(18) Roth, S.; Freund, I. *J.Chem.Phys.* **1979**, *70*, 1637-1643.

(19) Dehring, K. A.; Smukler, A. R.; Roessler, B. J.; Morris, M. D. *Appl. Spectrosc.* **2006**, *60*, 366-372.

(20) Diem, M.; Bhatnagar, R. S.; Druyan, M. E.; Renugopalakrishnan, V. *Biopolymers* **1984**, *23*, 2955-2961.

(21) Dingari, N. C.; Horowitz, G. L.; Kang, J. W.; Dasari, R. R.; Barman, I. *PLoS ONE* **2012**, *7*.

(22) Dong, R.; Yan, X.; Pang, X.; Liu, S. *Spectrochim Acta A* **2004**, *60*, 557-561.

(23) Erckens, R. J.; Motamedi, M.; March, W. F.; Wicksted, J. P. *J. Raman Spectrosc.* **1997**, *28*, 293-299.

(24) Frank, C. J.; McCreery, R. L. *Anal. Chem.* **1995**, *67*, 777-783.

(25) Jaisson, S.; Lorimier, S.; S.;, R.-B.; Sockalingum, G. D.; C.;, D.-F.; Kegelaer, G.; Manfait, M.; Garnotel, R.; Gillery, P. *Chem. Biol.* **2006**, *13*, 149-159.

(26) Jastrzebska, M.; Wrzalik, R.; Kocot, A.; Zalewska-rejdak, J.; Cwalina, B. *J. Jomater. Sci. Polymer Edn* **2003**, *14*, 185-197.

(27) Sebag, J.; Nie, S.; Reiser, K.; Charles, M. A.; Yu, N. *Invest. Ophth. Vis. Sci.* **1994**, *35*, 2976-2980.

(28) Carey, P. R. *Biochemical Applications of Raman and Resonance Raman Spectroscopies*; Academic Press Inc.: New York, 1982.

(29) Parker, F. S. *Applications of Infrared, Raman and Resonance Raman Spectroscopy in Biochemistry*; Plenum Press: New York and London, 1983.

(30) Spiro, T. G. *Biological Applications of Raman Spectroscopy; Volume 1 Raman Spectra and the Conformations of Biological Molecules*; John Wiley & Sons: New York, 1987.

(31) Tfayli, A.; Piot, O.; Draux, F.; Pitre, F.; Manfait, M. *Biopolymers* **2007**, *87*, 261-274.

(32) Agarwal, l. A.; Coleno, M. L.; Wallace, V. P.; Wu, W.; Sun, C.; Tromberg, B. J.; Geroge, S. C. *Tissue engineering* **2001**, *7*, 191-202.

(33) Kirkpatrick, N. D.; Adndreou, S.; Hoying, J. B.; Utzinger, U. *Am. J. Physiol. Heart Circ Physiol* **2007**, *202*, 3198-3206.

(34) Miron-Mendoza, M.; Seemann, J.; Grinnell, F. *Mol. Bio. of the Cell* **2008**, *19*, 2051-2058.

(35) Pizzo, A. M.; Kokini, K.; Vaughn, L. C.; Waisner, B. Z.; Voytik-Harbin, S. L. *J.Appl. Physiol* **2005**, *98*, 1909-1921.

(36) Brightman, A. O.; Rajwa, B. P.; Sturgis, J. E.; McCallister, M. E.; Robinson, J. P.; Voytik-Harbin, S. L. *Biopolymers* **2000**, *54*, 222-234.

(37) Williams, B. R.; Gelman, R. A.; Poppke, D. C.; Piez, K. A. *J. Biol. Chem.* **1978**, *253*, 6578-6585.

(38) When the collagen concentration was 0.1 mg/ml, a. t. o. f., where the stained region in the single D-period band is narrower than the unstained region, was observed. The presence of this type of collagen fibril was previously reported to occur during collagen assembly from high phosphate concentrations. It probably occurs due to insufficient availability of collagen molecules during the self-assembly process, which results in closer spacing between the collagen molecules. These fibrils were previously observed in Williams, B. R. G., R.A.; Poppke, D. C.; Piez, K.A. J. Biol. Chem. 1978, 253, 6578-6585.

(39) Graham, H. K.; Holmes, D. F.; Watson, R. B.; Kadler, K. E. *J. Mol. Biol.* **2000**, *295*, 891-902.

(40) Kadler, K. E.; Holmes, D. F.; Trotter, J. A.; Chapman, J. A. *Biochem. J.* **1996**, *316*, 1-11.

(41) Gobeaux, F.; Mosser, G.; Anglo, A.; Panine, P.; Davidson, P.; Giraud-Guille, M. M.; Belamie, E. *J. Mol. Biol.* **2008**, *376*, 1509-1522.

(42) Ottani, V.; Raspanti, M.; Ruggeri, A. *Micron* **2001**, *32*, 251-260.

(43) Ottani, V.; Martini, D.; Franchi, M.; Ruggeri, A.; Raspanti, M. *Micron* **2002**, *33*, 587-596

(44) Wood, G. C.; Keech, M. K. *Biochem. J.* **1960**, *75*, 588-598.

(45) Bruns, R. R. *J. Cell. Biol.* **1976**, *68*, 521-538.

(46) Hayashi, T.; Nagai, Y. *J. Biochem.* **1973**, *73*, 999-1006.

(47) Kuznetsova, N.; Leikin, S. *J. Biol. Chem.* **1999**, *274*, 36083-36088.

(48) Wood, G. C. *Biochem. J.* **1960**, *75*, 598-605.

(49) Wood, G. C. *Biochem.J.* **1960**, *75*, 598.

(50) Gross, J.; Kirk, D. *J. Biol. Chem.* **1958**, *233*, 355-360.

(51) Yeh, A.; Choi, B.; Nelson, J. S.; Tromberg, B. J. *J. Invest. Dermatol.* **2003**, *121*, 1332-1335.

(52) Sun, Y.; Chen, W. L.; Lin, S. J.; Jee, S. H.; Chen, Y. F.; Lin, L. C.; So, P. T. C.; Dong, C. Y. *Biophys J.* **2006**, *91*, 2620-2625.

(53) Lyubovitsky, J. G.; Xu, X.; Sun, C.; Krasieva, T. B.; Andersen, B.; Tromberg, B. J. *Proc. SPIE* **2008**, *6859*, 685902

(54) Laiho, L. H.; Pelet, S.; Hancewicz, T. M.; Kaplan, P.; So, P. T. C. *Journal of Biomed. Optics* **2005**, *10*, 024016.

(55) Stoller, P.; Celliers, P. M.; Reiser, K. M.; Rubenchik, A. M. *Appl. Optics.* **2003**, *42*, 5209-5219.

(56) Yasui, T.; Tohno, Y.; Araki, T. *J. Biomed. Opt.* **2004**, *9*, 259-264.

(57) Stoller, P.; Celliers, P. M.; Reiser, K. M.; Rubenchik, A. M. *Biophys. J.* **2002**, *82*, 3330-3342.

(58) Stoller, P.; Kim, B. M.; Rubenchik, A. M.; Reiser, K. M.; Da Silva, L. B. *J. Biomed. Opt.* **2002**, *7*, 205-214.

(59) Bayan, C.; Levitt, J. M.; Miller, E.; Kaplan, D.; Georgakoudi, I. *J. of Applied Physics* **2009**, *105*, 102042.

(60) Yeh, A. T.; Gibbs, H.; Hu, J.; Larson, A. M. *Tissue Engineering: Part B* **2008**, *14*, 119-131.

(61) Miron-Mendoza, M.; Seemann, J.; Grinnell, F. *Biomaterials* **2010**, *31*, 6425-6435.

(62) Hwang, Y.; Kolettis, N.; Yang, M.; Gillard, E.; Sanchez, E.; Sun, C.; Tromberg, B.; Krasieva, T.; Lyubovitsky, J. *Photochem. Photobiol.* **2010**, *In Press*.

(63) Niklason, L. E.; Yeh, A. T.; Callea, E. A.; Baib, Y.; Arturo, V.; Humphrey, J. D. *Proc. Natl. Acad. Sci. USA.* **2009**, *107*, 3335-3339.

CHAPTER 3

CHARACTERIZATION OF CROSS-LINKED COLLAGEN HYDROGELS: A multi-photon optical image guided spectroscopy method for characterization of collagen-based materials modified by glycation

Abstract

The cross-linking with reducing sugars, known as glycation, is used to increase stiffness and strength of tissues and artificial collagen-based scaffolds. Non-destructive characterization methods that report on the structures within these materials could clarify the effects of glycation. For doing this non-destructive evaluation, we employed an *in-situ* one-photon fluorescence as well as multiphoton microscopy method that combined two-photon fluorescence and second harmonic generation signals. We incubated collagen hydrogels with glyceraldehyde, ribose and glucose and observed an increase in the *in situ* fluorescence and structural alterations within the materials during the course of glycation. The two-photon fluorescence emission maximum was observed at about 460 nm. The fluorescence emission in the one-photon excitation experiment (λ_{ex}=360 nm) was broad with peaks centered at 445 nm and 460 nm. The 460 nm emission component subsequently became dominant during the course of glycation with glyceraldehyde. For the ribose, in addition to the 460 nm peak, the 445 nm component persisted. The glucose glycated hydrogels, exhibited broad fluorescence that did not increase significantly even after six weeks. As determined from measuring the fluorescence intensity at 460 nm maximum, glycation with glyceraldehyde was faster compared to ribose and generated

stronger fluorescence signals. Upon excitation of glycated samples with 330 nm light different emission peaks were observed.

Introduction

In spite of the adverse aging effects of glycation[1-4] *in vivo, in vitro* this process is widely employed to increase stiffness and strength of tissues' and artificial scaffolds'.[2, 3, 5-7] Most present studies, however, are focused on following changes in the mechanical strength of the glycated samples after the exposures to reducing sugars with little reference to the structures within. Characterization of the microstructures is necessary to clarify the effects of non-enzymatic crosslinking on tissues and biologically derived scaffolds.

We now report the effects of non-enzymatic crosslinking with glyceraldehyde, ribose and glucose on three-dimensional (3D) collagen-based hydrogels characterized by *in-situ* multi-photon microscopy (MPM) and fluorescence spectroscopy. The data and methods developed provide an outline to follow the mechanisms of glycation of protein-based materials by reducing sugars *in situ*.

MPM is a non-destructive optical method that utilizes femto-second pulses of near-infrared (NIR) laser light and performs high resolution and three-dimension imaging of biological samples. Its advantages include reduced scattering because NIR wavelengths are employed, no out-of focus absorption, very small sample volumes and deeper tissue penetration compared to confocal microscopy.[8] The interaction between fibrillar collagen and NIR pulsed, femto-second laser light of MPM has been identified to result in second harmonic generation (SHG) and two-photon excited fluorescence (TPF)[8, 9] signals. SHG

is produced when photons interacting with fibrillar collagen are combined to form new photons with exactly twice the energy.[10] SHG gained recognition in tissue imaging[8-17] because this source of contrast resists photo-bleaching and had been used to successfully image structural proteins in various non-animal and animal sources[18] with strong enhancement suitable for biomedical assessment of tissue structure.[17] It is believed that the interaction between laser pulses and collagen's non-centrosymmetric, triple helix structure in addition to molecular packing within collagen materials leads to scattering from the tertiary (fibrils),[17] and quaternary (fibers)[10] level of organization thus producing SHG.[19] The intrinsic fluorescence is generated by UV/VIS absorbing molecules and proteins. In collagen protein, the non-enzymatic glycation products collectively known as advanced glycation endproducts (AGEs)[20] absorb in the near-UV (320-370 nm) and fluoresce in the 380 to 460 nm range.

Experimental Section

Collagen materials formation and cross-linking

Soluble rat-tail type I collagen, 9.58 mg/ml (BD Biosciences) was in 0.02N acetic acid. The purity of this stock solution was verified with 4%-20% Tris-HCl gels (Bio-Rad) following a standard protocol. The stock solution was diluted with 0.02N acetic acid to obtain the 2X collagen aliquots. The reverse pipetting technique was used to pipette collagen stock solution. 2X initiation buffer were prepared from NaCl and phosphate buffer. The concentration of mono-and dibasic phosphate in the buffer at pH=7.4 were calculated with Henderson-Hasselbalch equation. The pH was adjusted drop-wise with

1N NaOH or HCl. Ionic strength was adjusted with NaCl. The initiation buffer had the following components: 6.40 g/l K_2HPO_4; 3.16 g/l KH_2PO_4; 38.55 g/l NaCl (ionic strength = 0.44 M). After the pH was adjusted to a desired value, the initiation buffer was filtered with a 0.22 μm, 25 mm syringe filter (Fisher) and stored at 4℃. Prior to the beginning of material formation, both 2X collagen aliquots and initiation buffer were de-airated by placing in a 1.5 L desiccator (Fisher) and applying house vacuum for 2 hrs. Material formation was initiated by mixing 2X collagen aliquot with 2X initiation buffer on ice at 1:1 ratio, verifying the pH to be 7.4±0.1, and then incubating at 37 ℃.

For multi-photon microscopy measurements collagen materials were prepared in the 8-well chambered coverglass (MP Biomedicals). For one photon experiments collagen materials were prepared in 96-well plates (BD Falcon). In both cases, after 24 hour incubation at 37 ℃, the materials were incubated in 0.1 M concentration of D, L-Glyceraldehyde, D-Ribose and D-Glucose (Sigma) at same temperature for the specified amount of times. The control reagents for the reducing sugars were 0.1 M sugar alcohols with the same number of carbons as respective reducing sugars. Glycerol, xylitol and sorbitol (Sigma) are the controls for glyceraldehyde, ribose and glucose respectively. When the samples incubated with ribose, glucose and sugar alcohols were stored for 6 weeks at 37° C, amphotercin B (Sigma) at 5.6 μg/ml final concentration and gentamicin sulphate salt (Sigma) at 50 μg/ml final concentration were added. The antibiotics were refreshed every couple of days.

One photon in-situ fluorescence measurements

Increase in fluorescence within the materials that was due to glycation was measured *in situ*, in a high-throughput format using a FlexStation microplate reader in the backscattering mode (Molecular Devices). The excitation wavelength was 360 nm and emission spectrum was collected from 420 to 530 nm. Additional excitation wavelength at 330 nm was used and the emission spectrum was collected from 360 nm to 500 nm. The spectra were collected with a 5 nm step. Measurements for glyceraldehyde were taken every 1 h during the first 9 hrs and subsequently 2 measurements every 24 hrs; measurements for ribose and glucose were taken once every week. Per one experimental run, a spectrum was independently acquired from two wells. The background fluorescence was subtracted from each spectrum and the spectra were averaged. All experimental runs were repeated on different days and up to three times using identical settings for the measurements. The error bars are standard deviations from the mean.

After the fluorescence intensity reached the plateau, glyceraldehyde-glycated samples were shaken thoroughly in a warm (~30°C) 0.1 M Tris-HCl (pH 4.5) buffer as previously described[2] to inactivate and remove adsorbed reducing sugars and/or other reactive carbonyl compounds.

In-situ multiphoton photon microscopy (MPM)

The inverted Zeiss LSM 510 NLO Meta laser scanning microscopy system was used in this work. It was based on the Axiovert 200M inverted microscope equipped with standard illumination systems for transmitted light and epi-fluorescence detection. It was

also equipped with an NLO interface for a femto-second Titanium:Sapphire laser excitation source (Chameleon-Ultra, Coherent, Incorporated, Santa Clara, California) for multi-photon excitation. The Chameleon laser provided femto-second pulses at a repetition rate of about 80 MHz, with the center frequency tunable from 690 to 1040 nm. A long working distance objective (Zeiss, 40X water, N.A. 0.8) was used to acquire images shown in this work. The two-photon signals from the sample were epi-collected and discriminated by the short pass 650 nm dichroic beamsplitter. The SHG images were collected with the 390-465 nm band pass filter (λ_{ex} = 800 nm). The TPF images were collected using META detection module with emission sampled in a 405-501 nm detection range (λ_{ex} = 720 nm). Each image presented in this work is 12 bit, 512x512 pixels representing 225 μm x 225 μm field of view. To obtain the spectra we averaged about twenty-five regions of interest (ROIs) in the areas of the image that displayed glycation-induced fluorescence (sample) and subtracted about twenty averaged ROIs obtained from the image in the regions that did not have induced fluorescence (background). All the imaging and spectra were successfully reproduced on separate days, using up to eight independent samples on each day (about five field of views per sample).

Results and Discussion

In-situ characterization of glycated collagen materials with one photon fluorescence

The incubation of acellular collagen hydrogels in 0.1 M solutions of reducing sugars caused the non-fluorescent samples to emit *in-situ* fluorescence. When the collagen hydrogels were exposed to glyceraldehydes and subsequently excited with 360 nm light,

the detected fluorescence emission maximum observed was a broad band with peaks centered at 445 nm and 460 nm (Figure 1A). The 460 nm emission component subsequently became dominant as reaction progressed. The shift, however, didn't occur for the materials incubated with ribose. In addition to a broad fluorescence maximum centered at 460 nm, the 445 nm component persisted (Supporting Information Figure S1A). The glucose glycated hydrogels, exhibited broad fluorescence that did not increase significantly even after 6 weeks (Supporting Information Figure S2A).

The excitation of samples with a different wavelength of light (λ_{ex} = 330 nm) produced a

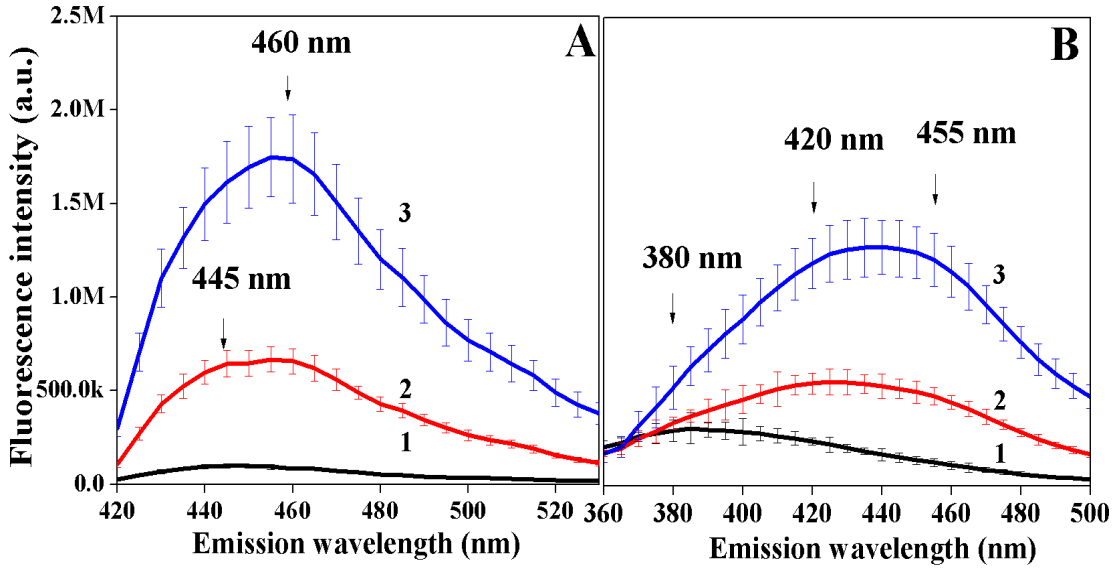

Figure 1. The effect of glycation with 0.1 M glyceraldehyde on the production of advanced glycation endproducts. (A) Fluorescence emission spectra (λ_{ex} = 360 nm) of the sample that was incubated with glyceraldehyde for 0 hr (1), 6 hr (2), 28 hr (3). (B) Fluorescence emission spectra (λ_{ex} = 330 nm) of the sample that was incubated with glyceraldehyde for 0 hr (1), 6 hr (2), 29 hr (3). All samples were measured in triplicate, and error bars represent standard deviations from the mean.

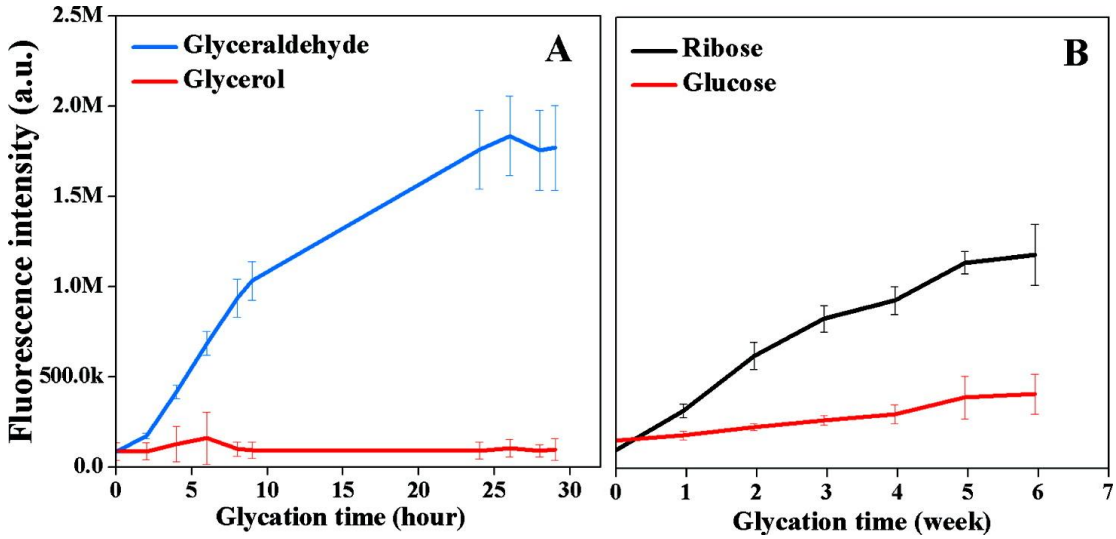

Figure 2. The effect of glycation with 0.1 M reducing sugars on the production of fluorescent advanced glycation endproducts. (A) The fluorescence intensity ($\lambda_{ex}/\lambda_{em}$ = 360 nm/460 nm) as a function of cross-linking time for glyceraldehyde and glycerol used as control. (B) The fluorescence intensity ($\lambda_{ex}/\lambda_{em}$= 360 nm/460 nm) as a function of cross-linking time for ribose and glucose. All samples were measured in triplicate, and error bars represent standard deviations from the mean.

different fluorescence emission spectrum. For glyceraldehyde modified hydrogels, the 330 nm light excited fluorescence appeared in a form of a shoulder at 380 nm and very broad maximum with at least two peaks centered at 420 nm and 455 nm (Figure 1B). For the ribose and glucose glycated materials the 330 nm light excited fluorescence maximum was observed at about 385 nm until week 3 with a subsequent shift to about 410 nm by week 6 (Supporting Information Figure S1B and Figure S2B). For glucose an increase was minimal.

Overall, glycation of collagen hydrogels with glyceraldehyde produced significantly higher final fluorescence intensity at 460 nm (λ_{ex} = 360 nm) compared to glycation with ribose or glucose and occurred with faster rate (Figure 2). The collagen hydrogels exposed to glyceraldehyde showed an increase in fluorescence intensity until reaching a

plateau at twenty-five hours (Figure 2A). The materials exposed to ribose showed a significant increase in fluorescence intensity at six weeks (Figure 2B). There was virtually no increase in fluorescence intensity in the samples incubated with glucose. The controls consisting of collagen hydrogels incubated in solutions of sugar alcohols didn't generate any detectable fluorescence.

One photon spectroscopy is a common technique for the identification of fluorescence generating advanced glycation endproducts (AGEs). For the collagen samples glycated with glyceraldehyde we detected the fluorescence emission maximum around 460 nm (λ_{ex} = 360 nm). This maximum is similar to fluorescence emission detected from biochemically identified lysine-OH-triosidine (LHT).[2, 4] Tessier et al.[2, 4] excited this product of non-enzymatic cross-linking formed by reacting glyceraldehyde and N^{α}-acetyl-L-lysine with 354 nm and observed fluorescence at 440 nm. Danilov et al.[2, 4] treated rabbit scleral tissue with glyceraldehyde and observed glycation products in papain-digest solutions to fluoresce at 453 nm upon excitation with 370 nm light. Treating a bovine kidney tubular basement membrane with glucose[21] lead to induction of 460 nm centered fluorescence emission (λ_{ex} = 360 nm). All previous studies, therefore, suggest that three reducing sugars employed in our work induce the formation of the LHT fluorophore. Additional peaks, however, persisted when we excited collagen hydrogels treated with ribose and glucose with 360 nm light.

The excitation of the glycated collagen materials with 330 nm light showed a different fluorescence emission spectrum compared to one obtained upon excitation of samples

with 360 nm light. This observed spectrum also differs from that measured in solution by other investigators.[4] The 380 nm fluorescence emission that in our work appeared as a shoulder upon excitation of samples with 330 nm light had been previously attributed to fluorescence from arginine-OH- triosidine (AHT).[2, 4,2, 4]

Our observations imply that 1) the *in-situ* fluorescence of LHT and AHT fluorophores is more complex compared to that observed in solution digests. *In situ*, either the AHT and LHT fluorophores are localized in different physico-chemical microenvironments or more extensive diversity of fluorophores is formed upon glycation of collagen hydrogels. Although not previously observed in solution, the different fluorophores or different states of the same fluorophore could be detected when we carry out fluorescence measurements *in-situ*. 2) overall, the fluorescence emission peaks were different for glyceraldehyde treated hydrogels compared to those treated with ribose and glucose. This difference is due to either the different advanced glycation endproducts (AGEs) formed as a result of treatment by the three sugars or to the difference in the overall time scales of forming AGEs. The rate of glycation is thought to depend on the amount of sugar present in the open chain form.[6] The glyceraldehyde exists only in the open-chain form and therefore exhibits the fastest glycation rate. Ribose is about 17 times more likely than glucose to be present in the open form[6] and modifies collagen materials at a faster rate compared to glucose.

In-situ characterization of glycated collagen materials with multiphoton microscopy and spectroscopy using second harmonic generation (SHG) and two photon fluorescence (TPF) signals.

Multi-photon microscopy provides an opportunity to monitor the microscopic structures *in situ* during glycation of collagen-based materials with reducing sugars.

To follow the extent of glycation we excited the collagen hydrogels with 720 nm light and monitored the evolution of two-photon fluorescence intensity in the X-Y plane through the 405-501 nm filter (Figure 3A-C). At 8 hours of glyceraldehyde glycation time, the bright fluorescence spots were observed (Figure 3B). When the glycation time reached 48 hours, the accumulated fluorescence spots exhibited higher fluorescence intensity, grew in diameter and merged into larger structures (Figure 3C, white outline). The TPF images taken in X-Z plane showed that upon extended glycation (24 hrs and more) an increase of fluorescence occurred throughout the entire depth of collagen hydrogels (Figure 4D). After 6 weeks, the ribose-glycated samples produced strong fluorescence signals (Figure 5A). The glucose-glycated samples didn't generate significant fluorescence even after 6 weeks (Figure 5B). The control group that had collagen samples exposed to sugar alcohols also did not exhibit detectable fluorescence (Figure 4C and Supporting Information Figure S3C-S5C).

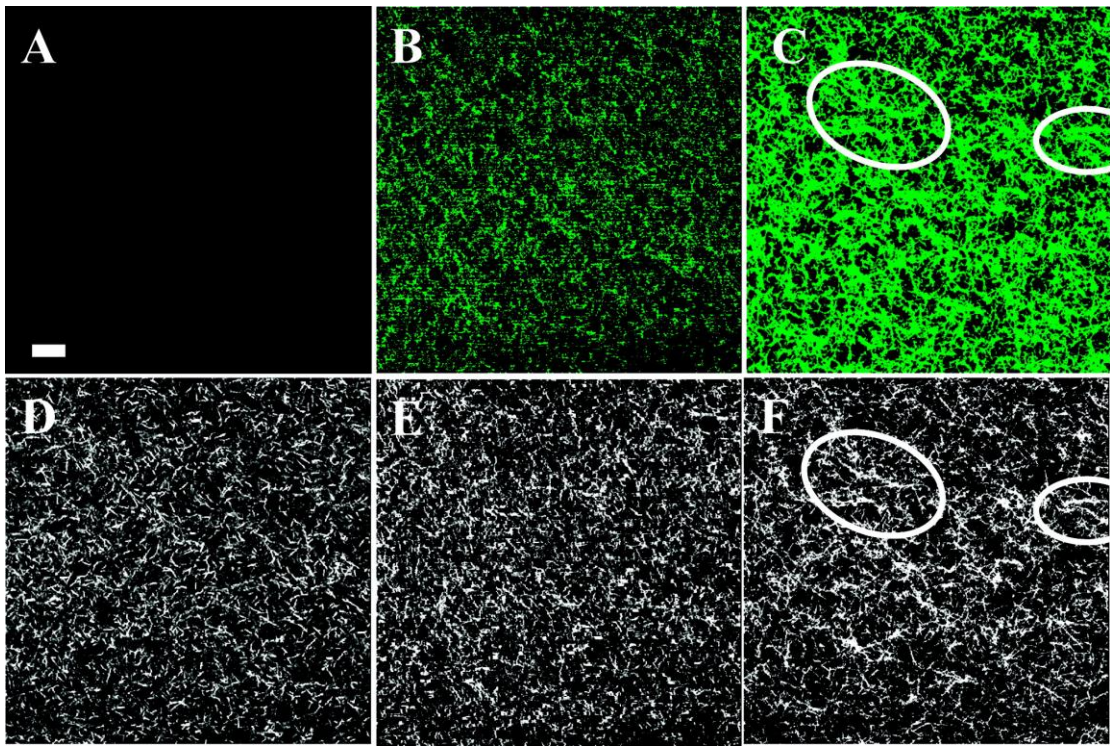

Figure 3. Typical two photon fluorescence (TPF) and second harmonic generation (SHG) images of a sample incubated with 0.1 M glyceraldehyde for different times. The images are taken in X-Y plane. TPF: (A) 0 hr. (B) 8 hr. (C) 48 hr. SHG: (D) 0 hr. (E) 8 hr. (F) 48 hr. The 'fiber-like' structures modified to long, aggregated fibers with length longer than 20 μm can be seen within the areas circled with the white outline. The collagen concentration of the sample was 2.0 g/l and the incubation temperature was 37℃. The scale bar is 20 μm.

To determine if there are structural modifications of collagen hydrogels that are caused by glycation, we obtained second harmonic generation (SHG) images in addition to fluorescence. As seen in SHG images (Figure 3D-F), extended glycation (24 hrs and more) clearly alters the microstructure of collagen hydrogels. When the glyceraldehyde glycation time was 8 hours, the "fiber-like" structures within collagen hydrogels remained short with lengths around 5 to 10 μm (Figure 3D and 3E). The short "fiber-like" structures began to disappear at about 24 hours. When the glycation time reached 48 hours, the short 'fiber-like' structures became modified to longer, aggregated threads

with length greater than 20 μm (Figure 3F). For ribose treated samples the collagen hydrogel remodeling began to occur after 1 week. After 6 weeks the short "fiber-like" structures began to transform to longer, aggregated fibers with length greater than 20 μm (Figure 5C). It took 2 weeks before any remodeling due to glucose could be detected and even after 6 weeks, the samples remain largely unchanged (Figure 5D). The control group, which had collagen samples exposed to sugar alcohols corresponding to glyceraldehydes, ribose and glucose did not have any structural changes that could be identified in the SHG images (Figure 4A and Supporting Information Figure S3A-S5A). In a separate set of imaging experiments we verified that there was no time dependent structural remodeling taking place within collagen hydrogels. When we employed the sterile technique, TPF and SHG images collected twenty-four hours after preparing samples looked identical to those acquired seven weeks later.

The SHG images show a clear glycation-induced remodeling of fibrils/fibers within the collagen materials. Our findings are in agreement with several previous studies that recognized the structural changes within various glycated collagen-based tissues and materials. For example, when tendons were exposed to reducing sugars, changes in collagen molecular packing were detected in the medium-angle X-ray diffraction studies.[22] When rat tail tendons were incubated in 0.2 M ribose, electron micrographs of tendons cross-sections showed an increased fibril packing density, fusion of fibrils and irregular fibril diameters.[23] Scanning force microscopy studies revealed structural alterations in the radius of fibrils gap depth when tendons were incubated with 0.5 M glucose for two weeks.[24] Interestingly, cellular behavior was altered when cells were

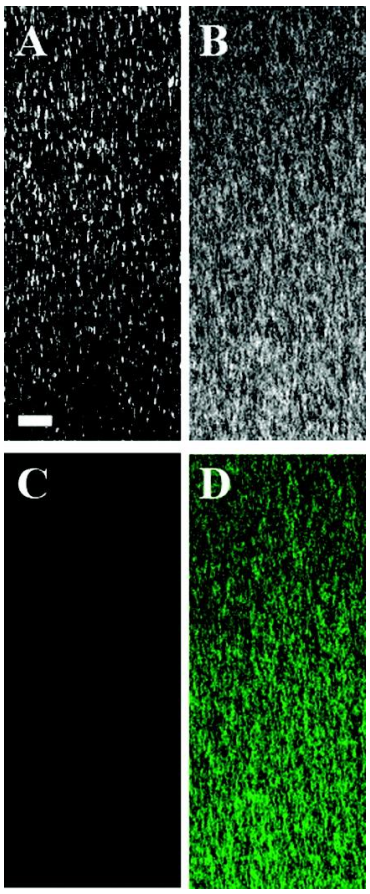

Figure 4. Typical second harmonic generation (SHG) and two photon fluorescence (TPF) images of a sample incubated with 0.1 M glyceraldehyde. The images were taken in X-Z plane. The collagen concentration was 4.68 g/l. Horizontal is X- axis, and vertical is Z- axis. SHG: (A) and (B), TPF: (C) and (D). Glycerol control: (A),(C). Glyceraldehyde: (B),(D). The scale is 20 μm. The top of each image represents the actual top of the imaged gel.

placed within the glycated collagen materials. For example, the fibroblasts underwent reorganization of actin cytoskeleton. Their morphology, attachment, proliferation, and migration were all altered.[25, 26] Glycated collagen materials suppressed the adhesive and migratory abilities of normal human keratinocytes from neonatal skin, therefore suggesting that modification diminished the binding capacity of type I collagen.[25, 26]

All the techniques employed in previous works that recognized the structural remodeling within glycated collagen tissues/materials have either imposed a non-reversible damage to the samples and/or provided only partial structural information. For example, the samples studied with X-ray and electron beams that are destructive in their nature, could not be used in any subsequent studies. The scanning force microscopy only provided

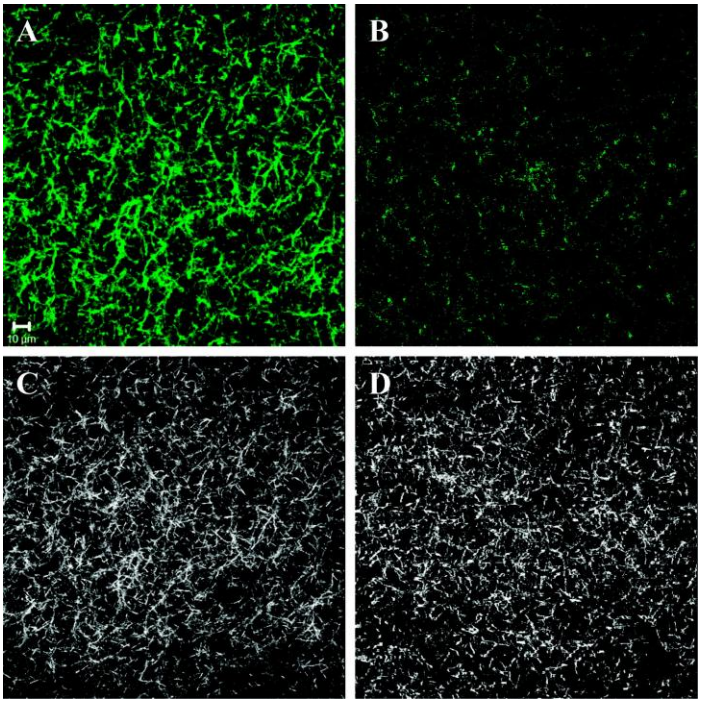

Figure 5. Typical two photon fluorescence (TPF) and second harmonic generation (SHG) images of the sample incubated with 0.1 M ribose and 0.1 M glucose for 6 weeks. These images were taken in X-Y plane. (A) Ribose, TPF. (B) Glucose, TPF. (C) Ribose, SHG. (D) Glucose, SHG. The scale is 10 μm.

information regarding collagen structures on the surface without penetrating deep into the tissues. The near-infrared wavelength of light utilized in our two-photon fluorescence (TPF) and second harmonic generation (SHG) imaging is non-destructive to protein-based samples like collagen 3D hydrogels. It can provide three-dimensional structural information regarding the extent of glycation within them. At present there is only one study reported in literature that briefly mentions a 40% decrease in the SHG intensity of a glycated human tendon as compared to the normal tendon.[27] That study did not provide data regarding structures and/or glycation-induced fluorescence.[27]

To relate the fluorescence observed in TPF images to the properties of the produced fluorophores, we obtained the two-photon emission spectra from the collagen hydrogels glycated with glyceraldehyde (Figure 6) and ribose (Supporting Information Figure S6). For the samples treated with glyceraldehydes, at six hours post initiation of glycation, the spectrum was a broad fluorescence band. At twenty-four hours, the band became centered at about 460 nm and the fluorescence intensity increased five-fold compared to six hours post initiation of glycation. For the ribose glycated hydrogels, the two-photon emission spectrum collected at six weeks looked similar to that collected at twenty four hours from the collagen hydrogels glycated with glyceraldehyde (Supporting Information Figure S6). The spectrum for the control group in which 0.1 M sugar alcohols were added to the collagen materials instead of reducing sugars indicated no increase of the TPF signals. The peak observed at about 460 nm possibly results from the fluorophore lysine-OH-triosidine (LHT). We believe it involves the same electronic transition excited with a 360 nm light (Figure 1).

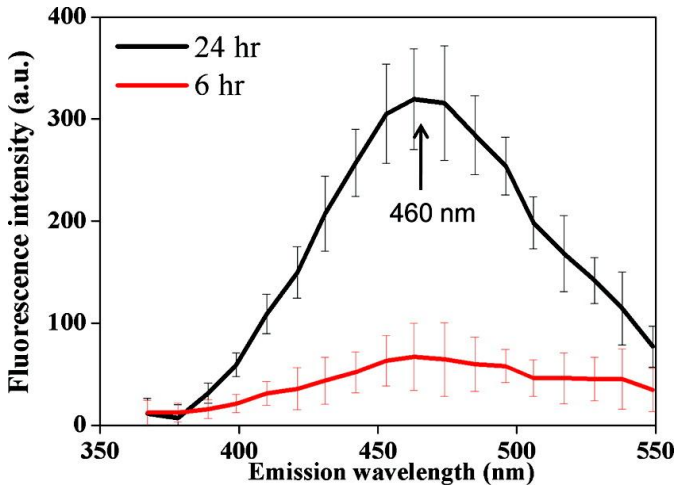

Figure 6. Two photon fluorescence emission spectra (λ_{ex} = 720 nm) of the sample incubated with 0.1M glyceraldehyde for different time.

Conclusion

We probed the effects of non-enzymatic cross-linking with multi-photon microscopy (MPM) and one-photon fluorescence methods *in situ*. In this study, collagen hydrogels were modified with glyceraldehyde, ribose and glucose. The glyceraldehyde and ribose modifications led to an induction of strong auto-fluorescence and significant micro-structural changes in 'fiber-like' features within collagen hydrogels. The glucose glycated hydrogels exhibited broad, weak auto-fluorescence. After six weeks the samples remained largely unchanged.

The two-photon fluorescence (TPF) emission maximum was observed at about 460 nm for the samples glycated with glyceraldehyde. The emission maximum in the one-photon excitation experiment was a broad band with peaks centered at 445 nm and 460 nm (λ_{ex} = 360 nm). For the glyceraldehyde, the 460 nm emission component subsequently became dominant as reaction progressed. For the ribose, in addition to the 460 nm peak, the 445 nm component persisted. With 330 nm excitation wavelength different emission peaks were observed. Glyceraldehyde-glycated collagen hydrogels generated stronger fluorescence signals and were modified at a faster rate compared to ribose and glucose-glycated samples.

The second harmonic generation (SHG) images were effective in demonstrating remodeling of 'fiber-like' structures throughout the collagen hydrogels. For glyceraldehyde, when the glycation time reached forty eight hours, the short 5 to 10 μm structures became modified to long, aggregated threads with length longer than 20 μm.

The potential *in situ* applications of the presented optical methods go beyond evaluating the effects of non-enzymatic cross-linking on tissues and biologically derived scaffolds. They range from diagnosing pathological complication to evaluating food processing strategies and skin products that target glycation.

References

(1) Bailey, A. J.; Paul, R. G.; Knott, L. *Mech. Ageing Dev.* **1998**, *106*, 1-56.

(2) Danilov, N. A.; Ignatieva, N. Y.; Iomdina, E. N.; Semenova, S. A.; Rudenskaya, G. N.; Grokhovskaya, T. E.; Lunin, V. V. *Biochim. Biophys. Acta* **2008**, *1780*, 764-772.

(3) Francis-Sedlak, M. E.; Uriel, S.; Larson, J. C.; PGreisler, H. P.; Venerus, D. C.; Brey, E. M. *Biomaterials* **2009**, *30*, 1851-1856.

(4) Tessier, F.; Monnier, V. M.; Sayre, L. M.; Kornfield, J. A. *Biochem. J.* **2003**, *369*, 705-719.

(5) Girton, T. S.; Oegema, T. R.; Grassl, E. D.; Isenberg, B. C.; Tranquillo, R. T. *ASME* **2000**, *122*, 216-223.

(6) Girton, T. S.; Oegema, T. R.; Tranquillo, R. T. *J. Biomed. Mater. Res.* **1998**, *46*, 87-92.

(7) Reddy, G. K. *Exp. Diab. Res.* **2004**, *5*, 143-153.

(8) Zipfel, W. R.; Williams, R. M.; Christie, R.; Nikitin, A. Y.; Hyman, B. T.; Webb, W. W. *Proc. Natl. Acad. Sci. USA.* **2003**, *100*, 7075-7080.

(9) Yeh, A. T.; Nassif, N.; Zoumi, A.; Tromberg, B. J. *Optics Letters* **2002**, *27*, 2082-2084.

(10) Raub, C. B.; Suresh, V.; Krasieva, T.; Lyubovitsky, J.; Mih, J. D.; Putnam, A. J.; Tormberg, B. J.; Geroge, S. C. *Biophys. J.* **2006**, *92*, 2212-2222.

(11) Brown, E.; McKee, T.; DiTomaso, E.; Pluen, A.; Seed, B.; Boucher, Y. *Nat. Med.* **2003**, *9*, 796-801.

(12) Campagnola, P. J.; Millard, A. C.; Terasaki, M.; Hoppe, P. E.; Malone, C. J.; Mohler, W. A. *Biophys. J.* **2002**, *82*, 493-508.

(13) Guo, Y.; Savage, H. E.; Liu, F.; Schantz, S. P.; Ho, P. P.; Alfano, R. R. *Proc. Natl. Acad. Sci. USA* **1999**, *96*, 10854-10856.

(14) Masters, B. R.; So, P. T. C. *Microsc. Res. Techniq.* **2004**, *63*, 3-11.

(15) Moreaux, L.; Sandre, O.; Charpack, S.; Blanchard-Desce, M.; Mertz, J. *Biophys. J.* **2001**, *80*, 1568-1574.

(16) Schenke-Layland, K.; Riemann, I.; Damour, O.; Stock, U. A.; Konig, K. *Advance Drug Delivery Reviews* **2006**, *58*, 878-896.

(17) Williams, R. M.; Zipfel, W. R.; Webb, W. W. *Biophys. J.* **2005**, *88*, 1377-1386.

(18) Legare, F.; Pfeffer, C.; Olsen, B. R. *Biophys. J.* **2007**, *93*, 1312-1320.

(19) Roth, S.; Freund, I. *J.Chem.Phys.* **1979**, *70*, 1637-1643.

(20) Baynes, J. W.; Monnier, V. M.; Ed. *Alan R. Liss, Inc.: New York,* **1988**.

(21) Anderson, S. S.; Tsilibary, E. C.; Charonis, A. S. *J. Clin. Invest.* **1993**, *92*, 3045-3052.

(22) Tanaka, S.; Avigad, G.; Brodsky, B.; Eikenberry, E. F. *J. Mol. Biol.* **1988**, *203*, 495-505.

(23) Bai, P.; Phua, K.; Hardt, T.; Cernadas, M.; Brodsky, B. *Connect. Tissue Research* **1991**, *28*, 1-12.

(24) Odetti, P.; Aragno, I.; Rolandi, R.; Garibaldi, S.; Valentini, S.; Cosso, L.; Traverso, N.; Cottalasso, D.; Pronzato, M. A.; Marinari, U. M. *Diabetes Metab. Res. Rev.* **2000**, *16*, 74-81.

(25) Liao, H.; Zakhaleva, J.; Chen, W. *Biomaterials* **2009**, *30*, 1689-1696.

(26) Morita, K.; Urabe, K.; Moroi, Y.; Koga, T.; Nagai, R.; Horiuchi, S.; M., F. *Wound Repair Regen.* **2005**, *13*, 93-101.

(27) Kim, B. M.; Eichler, J.; Reiser, K. M.; Rubenchik, A. M.; Da Silva, L. B. *Laser Surg. Med.* **2000**, *27*, 329-335.

Appendices

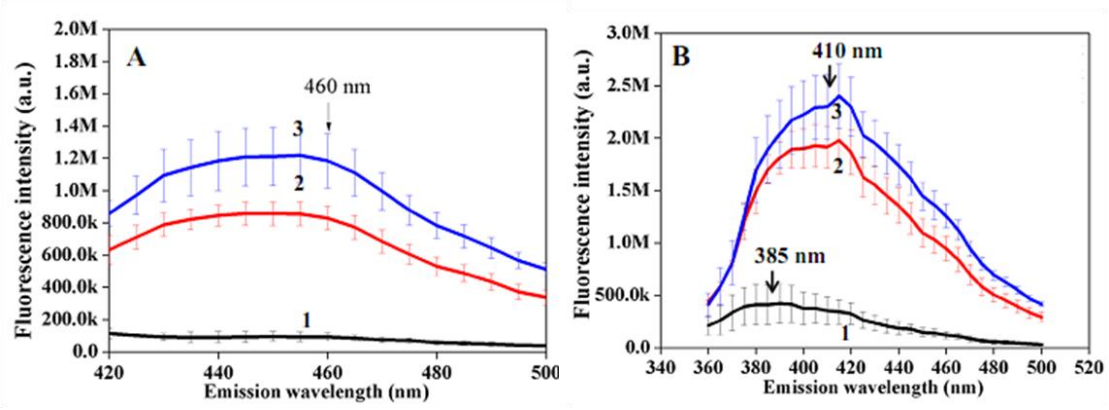

Figure S1. The effect of glycation with 0.1 M ribose on the production of advanced glycation endproducts. (A) Fluorescence emission spectra (λex = 360 nm) of the samples that were incubated with ribose for 0 hr (1), 3 weeks (2), 6 weeks(3). (B) Fluorescence emission spectra (λex = 330 nm) of the samples that were incubated with ribose for 0 hr (1), 3 weeks (2), 6 weeks (3).

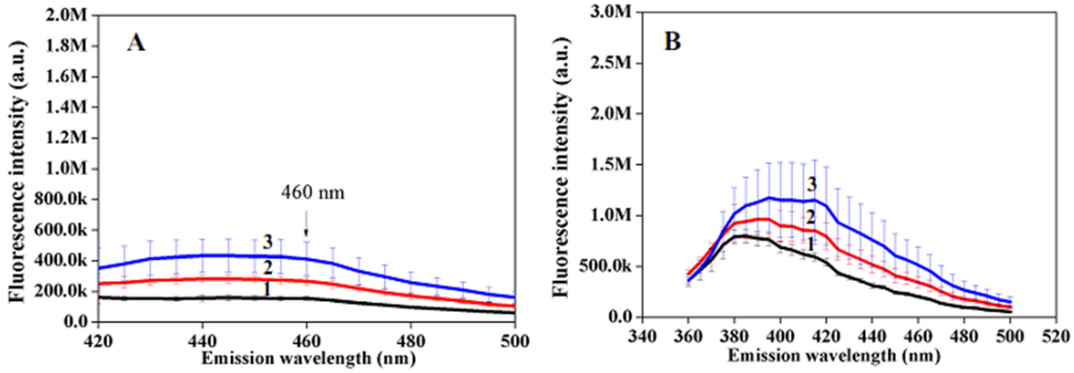

Figure S2. The effect of glycation with 0.1 M glucose on the production of advanced glycation endproducts. (A) Fluorescence emission spectra (λex = 360 nm) of the samples that were incubated with glucose for 0 hr (1), 3 weeks (2), 6 weeks(3). (B) Fluorescence emission spectra (λex = 330 nm) of the samples that were incubated with glucose for 0 hr (1), 3 weeks (2), 6 weeks (3).

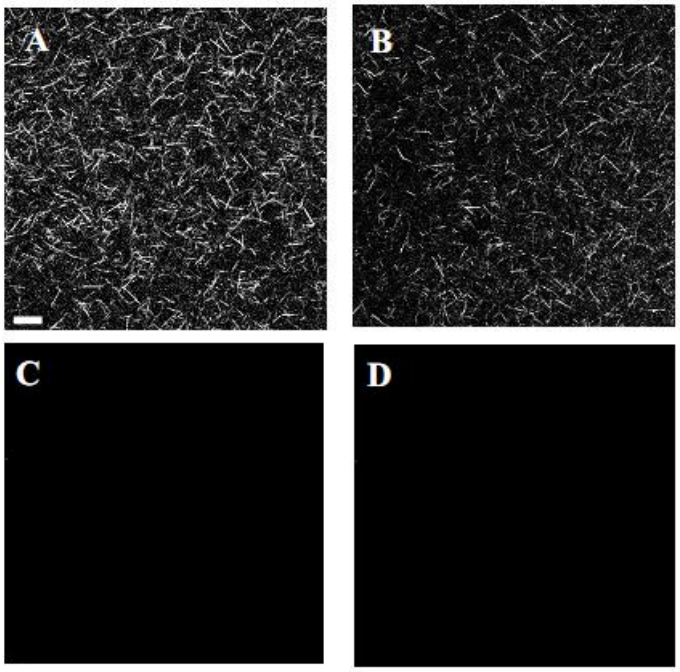

Figure S3. Typical second harmonic generation (SHG) and two photon fluorescence (TPF) images of the 2 g/l collagen hydrogels incubated with 0.1M glycerol. (A) SHG and (C) TPF; The 2 g/l collagen gels that have not been exposed to glycerol are shown for comparison (B) SHG and (D) TPF ; These images were taken in X-Y plane. The scale is 20 µm.

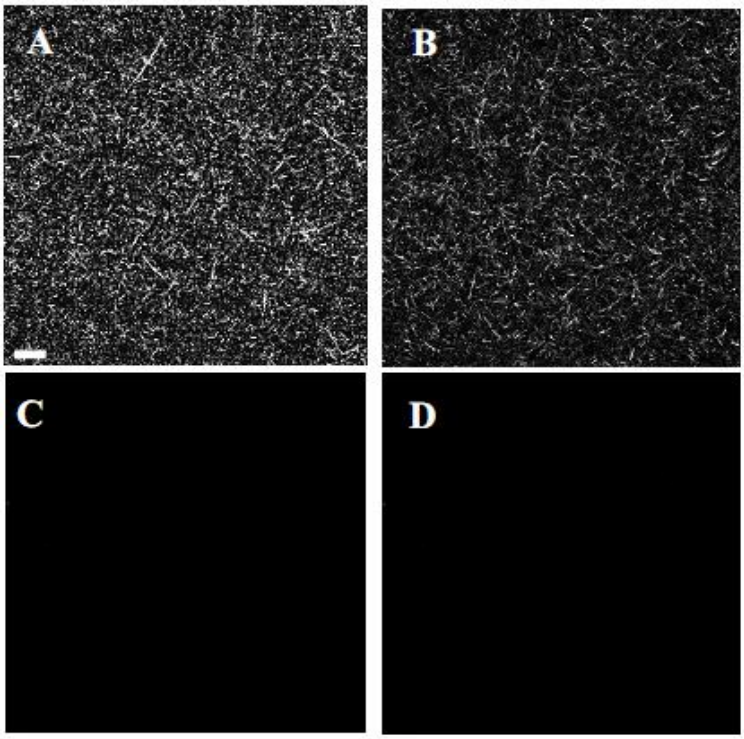

Figure S4. Typical second harmonic generation (SHG) and two photon fluorescence (TPF) images of the 3 g/l collagen hydrogels incubated with 0.1M xylitol. (A) SHG and (C) TPF; 3 g/l collagen gels that have not been exposed to xylitol are shown for comparison (B) SHG and (D) TPF ; These images were taken in X-Y plane. The scale is 20 μm.

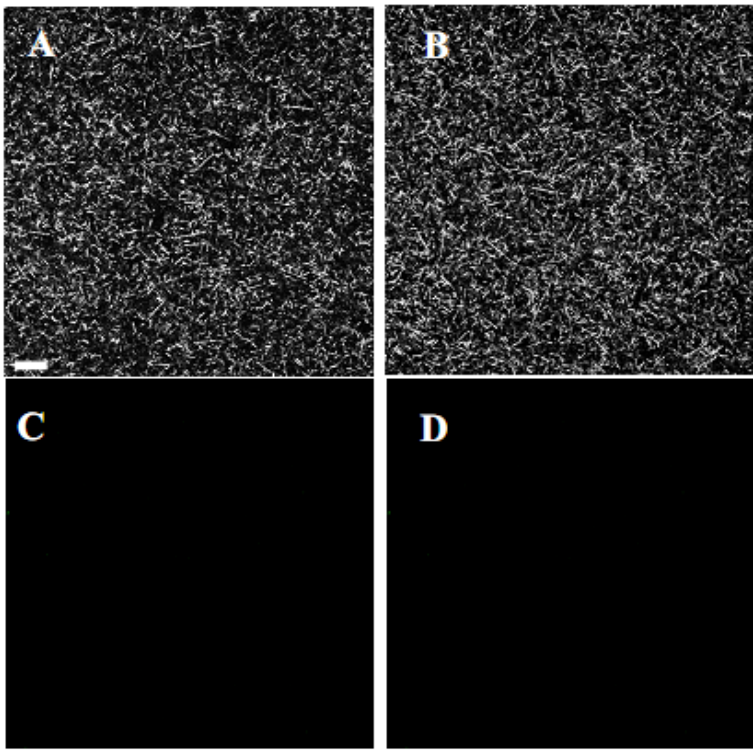

Figure S5. Typical second harmonic generation (SHG) and two photon fluorescence (TPF) images of the 4.68 g/l collagen hydrogels incubated with 0.1M sorbitol. (A) SHG and (C) TPF; The 4.68 g/l collagen gels that have not been exposed to sorbitol are shown for comparison (B) SHG and (D) TPF ; These images were taken in X-Y plane. The scale is 20 µm.

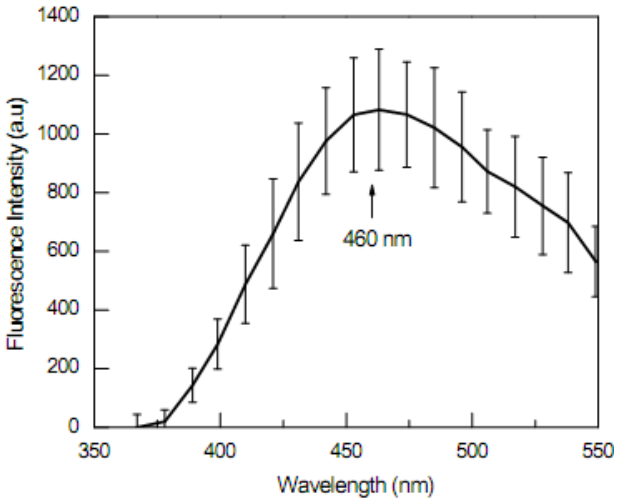

Figure S6. Two photon fluorescence emission spectra (λex = 720 nm) of the collagen hydrogel that was incubated with 0.1M ribose for 6 weeks.

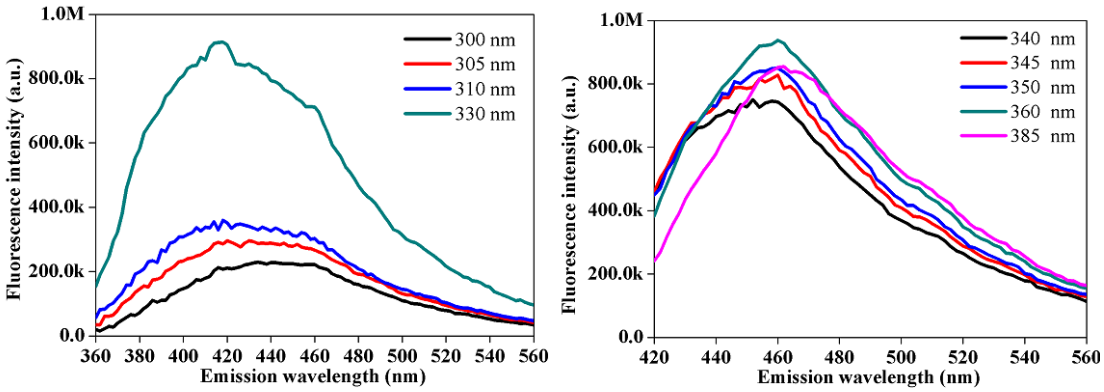

Figure S7. The effect of changing the excitation wavelength on fluorescence of advanced glycation endproducts formed with 0.1 M glyceraldehyde (24-hr product).

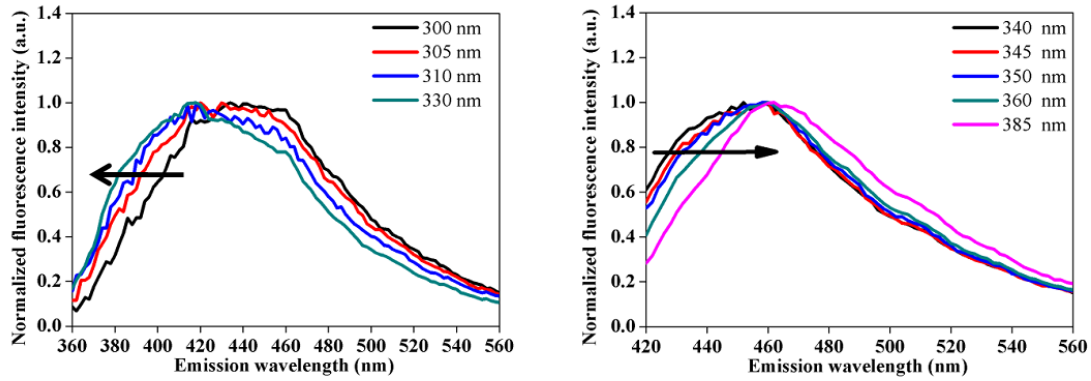

Figure S8. The effect of changing the excitation wavelength on fluorescence of advanced glycation endproducts formed with 0.1 M glyceraldehydes (24-hr product). The data is the same as in Supporting Information Figure 7, however, normalized

CHAPTER 4

CHARACTERIZATION OF CROSS-LINKED COLLAGEN HYDROGELS: The effects of zero-length and non-zero length cross-linking reagents on the optical spectral properties and structures of collagen hydrogels

Abstract

We compared the effects of zero-length cross-linkers 1-Ethyl-3 (3dimethylaminopropyl) carbodiimide (EDC) and non zero-length cross-linkers glycolaldehyde and glyceraldehyde on the optical and structural properties of three dimensional (3D) collagen hydrogels. We evaluated these effects by multiphoton microscopy (MPM) that combined two-photon fluorescence (TPF) and second harmonic generation (SHG) contrasts and transmission electron microscopy (TEM). The collagen hydrogels were incubated separately with the above-mentioned reagents present at the concentration of 0.1 M. The incubation with glycolaldehyde and glyceraldehyde induced strong auto-fluorescence within the gels. We followed the formation of fluorescence with TPF signals *in situ* and in real time as well as characterized the micro- and nano-structures within cross-linked hydrogels by examining SHG and TEM images respectively. As detected in the SHG images, glycolaldehyde and glyceraldehyde modified 5 – 10 μm 'fiber-like' collagen structures to longer, 20 μm and more, aggregated strands while EDC had minimal effect on the microstructure. TEM revealed that glycolaldehyde and glyceraldehyde either completely eliminated collagen's characteristic native fibrillar striations or generated uncharacteristic fibrils with extensions. EDC preserved the native

striation patterns, decreased the fibril diameters and effectively homogenized the fibrils within hydrogels assembled at 1.8 g/l to 4.68 g/l collagen concentrations and 37 °C. Our findings provide a clear understanding on how different cross-linking reagents have very different effects on the collagen hydrogels. This understanding is critical for advancing tissue engineering and wound healing applications.

Introduction

Collagen hydrogels are natural biomaterials known for their biocompatibility and low cytotoxicity. However, for tissue engineering applications, collagen hydrogels need to be more mechanically stable and durable which led to the use of various cross-linking reagents (CLR) to strengthen them. In spite of many CLRs routinely employed to stabilize collagen-based scaffolds, their effect on the optical spectral properties and hierarchical structure of collagen within scaffolds has not been systematically investigated. To understand the effects of CLRs on the optical properties and structures within the collagen-based hydrogels, investigating the correlation between different reagents and collagen hierarchical structure is necessary.

In this study, we compared the effects of zero-length cross-linker 1-Ethyl-3 (3-dimethylaminopropyl) carbodiimide (EDC) and the non zero-length crosslinkers, glyceraldehyde and glycolaldehyde on the optical and structural properties of three-dimensional (3D) collagen hydrogels. The study was set to investigate how these two different types of cross-linking reagents influence collagen hierarchical organization ranging from the micro- to nano-scale. This goal was accomplished by employing

multiphoton microscopy (MPM) to examine the production of two-photon fluorescence (TPF) within collagen microstructure, excitation wavelength dependence of TPF as well as the micro-structure itself via second harmonic generation (SHG) contrast; transmission electron microscopy (TEM) was used to evaluate changes in the collagen nanostructure.

Water soluble carbodiimide EDC is a common zero-length crosslinker, which has been utilized to modify collagen[28-44], gelatin[45-48], fibrinogen[49] and chitosan.[50, 51] Cross-linking of proteins with EDC results in the formation of the amide bonds and since carbodiimide doesn't become a part of the final protein conjugate, this cross-linking reagent was defined as zero-length. Glyceraldehyde and glycolaldehyde are the glycation reagents and produce non-zero length cross-linking.[2, 3, 5-7, 52] The glycation begins with a Maillard reaction during which an amino group of the protein reacts with a carbonyl group of sugar. Upon several subsequent reactions and rearrangements, the sugars become incorporated into the protein conjugate to form adducts collectively known as advanced glycated end-products (AGEs). AGEs from various tissues had been long thought to absorb in the near-UV (320-370 nm) and fluoresce in the 380-460 nm range.[53]

Experimental Section

Collagen Materials Formation and Cross-Linking

Soluble rat-tail type I collagen, 8.58 mg/mL (BD Biosciences) was **dissolved** in 0.02 N acetic acid. The purity of this stock solution was verified with 4%-20% Tris-HCl gels (Bio-Rad) following a standard protocol. The stock solution was diluted with 0.02 N acetic acid to obtain the 2X collagen aliquots. 2X initiation buffers were prepared from

NaCl and phosphate buffer. The concentration of mono-and dibasic phosphate in the buffer at pH 7.4 were calculated with Henderson-Hasselbalch equation. The pH was adjusted drop-wise with 1N NaOH or HCl. Ionic strength was adjusted with NaCl. The initiation buffer had the following components: 6.40 g/L K_2HPO_4; 3.16 g/L KH_2PO_4; 38.55 g/L NaCl (ionic strength =0.6 M). After the pH was adjusted to a desired value, the initiation buffer was filtered with 0.22 μm, 25 mm syringe filter (Fisher) and stored at 4 ℃. Prior to the beginning of material formation, both 2X collagen stock and initiation buffer were de-airated by placing in a 1.5 L desiccator (Fisher) and applying house vacuum for 2 h. Material formation was initiated by mixing 2X collagen aliquot with 2X initiation buffer on ice at 1:1 ratio, verifying the pH to be 7.4 ±0.1, and then incubated at 37 °C. The final collagen concentration of the materials is 2 mg/ml unless noted. For multi-photon microscopy and confocal microscopy measurements collagen materials were prepared in 8-well chambered coverglass (MP Biomedicals). For one-photon experiments collagen materials were prepared in 96-well plates (BD Falcon). In both cases, after 24 h incubation at 37 ℃, the materials were incubated in 0.1 M glyceraldehyde, 0.1M glycolaldehyde, 0.1M EDC and 0.1 M EDC/.025 M NHS solutions (Sigma) at the same temperature for the specified times.

Multiphoton Microscopy (MPM) and Spectroscopy

The inverted multiphoton laser scanning microscope used in this work was the Zeiss LSM 510 NLO Meta microscopy system. It is based on an Axiovert 200M inverted microscope equipped with standard illumination systems for transmitted light and epi-

fluorescence detection. It was also equipped with an NLO interface for a femtosecond titanium: sapphire laser excitation source (Chameleon-Ultra, Coherent, Incorporated, Santa Clara, CA) for multiphoton excitation. The Chameleon laser provided femtosecond pulses at a repetition rate of about 80 MHz, with the center frequency tunable from 690 to 1040 nm. A long working distance objective (Zeiss, 40X water, N.A. 0.8) was used to acquire images shown in this work. The two-photon signals from the samples were epi-collected and discriminated by the short pass 650 nm dichroic beamsplitter. The SHG and TPF images were collected using the META detection module with the signals sampled in a 375 – 415 nm and 470–500 nm detection range respectively (λ_{ex} = 800 nm). Each image presented in this work is 12 bit, 512 x 512 pixels representing 225 μm x 225 μm field of view. All the experiments were repeated on separate days, using up to 8 independent samples on each day (about 5 fields of view per sample). The upright multiphoton laser-scanning microscope used to acquire spectra was the modified Zeiss Axioexaminer.Z1. It was equipped with a femtosecond titanium:sapphire laser excitation source (Mai-Tai HP, Spectra Physics, Santa Clara, CA) that provided femtosecond pulses at a repetition rate of about 80 MHz, with the center frequency tunable from 690 to 1040 nm. A long working distance objective (Zeiss, 10x water, N.A. 0.3) was used to acquire spectra. The two-photon signals generated by the samples were epi-collected, discriminated by a long pass 665 nm single-edge dichroic beamsplitter and filtered through a 720 nm short pass filter. Spectra were obtained with a Acton SP2300 spectrograph equipped with a 68x68 mm 300 grooves/mm ruled grating blazed at 500 nm and a Pixis1024B CCD camera (Princeton Instruments, Trenton, New Jersey). The

spectrograph and camera settings were PC-controlled through WinSpec/32 v.2.5K software. The CCD temperature was maintained at –75 ℃ for all the experiments to ensure low dark noise. The entrance slit of the spectrograph was set to a width of 0.5 mm. The typical spectral acquisition time was 4 s. The multi-photon spectra were corrected for the non-linearity of the laser excitation power, quantum efficiency of the CCD camera and dark noise background.

Transmission Electron Microscopy (TEM) Imaging

After 24 h of incubation, entire portion of an incubated sample was retrieved. A drop of sample containing cross-linked material was added on a formvar film coated with a layer of carbon supported on a 300-mesh copper grid (Carbon type A, Ted Pella, Inc.). Excess liquid was drained with filter paper after 10 min. A drop of double de-ionized water was then added to the sample on the grid for 1 s to remove the excess NaCl, and was drained slowly with filter paper. A drop of same-day-prepared 10 g/L sodium phosphotungstate (Sigma), pH 7.4 was added to the sample on the grid. After 5 minutes of staining, the grid was drained slowly with filter paper. A drop of double de-ionized water was then added to the sample on the grid for 1 s to remove the excess stain and then air-dried for about 15 minutes. The grids were examined immediately in a Tecnail 12 electron microscope operated at 120 kV.

Results and Discussion

The reaction between carbodiimide and proteins follows the mechanism expressed in Figure 1A. The carboxyl groups of aspartic or glutamic acid side chains in collagen react with this compound to form an activated O-acylurea. This intermediate can then react with a neighboring amino group of lysine side chain of collagen to form an amide bond while releasing urea derivative of the reagent.[54] However, since O-acylurea is susceptible to hydrolysis in the aqueous physiological solutions, the insufficient stability of this

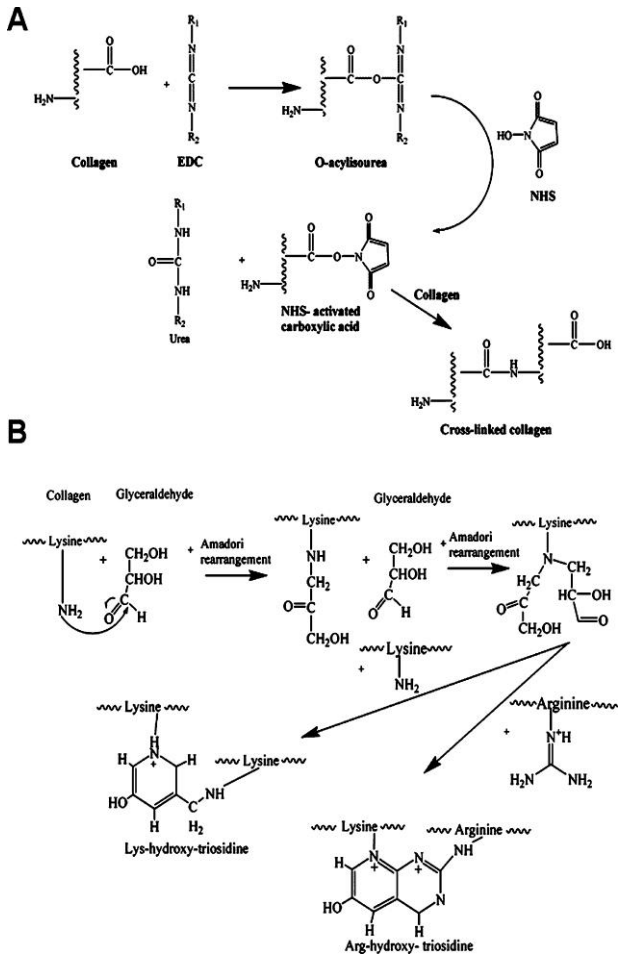

Figure 1. Schematics for the cross-linking reaction of collagen with (A) 1-ethyl-3 (3dimethylaminopropyl)carbodiimide (EDC) and (B) glyceraldehyde.

intermediate decreases the overall efficiency of the cross-linking reaction. The addition of N-hydroxysuccinimide (NHS), which reacts through O-acylurea to form a more hydrolysis resistant compared to O-acylurea amine-reactive ester, increases the yield of carbodiimide cross-linking.[55]

On the other hand, the highly reactive sugars glyceraldehyde and glycoaldehyde cross-link proteins through a Millard reaction. Figure 1B shows a possible collagen cross-linking mechanism with the glyceraldehyde that involves two glyceraldehyde molecules as proposed in Ref. [56]. In that work, the major fluorescent products detected from the incubation of glyceraldehyde with N^{α}acetyl-L-lysine and N^{α}-acetyl-L-arginine were lys-hydroxytriosidine (LHT), which is the lysine-lysine cross-link and arg-hydroxy-triosidine (AHT), which is the arginine-lysine cross-link. LHT and AHT structures shown in Figure 1B were also detected in human and porcine corneas treated with glyceraldehyde. Supplementary Information Figure S1 expresses the possible mechanism for collagen cross-linking by glycoaldehyde. Similar to modification with the glyceraldehyde, it involves a Schiff base adduct. The subsequent Amadori rearrangement generates a new aldehyde function in a form of an aldoamine leading to pirazine formation and covalent cross-linking of collagen.[57, 58] The fluorescent structures, however, have not been unequivocally identified.

In situ Microscopic Characterization of Cross-Linked Collagen Hydrogels: Two Photon Fluorescence (TPF) and Second Harmonic Generation (SHG)

To examine the effect of cross-linking on microstructure of collagen hydrogels, we employed multiphoton microscopy. TPF signals are utilized to monitor the extent of cross-linking and SHG signals are used to identify the microstructure of collagen fibers.

Generally we find that it is useful to initially obtain TPF spectra of our modified hydrogels prior to visualizing fluorescent structures with the multiphoton microscope. This approach aids in setting the appropriate filters to collect the TPF signals that can be used to generate TPF images at a specific excitation wavelength. The TPF spectra acquired on the glycated samples (Figure 2) illustrated that 800 nm excitation wavelength generated glycation induced TPF centered at approximately 485 nm and that the 470–500 nm range of emission wavelength set for the detection of TPF signals would be suitable.

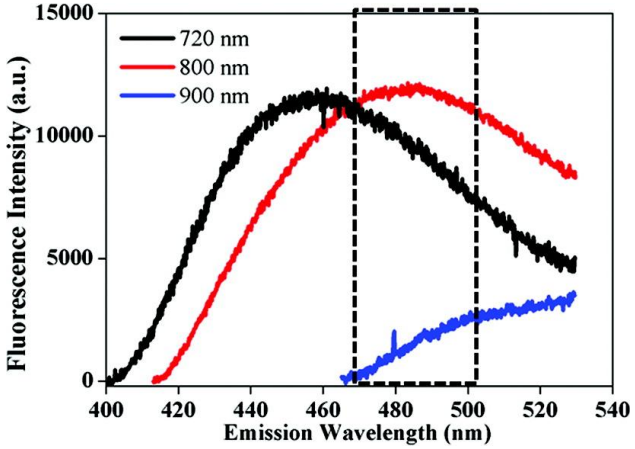

Figure 2. The two-photon fluorescence (TPF) spectrum of glyceraldehyde treated collagen hydrogels excited with different wavelengths. The rectangle indicates the range of emission wavelength that was set for the detection of TPF signals in this study.

As seen in Figure 2, the TPF spectrum undergoes a bathochromic (red) shift when the excitation wavelength is changed from 720 nm to 800 nm while no appreciable fluorescence can be excited with 900 nm light. This wavelength dependent shift of the multi-photon fluorescence spectra agrees with a trend previously reported by our group[59] for the one photon fluorescence spectra of the fluorophores generated upon glycating collagen hydrogels.

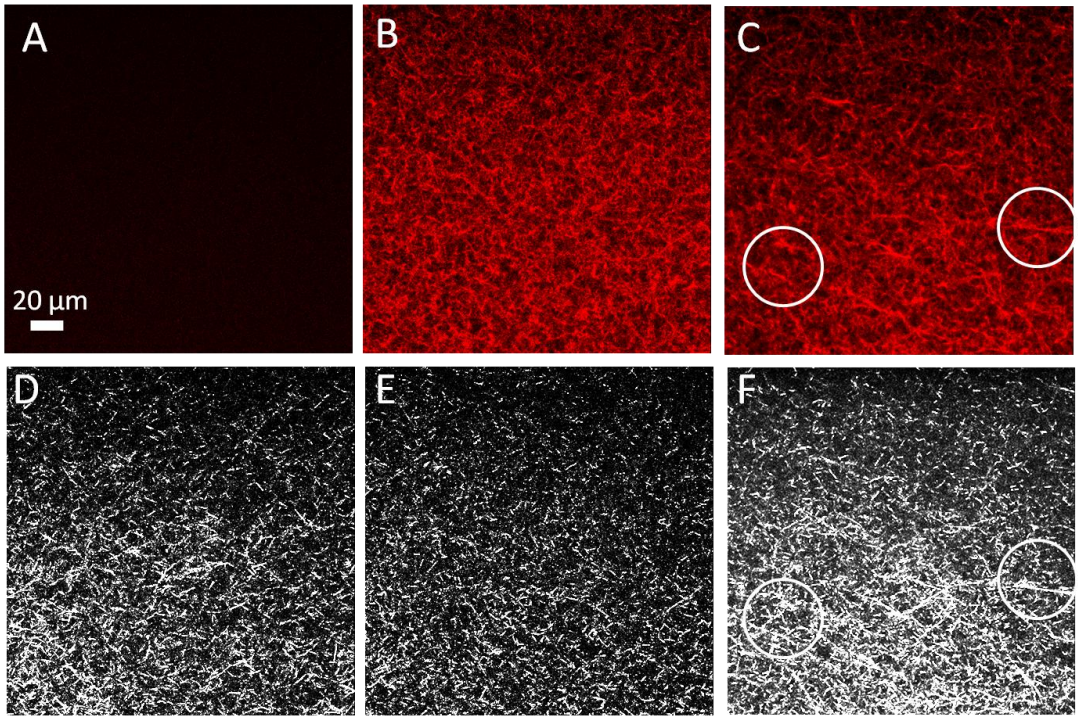

Figure 3. Typical two photon fluorescence (TPF) and second harmonic generation (SHG) images of a sample incubated with 100 mM glyceraldehyde for a different amount of time. The images are taken in XY plane. TPF, (A) 0 hours, (B) 48 hours and (C) 4 weeks; SHG, (D) 0 hours, (E) 48 hours and (F) 4 weeks. Formation of the long, aggregated strands with length longer than 20 µm can be seen in the TPF and SHG images within the areas circled with the white outline. The collagen concentration of the sample is 2.0 mg/mL and the incubation temperature is 37 °C. The scale bar is 20 µm. The filters for SHG and TPF are 375–415 nm and 470–500 nm respectively. The excitation wavelength is 800 nm.

To follow the extent of cross-linking with glycation reagents, we monitored the fluorescence intensity throughout the course of glycation via the excitation with 800 nm light. The evolution of two-photon fluorescence was detected in X-Y plain through a 470—500 nm filter as shown in Figure 2. No fluorescence was detected before the addition of sugars (Figure 3A). When the incubation reached 48 hours, elongated and very strongly fluorescing structures were present (Figure 3B). The long fluorescent structures would get even longer after 1 month of incubation (Figure 3C). It is notable that TPF of the glyceraldehyde-induced cross-links has soft appearance without clear edges and extends into the background. The spectrally and structurally similar development of fluorescence was observed when the samples were treated with glycolaldehyde instead of glyceraldehydes. As judged from the kinetic profiles obtained by detecting one-photon fluorescence intensity, the reaction between the glycolaldehyde and collagen was approximately two times faster compared to the one between glyceraldehyde and collagen.

To identify if the original fiber structure within collagen hydrogels was modified due to glycation, we acquired the second harmonic generation (SHG) images at the same time as TPF images using the same 800 nm excitation wavelengths. As seen in SHG images, glycation reagents clearly modified the original microstructure of fibers in collagen hydrogels. The short fibers with length approximately 5 – 10 μm were observed within hydrogels prior to glycation (Figure 3D). After 48 hours of glycation, few short fibers were modified to become longer fibers with length approximately 20 μm (Figure 3E). The formation of these longer fibers was even more evident when the hydrogels were

allowed to react with glycation reagents for 1 month (Figure 3F). Interestingly, the SHG generated by collagen fibers did not simply co-localize with the induced TPF signals. In the TPF images, there were some fluorescent structures, which did not have the corresponding structure in the SHG image. These newly formed fluorescent structures are possibly the linkages between adjacent fibrils, which do not contribute to the SHG generating features.

Upon detecting with multiphoton microscopy the significant changes to the microstructure within collagen hydrogels induced by glycation reagents, we proceeded to examine the effects of EDC and EDC/NHS on the microstructure of collagen hydrogels as well.

Because EDC or EDC/NHS does not generate any fluorescence when they react with collagen, only the SHG signal was detected. The SHG images clearly showed that a modification of collagen hydrogels with EDC did not cause a significant alteration to the microstructure (Figure 4B). The microstructure of the EDC-modified samples appeared similar to the controls consisting of samples without the addition of any EDC (Figure 4A). Upon addition of NHS, the microstructure of fibers remained very similar to those cross-linked with EDC only (Figure 4C).

The application of SHG and TPF signals can be successfully utilized to characterize the glycation effect. These two signals show that sugars significantly modify both: the spectral optical properties and the microscopic architecture within collagen hydrogels. On

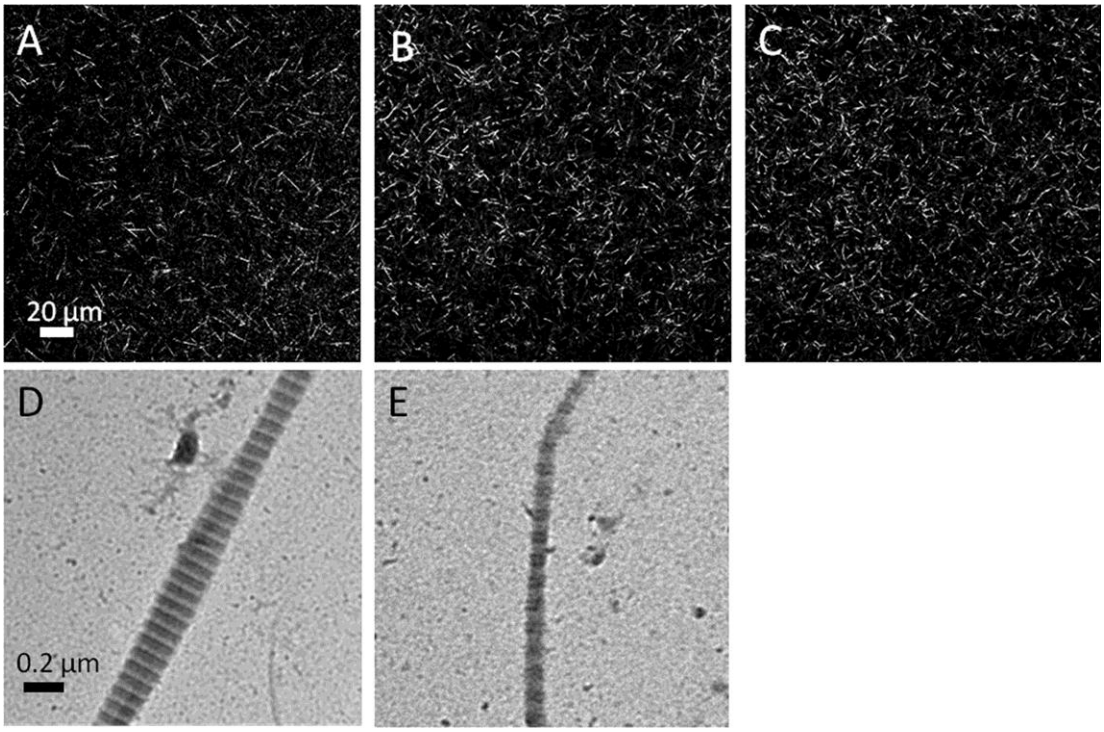

Figure 4. Typical second harmonic generation (SHG) and transmission electron microscopy (TEM) images of a sample incubated with 100 mM EDC or 100 mM EDC /25mM NHS. The images are taken in XY plane. SHG (A) collagen hydrogels only, (B) collagen hydrogels treated with EDC and (C) collagen hydrogels treated with EDC/NHS; TEM, (D) collagen hydrogels only, (E) collagen hydrogels treated with EDC. The collagen concentration of the sample is 2.0 mg/mL and the incubation temperature is 37 °C. The scale bar is 20 μm for SHG and 0.2 μm for TEM.

the other hand, EDC has no effect on the collagen structures at the microscopic level of organization and does not alter the spectral optical properties of collagen hydrogels.

We believe that the significant differences in which sugars and EDC affect the microstructure within collagen hydrogels can be attributed to the differences in their cross-linking mechanisms. The glycation occurs both intra- and inter-molecularly, resulting in sugars becoming integral parts of the cross-linked structures collectively known as advanced glycation endproducts (AGEs). The newly created AGE bridges perhaps then exert certain forces that aggregate the nearby fibrils into a longer 'fiber-like'

feature. It is interesting that although the fiber grows in length, the diameter of the fiber remains roughly the same. Our observation would imply that the previously detected with medium angle X-rays[21] highly directional lateral expansion of the collagen unit cell at the molecular level remarkably extends to the microscopic structures within our hydrogels as well. In this earlier X-ray work, specific glycation induced cross-links were thought to be primarily responsible for the expansion of the unit cell due to pushing the collagen molecules apart and away from the cross-link sites, allowing water to enter the structure in response.

On the other hand, EDC induces only the formation of amide bonds within and between collagen molecules without introducing any additional chemical moieties. Even if these newly established amide bonds could cause expansion of the collagen unit cell at the molecular level, it does not appear to extend to the microscopic scale to a visually detectable degree. As a result, the microstructure within EDC cross-linked hydrogels as determined from visualizing SHG signals is maintained.

The near-infrared wavelength of light utilized in our two-photon fluorescence (TPF) and second harmonic generation (SHG) imaging is non-destructive to collagen 3D hydrogels. A combination of TPF and SHG imaging can provide high-contrast, three-dimensional micro-structural details regarding the effects of cross-linking within these soft biomaterials. At this time, there are not many studies in the literature that had relied on the optical properties of the collagen hydrogels to obtain micro-structural details. Our non-destructive observations on the effect of glycating collagen within hydrogels clearly

show the significant changes to the microstructure introduced by the glycation.[59] The other optical studies are, however, less clear concerning the effects of modifying the structures within collagen-based scaffolds with the glycation reagents. For example, the 40% decrease in the SHG signal when the human tendon was glycated[27] was previously observed and could be interpreted as some change of structure. A reflectance confocal microscopy study showed the microstructure remaining unchanged in the collagen gels glycated with glucose-6-phosphate.[3] EDC not having any effect on the microstructure within collagen hydrogels is well shown in our SHG images presented in this work while no relevant previous optical imaging characterization was located.

Characterization of Cross-Linked Collagen Hydrogels with Transmission Electron Microscopy

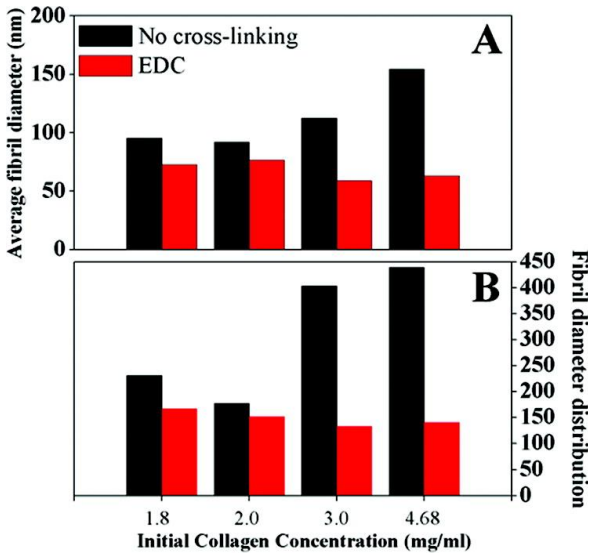

Figure 5. The effect of 100mM EDC on the average collagen fibril diameters and fibril diameter distribution. (A) Average fibril diameter. (B) Fibril diameter distributions.

We used transmission electron microscopy to determine if in addition to their effect on the microstructure, the cross-linking reagents affect the nanostructure of collagen fibrils within hydrogels as well. The TEM images show that EDC didn't alter much of the nanostructure of collagen fibrils. The collagen fibrils treated with EDC (Figure 4E) maintained the native-like

striation with D-periods ranged from 62 to 67 nm (Figure 4D). However, based on the histograms constructed from TEM image measurements we detected a decrease in the fibril diameters (Figure 5A) and a decrease in the fibril diameter distribution (Figure 5B) within EDC-treated collagen hydrogels. The apparent homogenization in the fibrillar diameters upon EDC-treating hydrogels assembled from different initial collagen concentrations was observed. The previous investigations are less clear concernng the effects of modifying the structures within protein-based scaffolds with EDC. For example, when electrospun fibrinogen scaffolds were treated with EDC, scanning electron microscopy studies showed no change in morphology and pore size compared to untreated controls.[49] Another study which used transmission electron microscopy[37] showed that EDC treatment of amniotic membranes causes aggregation of collagen fibers at certain EDC concentrations while leaving the rest of the structure unchanged.

As opposed to the modification done by EDC, the TEM images show that the glycation reagents significantly altered the nanostructures of collagen fibrils. When collagen hydrogels were treated with either glyceraldehyde or glycolaldehyde, collagen fibrils with native striation patterns (Figure 6A) could no longer be observed. Instead, the only nanostructures we were able to detect in the glycated samples were the non-striated filaments (Figure 6B) and uncharacteristic fibrils with thin fibrous extensions emanating from them (Figure 6C).

Our previous work demonstrated that the non-striated filaments can occur within 3D collagen hydrogels assembled at the initial collagen concentrations and incubation

temperatures used in this work.[60] In filaments, collagen molecules are not assembled in staggered alignment and the distance between them might be too close for the phosphotungstate stain to enter; hence, filaments do not exhibit banding patterns. We believe that the disruption of the banding patterns is exuberated by glycation. We could

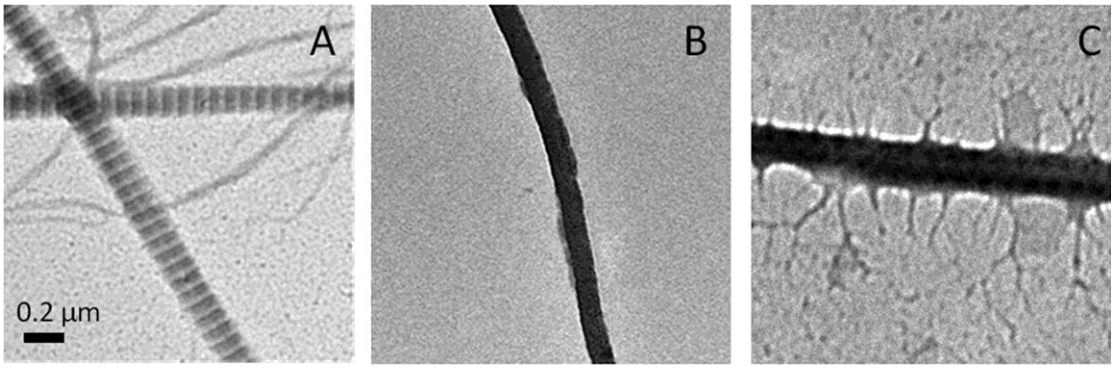

Figure 6. Transmission electron micrographs of negatively stained collagen fibrils cross-linked with 100 mM glyceraldehyde. (A) Typical collagen fibril with native banding observed in non-treated control samples. (B) Typical non-striated filaments observed in the glyceraldehyde treated samples and (C) Collagen uncharacteristic fibrils observed in the glyceraldehyde treated samples. The scale bar is 0.2 μm.

not locate any prior TEM record of uncharacteristic fibrils with fibrous extensions emanating from them that we observed in our glycated hydrogels. We speculate that the thin fibrous extensions are the bridging cross-links that held together larger fibrillar structures disrupted by smearing the samples on the grids for the TEM visualization. These findings are in good agreement with most studies that recognized the ultrastructural changes within various glycated collagen-based tissues and materials. Scanning force microscopy work revealed structural alterations in the radii and cleft depth of tendons incubated with 0.5 M glucose for two weeks and detected connections between the fibrils.[24] The medium-angle X-ray diffraction studies[21] detected changes in collagen molecular packing within tendons exposed to reducing sugars, when rat tail

tendons were incubated in 0.2 M ribose. The electron micrographs of tendons' cross-sections showed an increased fibril packing density, fusion of fibrils and irregular fibril diameters.[23] Scanning electron microscopy study showed an apparent increase in the number of large pores (diameters > 12.5 nm) in the bovine kidney tubular basement membrane treated with glucose.[21]

In short, our TEM images indicate that two sugars (glyceraldehyde and glycolaldehyde) acted on collagen hydrogels to either completely remove the striation patterns within fibrils or to transform the remaining fibrils to develop uncharacteristic extension. On the other hand, treatment with EDC reduced the fibril diameters, however, maintained the native fibrillar striation patterns. Based on the cross-linking mechanism of sugars in which the sugar molecules incorporate into the final protein-conjugated product, this intra- and inter-molecular incorporation likely to disrupt the native staggered alignment of collagen molecules within collagen fibrils thus altering the striation patterns. On the other hand, because EDC doesn't become part of the final cross-linking products, the striation pattern is preserved.

Conclusion

This study investigated the effects of zero-length crosslinker EDC and non zero-length crosslinker glycolaldehyde and glyceraldehyde on the optical and structural properties of 3D collagen hydrogels. As was seen in our studies, these two different groups of cross-linking reagents imposed very different effects on the collagen hydrogels. As detected in the SHG images, EDC didn't alter the short fiber microstructure while both sugars

modified the short collagen fibers to longer ones. The TEM images illustrated that EDC reduced the fibrillar diameter although preserved the fibrillar striation patterns while both sugars either completely eliminate the striation patterns within collagen fibrils or caused formation of very uncharacteristic fibrils with hanging fibrous nanostructures. Overall, this study is a comprehensive understanding of the effects of different kinds of cross-linking reagents. The results will potentially benefit tissue engineering, wound healing and food research. Moreover, since the physical interaction between cells and extracellular matrix are known to affect the cell fate, our findings provide a way to easily modify the structure of the matrix either in nano or micro-scale to benefit the design of the proper environment for target cells.

References

(1) Cao, H.; Xu, S. *J. Mater. Sci.: Mater. Med*. **2008**, 19, 567-575.

(2) Davidenko, N.; Campbell, J. J.; Thian, E. S.; Watson, C. *J. Acta Biomater.* **2010**, 6, 3857-3968.

(3) Duan, X.; Sheardonw, H. *J. Biomed. Mater. Res. Part A* **2005**, 75A, 510-518.

(4) Duan, X.; Sheardonw, H. *Biomaterials* **2006**, 27, 4608-4617.

(5) Gong, Z.; Xiong, H.; Long, X.; Wei, L.; Li, J.; Wu, Y.; Lin, Z. *Biomed. Mater.* **2010**, 5.

(6) Jorege-Herrero, E.; Fonseca, C.; Barge, A. P.; Turnay, J.; Olmo, N.; Fernandez, P.; Lizarbe, M. A.; Paez, J. M. G. *Artif. Organs* **2010**, 34, 168-176.

(7) Keogh, M. B.; O'Brien, F. J.; Daly, J. S. *Acta Biomater.* **2010**, 6, 4305-4313.

(8) Lai, E. S.; Anderson, C. M.; Fuller, G. G. *Acta Biomater.* **2011**, 7, 2448-2456.

(9) Liu, Y.; Gan, L.; Carlsson, D. J.; Fagerbolm, P.; Lagali, N.; Watsky, M. A.; Munger, R.; Hodge, W. G.; Priest, D.; Griffith, M. *Invest. Ophth. Vis. Sci.* **2006**, 47, 1869-1875.

(10) Ma, D.; Lai, J.; Cheng, H.; Tsai, C.; Yeh, L. *Biomaterials* **2010**, 31, 6647-6658.

(11) Madhavan, K.; Belchenko, D.; Motta, A.; Tan, W. *Acta Biomater.* **2010**, 6, 1413-1422.

(12) McLaughlin, C. R.; Acosta, M. C.; Luna, C.; Liu, W.; Belmonte, C.; MGriffith, M.; Gallar, *J. Biomaterials* **2010**, 31, 2770-2778.

(13) Nagai, N.; Mori, K.; Munekata, M. *J. Biomat. Appl.* **2008**, 23, 275-287.

(14) Tan, G.; Dinnes, D. L. M.; Cooper-White, J. J. *Acta Biomater.* **2011**, 7, 2804-2816.

(15) Yahyouche, A.; Zhidao, X.; Czernuszka, J. T.; Clover, A. J. P. *Acta Biomater.* **2011**, 7, 278-286.

(16) Yao, L.; Biliar, K. L.; Winderbank, A. J.; Pandit, A. *Tissue Eng. PT. C-Meth.* **2010**, 16, 1585-1596.

(17) Yunoki, S.; Mori, K.; Suzuki, T.; Nagai, N.; Munekata, M. *J. Mater. Sci.: Mater. Med.* **2007**, 18, 1369-1375.

(18) Kuijpers, A. J.; Engers, G. H. M.; Feijen, J.; De Smedt, S. C.; Meyvis, T. K. L.; Demeester, J.; Krijgsveld, J.; Zaat, S. A. J.; Dankert, J. *Macromolecules* **1999**, 32, 3325-3333.

(19) Lai, J.; Li, Y. *Mater. Sci. Eng.* **2010**, 30, 677-685.

(20) Lai, J.; Li, Y. *J. Biomat. Sci*. **2011**, 22, 277-295.

(21) Ratanavaraporn, J.; Rangkupan, R.; Jeeratawatchai, H.; Kanokpanaont, S.; Damrongsakkul, S. *Int. J. Bio. Macromol.* **2010**, 47, 431-438.

(22) Sell, S. A.; Francis, M. P.; Garg, K.; McClure, M. J.; Simpson, D. G.; Bowlin, G. L. *Biomed. Mater.* **2008**, 3.

(23) Custodio, C. A.; Alves, C. M.; R.L.;, R.; Mano, J. F. J. *Tissue Eng. Regen. M.* **2010**, 4, 316-323.

(24) Xu, H.; Yan, Y.; Li, S. *Biomaterials* **2011**, 32, 4506-4516.

(25) Danilov, N. A.; Ignatieva, N. Y.; Iomdina, E. N.; Semenova, S. A.; Rudenskaya, G. N.; Grokhovskaya, T. E.; Lunin, V. V. *Biochim. Biophys. Acta* **2008**, 1780, 764-772.

(26) Francis-Sedlak, M. E.; Uriel, S.; Larson, J. C.; PGreisler, H. P.; Venerus, D. C.; Brey, E. M. *Biomaterials* **2009**, 30, 1851-1856.

(27) Girton, T. S.; Oegema, T. R.; Grassl, E. D.; Isenberg, B. C.; Tranquillo, R. T. ASME **2000**, 122, 216-223.

(28) Girton, T. S.; Oegema, T. R.; Tranquillo, R. T. J. *Biomed. Mater. Res.* **1998**, 46, 87-92.

(29) Reddy, G. K. Exp. *Diab. Res*. **2004**, 5, 143-153.

(30) Wollensak, G.; Iomdina, E. *Acta Ophthalmol.* **2008**, 86, 887-893.

(31) Fujimori, E. Eur. *J. Biochem*. **1985**, 152, 299-306

(32) Wise, D. *Biomaterials And Bioengineering Handbook*, 2000.

(33) Staros, J.; Write, R.; Swingle, D. *Anal. Biochem.* **1986**, 156, 220-222.

(34) Tessier, F. J.; Monnier, V. M.; Sayre, L. M.; Kornfied, J. A. *Biochem. J.* **2003**, 369, 705-719.

(35) Glomb, M.; Monnier, V. M. *J. Biol. Chem.* **1995**, 270, 10017-10026.

(36) Acharya, A. S.; Manning, J. M. *Proc. Natl. Acad. Sci. USA* **1983**, 80, 3590-3594.

(37) Hwang, Y. J.; Granelli, J.; Lyubovitsky, J. G. *Anal. Chem.* **2011**, 83, 200-206.

(38) Anderson, S. S.; Tsilibary, E. C.; Charonis, A. S. *J. Clin. Invest*. **1993**, 92, 3045-3052.

(39) Kim, B. M.; Eichler, J.; Reiser, K. M.; Rubenchik, A. M.; Da Silva, L. B. *Laser Surg. Med*. **2000**, 27, 329-335.

(40) Hwang, Y. J.; Lyubovitsky, J. G. *RSC Anal. Methods* **2011**, 3 529-536.

(41) Odetti, P.; Aragno, I.; Rolandi, R.; Garibaldi, S.; Valentini, S.; Cosso, L.; Traverso, N.; Cottalasso, D.; Pronzato, M. A.; Marinari, U. M. *Diabetes Metab. Res. Rev.* **2000**, 16, 74-81.

Appendices

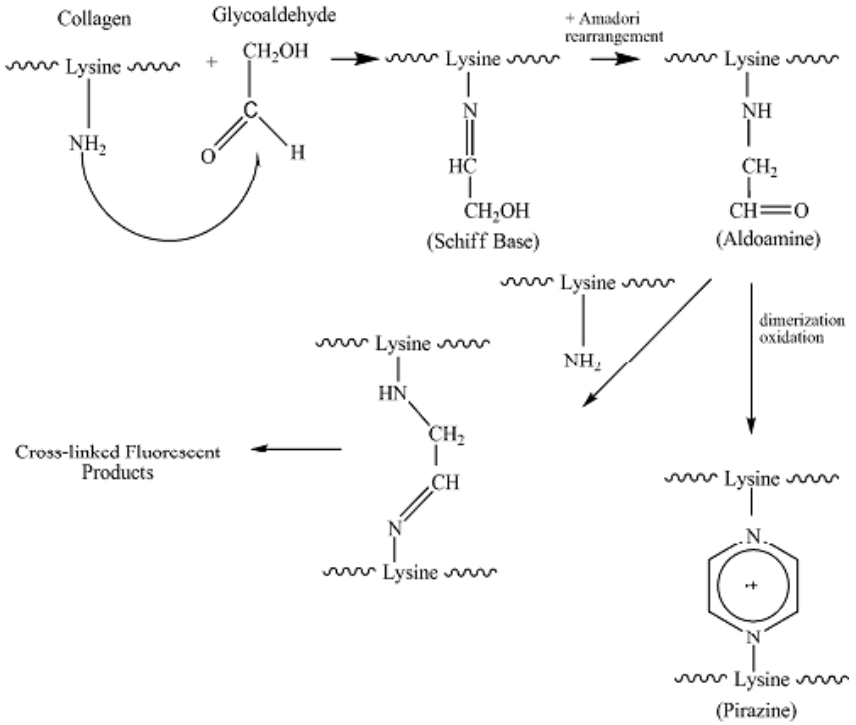

Figure S1. Schematics for the cross-linking reaction of collagen with glycolaldehyde

CHAPTER 5

CHARACTERIZATION OF CROSS-LINKED COLLAGEN HYDROGELS: The structural analysis of cross-linked three-dimensional collagen hydrogels by Raman microspectroscopy

Abstract

The molecular effects of 1-Ethyl-3-(3-dimethylaminopropyl) carbodiimide (EDC), EDC/N-hydroxysuccinimide (NHS) and glyceraldehyde cross-linking reagents on the three-dimensional (3D) collagen hydrogels were evaluated by Raman microspectroscopy. The increased intensity of the 814 cm^{-1} and 936 cm^{-1} Raman bands corresponding to the C-C stretch of a protein backbone indicated the change in packing of collagen molecules upon glyceraldehyde treatment. A shift in the amide III bands from 1241 cm^{-1} and 1268 cm^{-1} in controls to 1247 cm^{-1} and 1283 cm^{-1} in glyceraldehyde-treated gels indicated changes to the alignment of the collagen molecules, fibrils/fibers and/or changes to the secondary structure. The increased intensity of the 1450 cm^{-1} band and the appearance of a strong peak at 1468 cm^{-1} reflected a change in the motion of lysine/arginine CH_2 groups due to the cross-linking reaction between the glyceraldehyde and lysine/arginine resides. For the EDC-treated collagen hydrogels, the increased intensity of 823 cm^{-1} peak corresponding to the C-C stretch of the protein backbone indicated that EDC also changed the packing of collagen molecules. The 23% decrease in the ratio of 1238 cm^{-1} to 1271 cm^{-1} amide III band intensities in the EDC-modified samples compared to the controls indicated changes to the alignment of the collagen molecules/fibrils and/or the

secondary structure. The 30% increase in the ratio of the amide III band (1238 cm^{-1}) area to the C-H twisting band (1316 cm^{-1}) area and a 85% increase in intensity of the C-H bending (1442 cm^{-1}) mode compared to the control reflected a change in length or environment of lysine and/or arginine residues. The addition of NHS did not induce additional Raman shifts compared to the effect of EDC alone with the exception of a 1416 cm^{-1} band corresponding to COO^- stretch becoming more prominent. Overall, the Raman spectra suggest that EDC affects the collagen states within 3D hydrogels to a lesser extent compared with glyceraldehyde.

Introduction

Three dimensional (3D) collagen hydrogels are often cross-linked to render them durable for the tissue-engineering applications. Two-photon fluorescence, second harmonic generation imaging and transmission electron microscopy provided initial understanding regarding the effects of two types of cross-linking reagents (CLRs) on the optical properties, micro- and nano-structure of these natural biomaterials.[1-3] One type of CLR was zero-length cross-linker carbodiimide (EDC) or EDC with an addition of N-hydroxysuccinimide (NHS). The other type of CLR was non zero-length cross-linker glyceraldehyde. In spite of this early successful development, many fundamental molecular insights regarding modifications of the collagen structures upon cross-linking 3D hydrogels remained unanswered.

Raman spectroscopy, used widely to examine variety of complex biomolecules and biological tissues,[4-13] is a powerful tool for studying molecular properties based on the

vibrational changes.[14-16] When compared to other techniques, which are used to study molecules, Raman spectroscopy has the advantages of being label-free, non-destructive and capable of providing real-time structural as well as molecular analysis.[17] It can furnish information to potentially determine the crystallinity, conformation, density, monomer content, degradation, stress-strain distribution and other properties relevant to supramolecular order of structures composed from collagen proteins. In the present study, we apply Raman microspectroscopy to study the molecular vibrations of the structural repeat units induced within the 3D collagen hydrogels upon modifying them with either EDC or glyceraldehyde. The results obtained provide a critical element to the in depth understanding of the cross-linking reactions used to stabilize collagen 3D hydrogels.

Experimental Section

Collagen Materials Formation and Cross-Linking

3D collagen hydrogels were prepared as described previously.[1-3] The stock concentration of soluble rat-tail type I collagen was 8.58 mg/mL (BD Biosciences). The final pH was 7.4 ± 0.1 and the hydrogels were polymerized at 37 ℃. The final collagen concentration of the materials is 4 mg/ml. The materials were prepared in the 8-well chambered coverglass (MP Biomedicals. In both cases, after 24 h polymerization at 37 ℃, the materials were separately incubated in 0.1 M glyceraldehyde, 0.1 M EDC and 0.1M EDC/.025M NHS solutions (Sigma) at the 37℃ for 24 hr.

Raman Microspectroscopy

Raman spectra were recorded directly on the control and cross-linked collagen gels with a DILOR XY microspectrometer. The samples were placed on a microstage and signals were collected with a Minolta 50mm/F1.7 lens in a backscattering manner. The 532 nm radiation from a diode-pumped solid state laser (Aixiz, USA) was used for excitation. The laser power at the sample was about 110 mW, and other experimental parameters were as following: grating 1800 gr/mm; 30 acquisitions of 30 s each. These parameters gave spectra that were measured at a spectral resolution of 2 cm^{-1}. The conditions were kept constant for all the measurements. Raman data were recorded in the 800–3000 cm^{-1} spectral range. All spectra were repeated on the separate days and at least 3 times, baseline corrected with Origin 8 software. No further spectral processing (smoothing, etc.) was performed.

Results and Discussion

The position of all observed vibrational Raman bands and corresponding assignments are summarized in Table 1. They are compared to a comprehensive list of Raman line assignments for collagen from bovine Achilles tendon of Ref. [10]. In general, the intensities of the absorption bands in the Raman spectra that could be obtained for collagen hydrogels were weak.

Collagen Hydrogel (cm^{-1})	Collagen Hydrogel modified with glyceraldehyde (cm^{-1})	Collagen Hydrogel modified with EDC (cm^{-1})	Collagen Hydrogel modified with EDC/NHS (cm^{-1})	Collagen from bovine Achilles tendon*	Assignment*
813	814	823	823	821	ν(C-C) backbone
846	855	846	846	856	ν(C-C) proline ring
871	877	869	869	876	ν(C-C) Hypro ring
		896	896	890	no assignment
921	921	918	921	921	ν(C-C) proline ring
936	936			938	ν(C-C) backbone/proline ring
984	990	983	983		no assignment
997	1001	996	996	1006	phenylalanine
1025	1032	1023	1023	1037	proline
		1054	1054	1067	no assignment
1078	1081	1081	1081	1087	ν(C-N)
1101	1101			1101	no assignment
		1140	1140	1128	NH3+
		1169	1169	1161	NH3+
				1178	Tyr
				1211	Hypro, Tyr
1241	1247	1238	1241	1248	Amide III
1268		1271	1272	1271	Amide III
1285	1283				Amide III
1316	1319	1316	1316	1314	$\gamma_t(CH_3,CH_2)$
1345	1350			1343	$\gamma_w(CH_3,CH_2)$
	1386	1371	1371	1392	no assignment
1422	1423	1416	1416	1422	ν(COO-)
1450	1453	1442	1442	1451	$\delta(CH_3,CH_2)$
	1468	1465	1465	1464	$\delta(CH_3,CH_2)$
1554	1550	1547	1548		no assignment
1604	1602				C=C Phe and Tyr
1636	1637	1635	1635	1642	Amide I, H_2O
2031	2063	2077	2031		no assignment

Table 1. The position of Raman spectral lines and their assignments in collagen hydrogels and collagen hydrogels treated with different cross-linking reagents. Information for the columns with asterisk is from ref 10.

Glyceraldehyde-modified collagen hydrogels

The Raman spectra obtained after treating collagen hydrogels with the glyceraldehyde at 37℃ for 24 hours and that of the untreated control are shown in Figure 1, 2 and 3. The fluorescence induced as a result of glyceraldehyde cross-linking[1, 2] did not interfere with the acquisition of Raman spectra. The bands observed for both modified and control collagen hydrogels in the low frequency region are those associated with the C-C stretches of the protein backbone and proline/hydroxyproline: control (814 cm^{-1}, 846 cm^{-1}, 871 cm^{-1}, 921 cm^{-1}) and glyceraldehyde modified (814 cm^{-1}, 855 cm^{-1}, 877 cm^{-1}, 921 cm^{-1}). The Raman shifts for the backbone C-C stretch (814 cm^{-1}), proline ring C-C stretch (846 cm^{-1}), hydroxyproline ring C-C stretch (876 cm^{-1}) observed for collagen from bovine Achilles tendon,[10] in the unmodified hydroges occur at lower values of 821 cm^{-1}, 856 cm^{-1} and 871 cm^{-1} respectively. This perhaps is due to an increase in tension due to

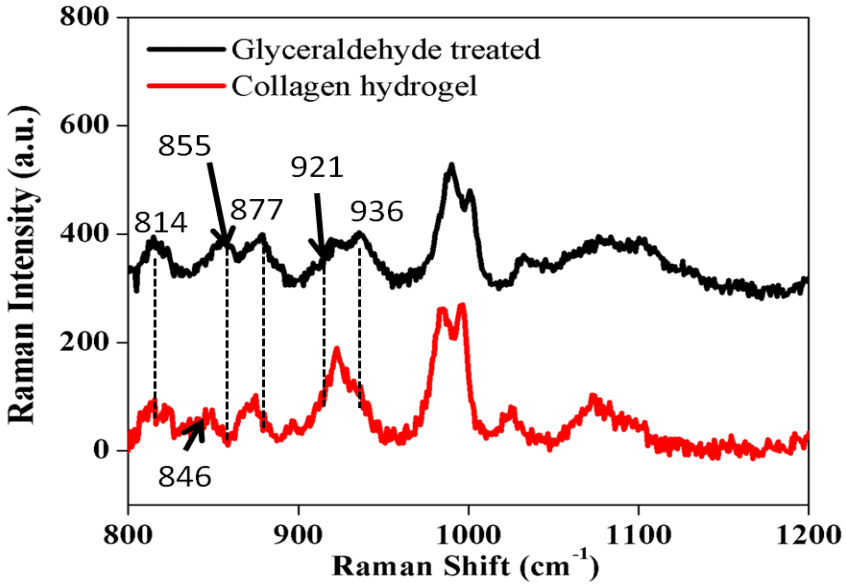

Figure 1. Raman spectra of the collagen hydrogel treated with glyceraldehyde and a corresponding control. The spectral range between 800 cm^{-1} to 1200 cm^{-1} is shown.

packing of collagen molecules within the hydrogels.[18]

As seen in Figure 1, the Raman bands in the low frequency region that undergo a change when collagen hydrogels are modified with the glyceraldehyde are those associated with the C-C stretch of the protein backbone: 814 cm^{-1}, 936 cm^{-1} and the C-C stretch of proline/hydroxyproline: 855 cm^{-1}, 877 cm^{-1}, 921 cm^{-1}. The increased relative intensity of 936 cm^{-1} band in the 936/921 doublet and slight sharpening of 814 cm^{-1} band in the glycated samples indicates a change in the packing of the collagen protein backbone and prolines/hydroxyprolines. The 814 cm^{-1} band however does not shift indicating that the collagen backbone remains intact upon glycation. The location of the 855 cm^{-1} and 877 cm^{-1} at the higher wavenumber values for the glycated samples as compared to the controls (846 cm^{-1} and 871 cm^{-1}) suggests that these vibrational models associated with

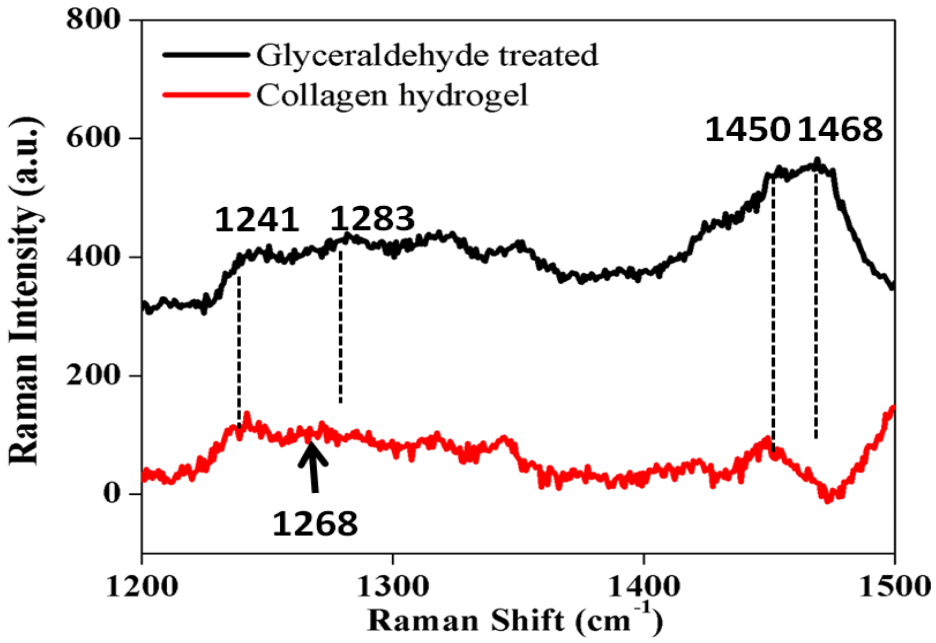

Figure 2. Raman spectra of the collagen hydrogel treated with glyceraldehyde and a corresponding control. The spectral range between 1200 cm^{-1} to 1500 cm^{-1} is shown.

proline/ hydroxyproline vibrations are normal to the collagen backbone and perhaps undergo compression.[18]

In addition to the lower frequency region, we examined the region of 1200 – 1500 cm^{-1} that is considered to be sensitive to the secondary structure of a polypeptide chain (Figure 2). The Raman bands in this high frequency region that undergo a change upon glycating collagen hydrogels are amide III (1241 cm^{-1} and 1268 cm^{-1}) corresponding to NH_2 deformations and a C-H bending mode (1450 cm^{-1}). The increase in the intensity of another peak at 1283 cm^{-1} we believe is another transition corresponding to the amide III peak in the glycated samples. This change in the amide III region indicates a possible alteration in the secondary structure upon glycation; this change might also be due to a modification and loss of order in the orientation of the collagen fibrils[19] and highlights the changes in the fibers orientation. The observed increased intensity of 1450 cm^{-1} and the appearance of a strong peak at 1468 cm^{-1} reflect a change in the length or an environment of lysine and/or arginine residues resulting in the changed deformation of CH_2 groups.[11] We believe this change occurs because amines of lysine and/or arginine residues react heavily upon glycation. The increase in the intensity in the broad range between 1200 cm^{-1} and 1400 cm^{-1} implies the formation of the aromatic ring configuration resulting upon glycation as well.[13]

The Raman vibrational bands between 1500 cm^{-1} to 2200 cm^{-1} are shown in Figure 3. The intensity of three bands which are 1604 cm^{-1}, 1636 cm^{-1} and 2063 cm^{-1} are all elevated in glycated collagen hydrogels. The 1604 cm^{-1} band observed is characteristic of the C=C

stretching vibration in the aromatic and π-conjugated rings of tyrosine and phenylalanine. Because the advanced glycation endproducts (AGEs) such as lysine-hydroxy-triosidine (LHT) and arginine-hydroxy-triosidine (AHT) contain the aromatic ring structures (Ref. [1] and references therein), we believe the elevated intensity of 1604 cm^{-1} band in glycated samples indicates the production of AGEs.[13] The increased intensity of the 1643 cm^{-1} band that corresponds to the C=O stretch of the peptide linkage (Amide I) had been interpreted to indicate the presence of additional C=O groups and/or closer packing of collagen fibers.[11] However, the O-H bending vibration of H_2O also contributes to the 1643 cm^{-1} band. Therefore, an increase in the intensity of this band cannot be attributed to the glycation and could be simply due to the difference in the H_2O content of the collagen hydrogels in general. The assignment of 2063 cm^{-1} is not known and the elevated

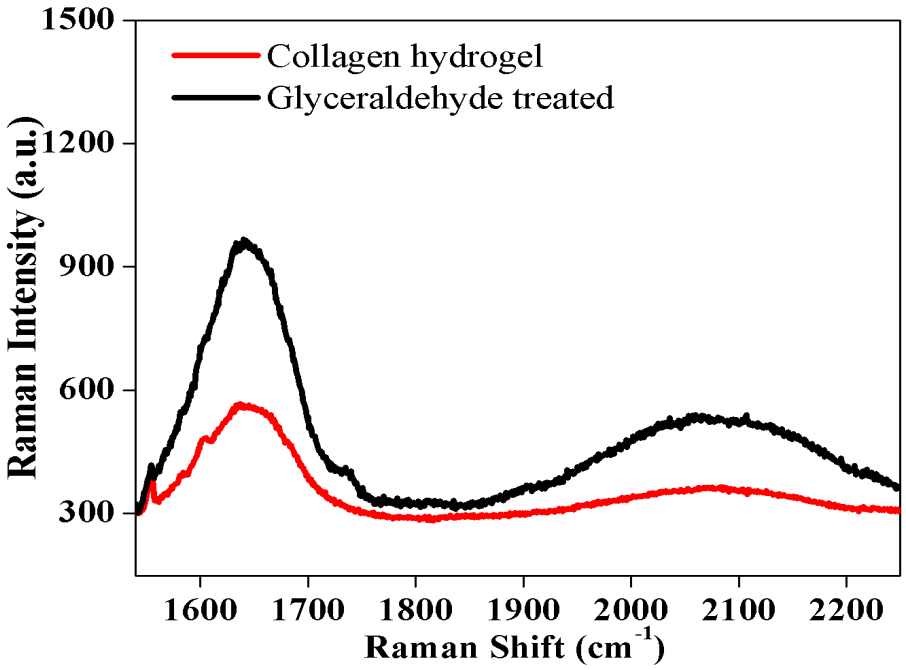

Figure 3. Raman spectra of the collagen hydrogel treated with glyceraldehyde and a corresponding control. The spectral range between 1500 cm^{-1} to 2250 cm^{-1} is shown.

intensity of this band was excluded from the scope of this study due to the need for an assignment.

EDC and EDC/NHS modified collagen hydrogels

The Raman spectra obtained after treating the collagen hydrogels with EDC and EDC/NHS at 37 ℃ for 24 hours and that of the control are shown in Figure 4 and 5. As shown in Figure 4, the Raman bands that display a change between modified and control collagen hydrogels in the low frequency region are those associated with the C-C stretches of protein backbone (814 cm^{-1} for the control and 823 cm^{-1} for the EDC-modified hydrogels), C-N stretch (1082 cm^{-1}) and tyrosine (1169 cm^{-1}). The increased intensity of 823 cm^{-1} band in the modified samples indicates a change in packing of the collagen molecule backbone. The increased intensity and sharpening of the 1082 cm^{-1} band indicates the formation of more amide bonds due the EDC crosslinking of collagen molecules. The increased intensity of 1169 cm^{-1} band possibly represents a conformational change of collagen molecules that lead to change in the environment of the bulky tyrosine residues.

Figure 5 shows the difference between EDC-modified and control collagen hydrogels in the region from 1200 cm^{-1} to 1500 cm^{-1}. The observed bands that change between modified and control collagen hydrogels are amide III (~1238 cm^{-1} and ~1271 cm^{-1}) corresponding to NH_2 deformations, C-H twisting (1316 cm^{-1}) and C-H bending (1442 cm^{-1}) modes. The approximately 23% decrease in the ratio of 1238 cm^{-1} to 1271 cm^{-1} amide III band intensities in EDC-modified samples as compared to controls indicates a

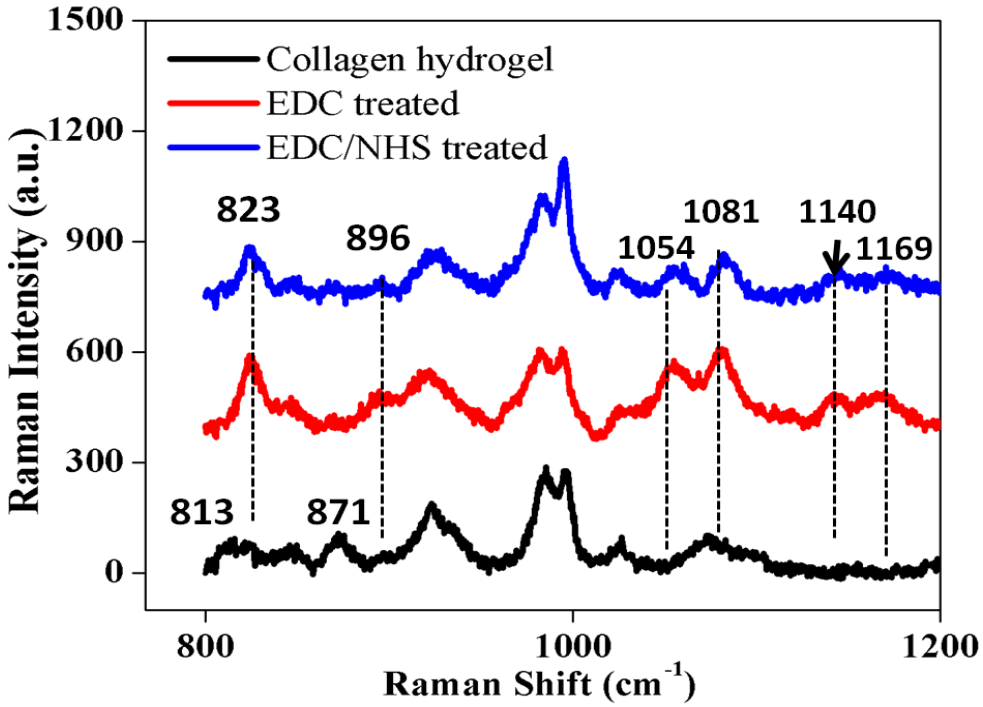

Figure 4. Raman spectra of the collagen hydrogel treated with EDC, collagen hydrogel treated with EDC/NHS and a corresponding control. The spectral range 800 cm^{-1} to 1200 cm^{-1} is shown.

change in the denaturation and disorder of the secondary structure upon EDC cross-linking. However, it could also be due to the modification and change in the order in orientation of the collagen fibrils[19] or molecules within them. In the EDC-modified samples, the 30% increase in the ratio of the amide III mode (~1238 $cm^{-1)}$ band area to the C-H twisting mode (1316 cm^{-1}) band area and a 85% increase in intensity for the C-H bending mode (1442 cm^{-1}) compared to control reflect a change in length or environment of lysine and/or arginine residue resulting in the changed motion of CH_2 groups due to packing of collagen molecules. Additional changes that are observed in the EDC and

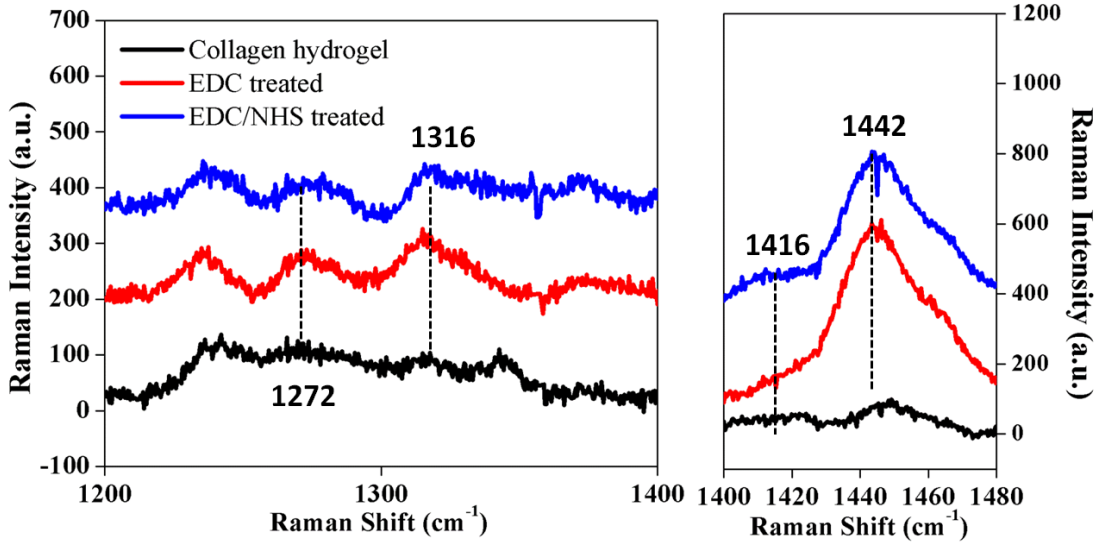

Figure 5. Raman spectra of the collagen hydrogel treated with EDC, collagen hydrogel treated with EDC/NHS and a corresponding control. The spectral range 1200 cm^{-1} to 1480 cm^{-1} is shown.

EDC/NHS modified samples are the following: appearance of 1140 cm^{-1} band corresponding to NH_3^+ (1128 cm^{-1} band assignment for collagen from the bovine Achilles tendon), disappearance of the 1345 cm^{-1} band corresponding to the C-H waging motion and 1416 cm^{-1} band corresponding to COO^- stretch becoming very prominent in the EDC/NHS modified samples. An increase in the intensity of 1416 cm^{-1} band (COO^- stretch) corresponds to the modification of aspartic and glutamic acid carbonyl containing residues with EDC. This observation suggests that the modification in presence of NHS, which reacts through an intermediate O-acylurea to form a more stable in solution activated ester, is more effective than with EDC alone.[20] Overall however, the addition of NHS doesn't induce additional molecular changes compare to the effect of EDC alone.

Our previous results clearly showed that glyceraldehyde modifies the collagen structure within hydrogels in both micro- and nano-scale. On the other hand, EDC even with an addition of NHS can't modify the structure within the collagen hydrogels on the microscale[1, 2]. Based on these earlier observations, glyceraldehyde was expected to have stronger modifying effect on the collagen at the most fundamental molecular structural level compared with the EDC. The findings of the current Raman study confirm this expectation. As from Figure 1 and Figure 4, glyceraldehyde affects more Raman bands than EDC in the region from 800 cm^{-1} to 1000 cm^{-1}, which represent the conformation of the collagen protein backbone.

Despite our previous studies have shown that the glyceraldehyde modifies the micro- (fibers) and nano-structure (fibrils) within collagen hydrogels and EDC have no effects on both structural levels as observed in SHG and TEM images[21], the Raman spectra showed that both reagents have dramatic effects on the molecular information of hydrogels. In addition to the change in the peak intensity and the shift in peak position which imply the conformation change in collagen molecules, these two changes also indicate the alteration in fiber orientation. The amide III bands at 1241 and 1268 cm^{-1} and the band at 921 cm^{-1} have been shown to be most affected by fiber orientation[19]. The Raman spectra show that the change in the ratio of 1241/1268 cm^{-1} peak intensity and the elevated intensity of 921 cm^{-1} in glyceraldehyde treated samples. Accompanied by the modification of micro-structure shown in SHG images which illustrates the realignment of micro-structure, this observation strongly suggests that the effect of glyceraldehyde on fiber orientation can be detected on both structural levels. Comparing to glyceraldehyde,

the Raman spectra also show that EDC changes the ratio of 1241/1268 cm^{-1} peak intensity; however EDC doesn't have any effect on the orientation of micro-structure. This observation indicates that the effect of EDC on the fiber orientation can only be detected on the molecular level but this effect is not strong enough to be detected at the micro-structural level. The difference between the effects of these two cross-linking reagents on the fiber orientation suggests that glyceraldehyde is a stronger crosslinking reagent than EDC on collagen hydrogels because glyceraldehyde can significantly modify the fiber structure and orientation on different structural levels but EDC only has its effect on molecular level.

Previous Raman spectroscopy studies related to collagen mainly focused on either the collagen molecules or collagen-based intact tissues. Our study on the 3D collagen hydrogels was designed to fill the void between these two fields. Our goal was to obtain the additional fundamental molecular insights regarding modifications of the collagen structures within hydrogels upon cross-linking. When the observed peaks in the Raman spectra of collagen hydrogels are compared to the Raman spectra of collagen-based tissues such as articular cartilage[4] and collagen from bovine Achilles tendon,[10] they are very similar. The major peaks including C-C stretch of proline and protein backbone (800 cm^{-1} - 1000 cm^{-1}), amide III (1242 cm^{-1}, 1268 cm^{-1}) and amide I (1636 cm^{-1}) can all be detected in the Raman spectra of collagen hydrogels. The major difference between the spectra of the control collagen hydrogels compared to the molecules/tissues is the disappearance of 1178 cm^{-1} band corresponding to the aromatic ring of tyrosine and

phenylalanine. For the collagen hydrogels, only a peak at 1604 cm^{-1}, which is also assigned to the π-conjugated and aromatic molecules was detectable.[11, 13]

Conclusion

This work is the first application of Raman micro-spectroscopy to examine the effect of different cross-linking reagents on molecular structure of the 3D collagen hydrogels. The Raman spectra clearly show that glyceraldehyde and EDC both modify the conformation of collagen molecules. Based on the changes we observed in the 800 cm^{-1} and 1000 cm^{-1} low frequency region corresponding to C-C streets of backbone and proline, we conclude that these reagents change packing of collagen molecules within fibrils. The reagents additionally affect the secondary structure and/or change order and orientation of collagen fibrils/fibers based on the changes associated with amide III bands (~1241 cm^{-1} and ~1268 cm^{-1}) that correspond to NH_2 deformations. When the modifying effect of EDC is compared with glyceraldehyde, glyceraldehyde has a stronger molecular modifying effect than EDC and affects more Raman bands. Our work successfully demonstrates the application of Raman spectroscopy to distinguish the molecular effects of different reagents during cross-linking of 3D collagen hydrogels. It indicated that Raman spectroscopy provides additional information in characterizing the molecular events underlying the cross-linking reactions taking place within hydrogels.

References

(1) Hwang, Y.; Granelli, J.; Lyubovitsky, J. G. *Analytical Chemistry* **2011**, *83*, 200–206.

(2) Hwang, Y.; Granelli, J.; Lyubovitsky, J. G. *Applied Materials and Interfaces* **2011**, *4*, 261-267.

(3) Hwang, Y.; Lyubovitsky, J. G. *Analytical Methods* **2011**, *3*, 529-536.

(4) Dehring, K. A.; Smukler, A. R.; Roessler, B. J.; Morris, M. D. *Appl. Spectrosc.* **2006**, *60*, 366-372.

(5) Diem, M.; Bhatnagar, R. S.; Druyan, M. E.; Renugopalakrishnan, V. *Biopolymers* **1984**, *23*, 2955-2961.

(6) Dingari, N. C.; Horowitz, G. L.; Kang, J. W.; Dasari, R. R.; Barman, I. *PLoS ONE* **2012**, *7*.

(7) Dong, R.; Yan, X.; Pang, X.; Liu, S. *Spectrochim Acta A* **2004**, *60*, 557-561.

(8) Erckens, R. J.; Motamedi, M.; March, W. F.; Wicksted, J. P. *J. Raman Spectrosc.* **1997**, *28*, 293-299.

(9) Frank, C. J.; McCreery, R. L. *Anal. Chem.* **1995**, *67*, 777-783.

(10) Frushour, B. G.; Koenig, J. L. *Biopolymers* **1975**, *14*, 379-391.

(11) Jaisson, S.; Lorimier, S.; S.;, R.-B.; Sockalingum, G. D.; C.;, D.-F.; Kegelaer, G.; Manfait, M.; Garnotel, R.; Gillery, P. *Chem. Biol.* **2006**, *13*, 149-159.

(12) Jastrzebska, M.; Wrzalik, R.; Kocot, A.; Zalewska-rejdak, J.; Cwalina, B. *J. Jomater. Sci. Polymer Edn* **2003**, *14*, 185-197.

(13) Sebag, J.; Nie, S.; Reiser, K.; Charles, M. A.; Yu, N. *Invest. Ophth. Vis. Sci.* **1994**, *35*, 2976-2980.

(14) Carey, P. R. *Biochemical Applications of Raman and Resonance Raman Spectroscopies*; Academic Press Inc.: New York, 1982.

(15) Parker, F. S. *Applications of Infrared, Raman and Resonance Raman Spectroscopy in Biochemistry*; Plenum Press: New York and London, 1983.

(16) Spiro, T. G. *Biological Applications of Raman Spectroscopy; Volume 1 Raman Spectra and the Conformations of Biological Molecules*; John Wiley & Sons: New York, 1987.

(17) Tfayli, A.; Piot, O.; Draux, F.; Pitre, F.; Manfait, M. *Biopolymers* **2007**, *87*, 261-274.

(18) Wang, Y. N.; Galiotis, C.; Bader, D. L. *J. Biomech.* **2000**, *33*, 483-486.

(19) Bonifacio, A.; Sergo, V. *Vib. Spectrosc.* **2010**, *53*, 314-317.

(20) Staros, J.; Write, R.; Swingle, D. *Anal. Biochem.* **1986**, *156*, 220-222.

(21) Hwang, Y.; Granelli, J.; Lyubovitsky, J. *ACS Appl. Mater. Interfaces* **2011**, *4*, 261-267.

CHAPTER 6

CHARACTERIZATION OF CROSS-LINKED COLLAGEN HYDROGELS: The effect of genipin crosslinking on the micro- and nano- structure of collagen hydrogels

Abstract

Genipin is a natural cross-linking reagent extracted from the fruits of *Gardenia jasminoides*. Due to its low cytotoxicity and high biocompatibility, it can be effectively employed in tissue engineering applications. To determine whether genipin cross-linking modifies the structure of collagen hydrogels, we followed this process *in-situ.* We incubated the hydrogels with 1 mM and 10 mM genipin solutions. The incubation with genipin induced strong fluorescence within the gels. The rate of fluorescence production upon modifying collagen hydrogels with genipin was three times faster with the 10 mM compared to 1 mM solution of the compound. However, both concentrations of genipin generated similar fluorescence intensity at twenty-four hours after the initiation of cross-linking reaction. The fluorescence maximum for the cross-linking products formed by genipin depended greatly on the excitation wavelengths. For example, the emission maximum was at 630 nm when we excited the cross-linked samples with 590 nm light and shifted to 462 nm when we used 400 nm light instead. We characterized the micro- and nano-structures within cross-linked hydrogels by examining second harmonic generation (SHG) and transmission electron microscopy (TEM) images respectively. As detected in the SHG images, genipin modified 10 μm 'fiber-like' collagen structures to longer, aggregated strands the density of which increased throughout the depth of

samples. TEM revealed that genipin largely eliminated collagen's characteristic native fibrillar striations. Moreover, fluorescence recovery after photobleaching (FRAP) was applied to examine the diffusion of genipin induced fluorophores within collagen hydrogels.

Introduction

The cross-linking of collagen-based scaffolds/gels is often employed to strengthen them for tissue engineering applications. The effects of these processes on collagen structures are usually not investigated. To clarify the effects of cross-linking on biologically derived scaffolds, characterizing these structures is critical. Different collagen structures contribute to batch-to-batch variability in the prepared biological scaffolds. They can potentially influence differently the cell proliferation, differentiation, and migration.[1]

This study investigates the effects of genipin cross-linking on the structure of three-dimensional (3D) collagen hydrogels. Specifically, the study is set to answer a question if genipin crosslinking modifies the nano- and micro- structures of collagen as well as establishing for the first time a combination of methods to follow this process *in-situ* and in real time. This was achieved through examining the genipin cross-linked collagen hydrogels with one-photon fluorescence spectroscopy, second harmonic generation, fluorescence, transmission electron microscopy and fluorescence recovery after photobleaching. The data and methods developed provide an outline to monitor *in-situ* the extent of cross-linking of collagen hydrogels with genipin.

Genipin compound is an iridoid derivative isolated from the fruits of *Gardenia jasminoides*. It generates both color and fluorescence in a single reaction with biopolymers containing primary amine groups. At this time, the molecular mechanism for genipin reaction with collagen is not well understood. It is believed to cross-link collagen through a nucleophilic attack of the collagen's primary amine of lysine, hydroxylysine and arginine residues on the C3 atom of genipin.[2] Subsequently, the tertiary nitrogen of collagen replaces an oxygen atom in the genipin's six-membered ring. The intramolecular and intermolecular crosslinks formed are the linked cyclic structures of nitrogen substituted genipin attached to collagen.[3] In addition to the cyclic structure constituted of genipin and collagen molecules, it has been found that genipin molecules might be polymerized before cross-linking to collagen. [4] This self-polymerized structure might also generate fluorescence. To date, genipin found practical use as a bioadhesive,[5] amino acid[6] and fingerprint[7, 8] detection reagent. Additionally, it had been employed to cross-link various hydrogels for biomaterial,[9, 10] drug delivery applications,[11] and preparation of porous constructs.[12]

The technique we used in this work to characterize the micro- structures of genipin-cross-linked collagen hydrogels is multi-photon microscopy (MPM). MPM imaging is a non-destructive optical method that utilizes femto-second pulses of near-infrared (NIR) laser light and can generate high resolution and contrast three-dimensional images of biological samples. Its advantages include reduced scattering because NIR wavelengths are employed, no out-of focus absorption, very small sample volumes and deeper tissue penetration compared to confocal microscopy.[13] The interaction between fibrillar

collagen and NIR pulsed, femto-second laser light of MPM has been identified to result in second harmonic generation (SHG) which is produced when photons interacting with fibrillar collagen are combined to form new photons with exactly twice the energy.[14] SHG gained recognition in tissue imaging[15-24] because this source of contrast resists photo-bleaching and had been used to successfully image structural proteins in various non-animal and animal sources[25] with strong enhancement suitable for biomedical assessment of tissue structure.[22] The interaction between laser pulses and collagen's non-centrosymmetric, triple helix structure in addition to molecular packing within collagen materials leads to scattering from the tertiary (fibrils),[22] and quaternary (fibers)[14],[26] thus producing SHG.[27] The intrinsic fluorescence is also generated by UV/VIS absorbing molecular structures and proteins. The cross-linking products formed by genipin when it reacts with biopolymers containing primary amine groups absorb in the mid-UV (250-300 nm),[28] near-UV (320-370 nm),[9] visible wavelength range (400-600 nm)[29] and fluoresces in the 380 to 700 nm wavelength region.

The MPM was used to examine the generation of genipin induced fluorescence due to the formation of self-polymerized structure composed of genipin molecules within collagen hydrogel and we then applied FRAP to confirm the induction of fluorescence. FRAP has been commonly used in measuring the diffusion of fluorescent molecules on different types of samples such as tissue[30], collagen gel[31-33] and plant[34]. A region of interest of the sample is scanned with the intense laser beam which causes an irreversible photobleaching of fluorophores in the region. The photobleached region is a dark spot which allows a gradual diffusion of the surrounding fluorescent molecules leading to the

recovery of fluorescence. The rate of fluorescence recovery is correlated to the diffusion coefficient of the fluorescent molecules. [35] In our study, we didn't use FRAP to investigate the diffusion of fluorophores. We took advantage of this technique which is capable of tracking fluorescence production *in situ* as a function of time to understand the process of fluorescence production via genipin cross-linking.

Experimental Section

Collagen materials formation and cross-linking

Soluble rat-tail type I collagen, 9.58 mg/ml (BD Biosciences) was in 0.02 N acetic acid. The purity of this stock solution was verified with 4%-20% Tris-HCl gels (Bio-Rad) following a standard protocol. The stock solution was diluted with 0.02 N acetic acid to obtain the 2X collagen aliquots. 2X initiation buffers were prepared from NaCl and phosphate buffer. The concentration of mono-and dibasic phosphate in the buffer at pH=7.4 were calculated with Henderson-Hasselbalch equation. The pH was adjusted drop-wise with 1N NaOH or HCl. Ionic strength was adjusted with NaCl. The initiation buffer had the following components: 6.40 g/l K_2HPO_4; 3.16 g/l KH_2PO_4; 38.55 g/l NaCl (ionic strength = 0.6 M). After the pH was adjusted to a desired value, the initiation buffer were filtered with 0.22 μm, 25 mm syringe filter (Fisher) and stored at 4°C. Prior to the beginning of material formation, both 2X collagen stock and initiation buffer were de-airated by placing in a 1.5 L desiccator (Fisher) and applying house vacuum for 2 hrs. Material formation was initiated by mixing 2X collagen aliquot with 2X initiation buffer on ice at 1:1 ratio, verifying the pH to be 7.4±0.1, and then incubated at 37 °C. The final

collagen concentration of the materials is 4.68 mg/ml. For multi-photon microscopy, confocal microscopy measurements and FRAP, collagen materials were prepared in 8-well chambered coverglass (MP Biomedicals). For one-photon experiments collagen materials were prepared in 96-well plates (BD Falcon). In both cases, after 24-hour incubation at 37 ℃, the materials were incubated in 1 mM or 10 mM genipin solutions (Sigma) at the same temperature for the specified times.

Fluorescence measurements

Increase in fluorescence intensity within the materials that was due to genipin cross-linking was measured *in situ*, in a high-throughput format using a FlexStation microplate reader in a backscattering mode (Molecular Devices). The excitation wavelength was 590 nm and emission spectrum was collected from 620 to 760 nm. Measurements were taken every 1 h during the first 9 hrs and subsequently 2 measurements every 24 hr. Per one experimental run, a spectrum was independently acquired from two wells. The background fluorescence was subtracted from each spectrum, and the spectra were averaged. All experimental runs were repeated on different days and up to three times using identical settings for the measurements. The error bars are standard deviations from the mean. After the fluorescence intensity reached the plateau, cross-linked samples were shaken thoroughly in a 0.3 M ionic strength phosphate buffer (NaCl added to adjust ionic strength) to remove the unreacted genipin.

Multiphoton microscopy (MPM) and confocal microscopy

The inverted multiphoton laser scanning microscope used in this work was the Zeiss LSM 510 NLO Meta microscopy system. It is based on an Axiovert 200M inverted microscope equipped with standard illumination systems for transmitted light and epi-fluorescence detection. It was also equipped with an NLO interface for a femtosecond titanium: sapphire laser excitation source (Chameleon-Ultra, Coherent, Incorporated, Santa Clara, CA) for multiphoton excitation. The Chameleon laser provided femtosecond pulses at a repetition rate of about 80 MHz, with the center frequency tunable from 690 to 1040 nm. A Helium-Neon 543 nm laser was also equipped for confocal excitation. A long working distance objective (Zeiss, 40x water, N.A. 0.8) was used to acquire images shown in this work. The signals from the samples were epi-collected and discriminated by the band pass 700/543 nm dichroic beamsplitter. The SHG images were collected with the 390-465 nm band-pass filter (λ_{ex} = 800 nm). The fluorescent images were collected with the 565-615 nm band-pass filter (λ_{ex} = 543 nm). Each image presented in this work is 12 bit, 512 x 512 pixels representing 225 μm x 225 μm field of view. All the images were repeated on separate days, using up to 8 independent samples on each day (about 5 fields of view per sample).

Transmission Electron Microscopy (TEM) imaging

After 24 hours of incubation, entire portion of an incubated sample was retrieved. A drop of sample containing cross-linked material was added on a formvar film coated with a layer of carbon supported on a 300-mesh copper grid (Carbon type A, Ted Pella, Inc.).

Excess liquid was drained with filter paper after 30 s. A drop of double de-ionized water was then added to the sample on the grid for 1 s to remove the excess NaCl, and was drained slowly with filter paper. A drop of same-day-prepared 1 g/l sodium phosphotungstate (Sigma), pH=7.4 was added to the sample on the grid. After 10 minutes of staining, the grid was drained slowly with filter paper and then air-dried for about 15 minutes. The grids were examined immediately in a Tecnail 12 electron microscope operated at 120 kV.

Fluorescence recovery after photobleaching (FRAP)

Images were captured with an inverted confocal laser-scanning microscope, Olympus FV1000. The laser and argon laser excitation wavelength were 405 nm and 488 nm respectively; the fluorescence emission was detected with the filter centered at 520 nm. A 60X water objective (1.2 NA) was used. Bleaching was done using a 405 nm beam and pre-bleaching and post-bleach imaging was done using a 488 nm beam. Pre-bleaching images were collected for 50 s and then a circular ROI with diameter of 45 μm was bleached for 50 s and 100 s for GA cross-linked and GE cross-linked hydrogels respectively. Recovery of fluorescence was recorded for 10 min. Images were collected at 512 pixels^2. The recovery of fluorescence was quantified with Olympus Fluoview software (Version 3.0). The kinetics of recovery of fluorescence was first-order exponential fitted with Origin8 software. Collagen hydrogels crosslinked with glyceraldehyde was served as the comparison. The experiment was repeated for two times with fresh samples and 6 different areas within collagen hydrogels were tested.

The percentage recovery was calculated

$$\% \text{ Recovery} = \frac{\text{F(min)} - \text{F(max)}}{\text{F(max)}}$$

where F(min) is the minimum fluorescence detected during the photobleaching and F(max) is the maximum fluorescence during the fluorescence recovery. The % recovery was calculated for each set of data and the % recovery for each set was then averaged.

Results and Discussion

Two potential molecular mechanisms for genipin modification of biopolymers containing primary amine groups are described in literature.[29, 36] For collagen, they are schematically shown in Figure 1. The first cross-linking pathway begins with a nucleophilic attack from a primary amine group of collagen on the genipin C3 carbon to form a nitrogen-iridoid.

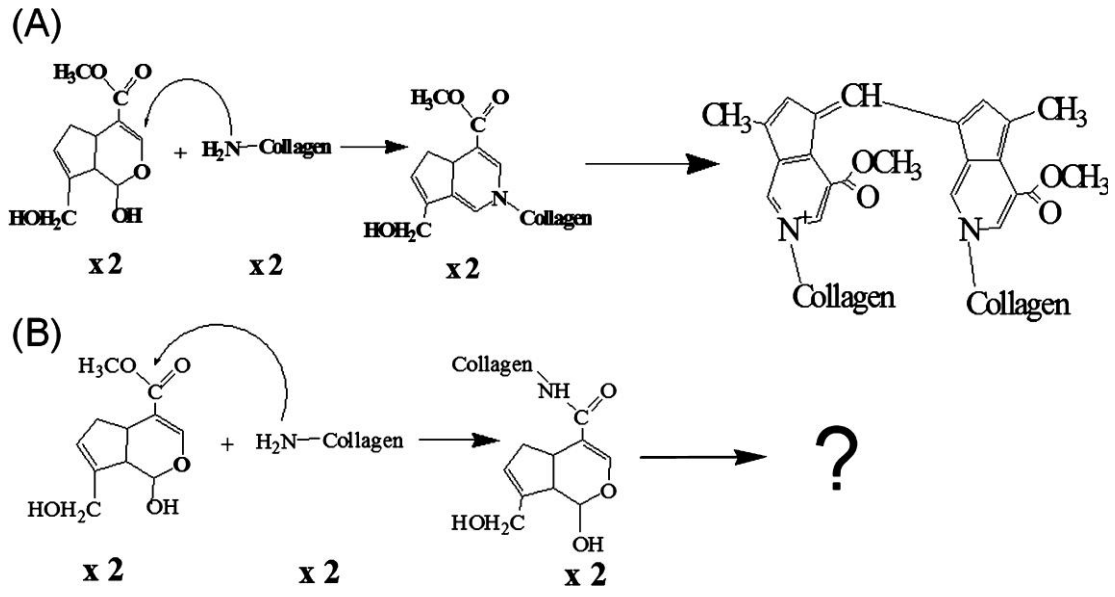

Figure 1. Schematics for the cross-linking reactions of collagen with a genipin compound.

Two iridoids subsequently dimerize through a radical reaction (Figure 1A).[5] The second proposed pathway starts with a nucleophilic substitution reaction that replaces the ester group of genipin by a secondary amide linkage.[36] The final product for this second possible pathway is unknown.

In-situ One-photon Fluorescence Characterization of Genipin in Crosslinked Collagen Hydrogels

The incubation of acellular collagen hydrogels in 1 mM or 10 mM solutions of genipin caused the non-fluorescent samples to emit fluorescence *in-situ*. When the collagen hydrogels exposed to genipin were subsequently excited with 590 nm light, the observed fluorescence emission maximum was a broad band with a peak centered at 625 nm (Figure 2A). The excitation of samples with different wavelengths of light produced very different fluorescence emission spectra (Supporting Information Figure S1). Overall, cross-linking collagen hydrogels with 10 mM versus 1 mM genipin solution occurred faster and fluorescence leveled off almost three times quicker. It reached a plateau at ten hours after initiation of reaction (Figure 2B).

The fluorescence emission maximum detected at 625 nm (λ_{ex} = 590 nm) from the genipin-modified hydrogels is the same as observed in one other study[29] using 590 nm light to excite genipin-modified collagen gels. An additional emission maximum that we detect at 464 nm (λ_{ex} = 300 to 400 nm) is similar to fluorescence emission at 469 nm observed by Chen et al.[37] from chitosan-genipin mixtures excited with 369 nm light. Our work and all previous relevant studies, therefore, suggest that cross-linking collagen

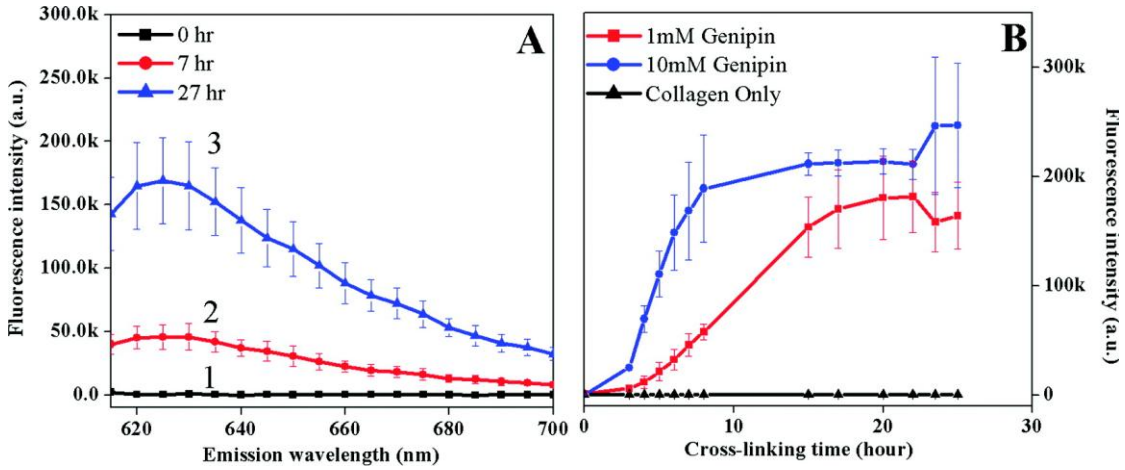

Figure 2. The effect of genipin cross-linking on the production of fluorophores (λ_{ex} = 590 nm): (A) *In situ* fluorescence emission spectra of the collagen hydrogels incubated with 1 mM genipin for 0 hr (1), 7 hr (2), and 27 hr (3). (B)The fluorescence intensity ($\lambda_{ex}/\lambda_{em}$ = 590 nm/630 nm) as a function of cross-linking time for collagen hydrogels incubated with 1mM, 10 mM genipin or no genipin (control). All samples are measured in triplicate, and error bars represent standard deviations from the mean.

hydrogels with genipin induces formation of multiple fluorophores. The fluorescence emission maxima of these fluorophores depend strongly on the excitation wavelength.

In Situ Microscopic Characterization of Genipin Cross-Linked Collagen Hydrogels: Second Harmonic Generation (SHG) and Fluorescence

To monitor the microstructures within collagen hydrogels during the cross-linking reaction with genipin, we employed LSM510 microscopy system equipped with both a Ti:Sapphire laser for SHG and a Helium-Neon 543 nm laser for fluorescence excitation.

To follow the extent of reaction during cross-linking collagen hydrogels with genipin, we excited samples with 543 nm light and monitored the evolution of fluorescence intensity in the x-y plane through the 565-615 nm filter (Figure 3A-C). At 6 hrs of cross-linking with genipin, we observed the fluorescence spots to appear and some of the spots to

accumulate into the larger structures (Figure 3B, white outline). When the cross-linking time reached 48 hr, the structures exhibited higher fluorescence intensity, and large structures were formed (Figure 3C, white outline). The fluorescence images taken in x-z plane showed that upon extended cross-linking (24 hr or more) an increase of fluorescence occurred throughout the entire depth of collagen hydrogels (Figure 4C). The control group consisting of collagen hydrogels incubated in 0.3 M phosphate buffer saline solution did not exhibit detectable fluorescence (Figure 4A).

To determine if there are structural modifications of collagen hydrogels that are caused by cross-linking with genipin, we acquired second harmonic generation (SHG) images at the same time as fluorescence images. To our knowledge, we are the first group to apply SHG and fluorescence imaging to carry out such evaluations. As seen in SHG images (Figure 3D-F), genipin cross-linking clearly alters the microstructure of collagen hydrogels. At the beginning of cross-linking, the "fiber-like" structures within the collagen hydrogels were short with lengths around 5- 10 μm (Figure 3D). When the cross-linking time was 6 hr, the short "fiberlike" structures began to disappear and became modified to longer, aggregated threads with a length greater than 20 μm (Figure 3E). When the cross-linking time reached 48 hr, the longer, aggregated threads became prominent (Figure 3F). The SHG images taken in X-Z planes also showed that the modification of structures was throughout the entire depth of collagen hydrogels and that there is an increase in the density of the "fiber-like" collagen structures (Figure 4D). The control group consisting of collagen hydrogels incubated in 0.3 M phosphate buffer

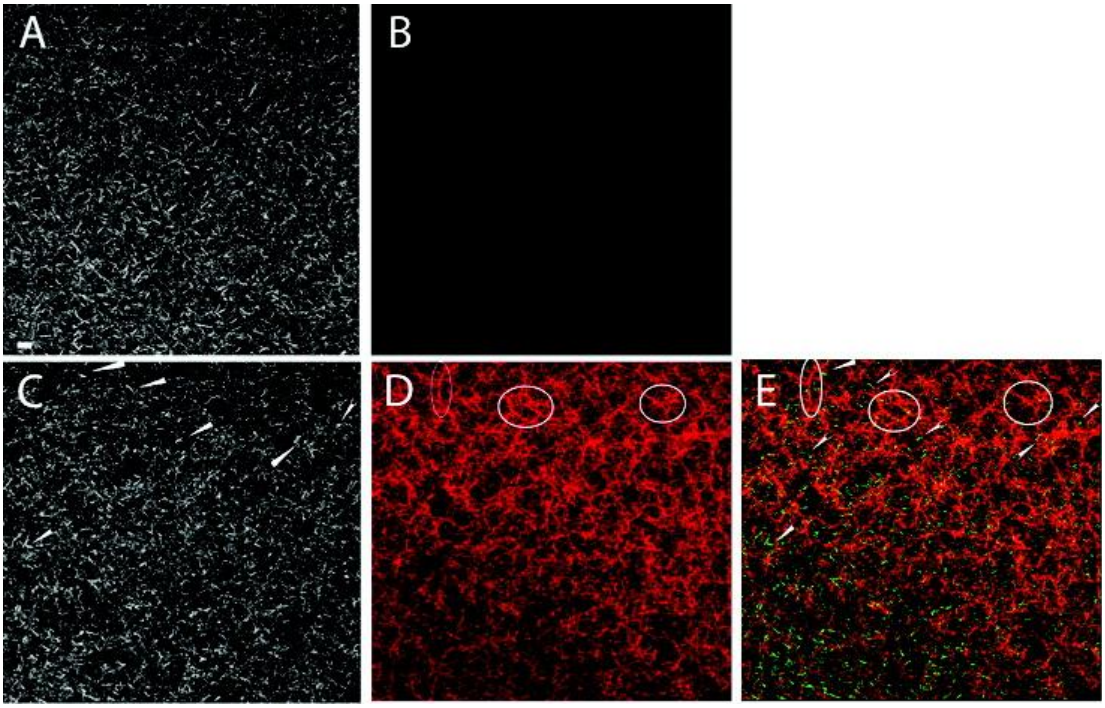

Figure 3. Typical fluorescence and second harmonic generation (SHG) images of a sample incubated with 1 mM genipin for a different amount of time. The images are taken in X-Y plane. Fluorescence: (A) 0 hr, (B) 6 hr, and (C) 48 hr. SHG: (D) 0 hr, (B) 6 hr, and (C) 48 hr. The original short "fiberlike" 5 μm structures modified to long, aggregated strands with length longer than 20 μm can be seen within the areas circled with the white outline. The collagen concentration of the sample is 2.0 mg/ml and the incubation temperature is 37 ℃. The scale bar is 20 μm.

saline did not have any structural changes that could be identified in the SHG images (Figure 4B).

The SHG images presented in our work clearly show that genipin cross-linking remodels the microscopic "fiber-like" features within collagen hydrogels. By non-invasively sampling the structures within these mechanically stabilized templates employed in tissue engineering we reconstructed their overall 3D architecture. This reconstruction validates and confirms previous studies that recorded structural changes within various genipin cross-linked collagen-based tissues and materials. For example, when electrospun gelatin

scaffolds were exposed to genipin, the morphology of pre-formed fibers was not maintained as detected with scanning electron microscopy.[38] Histological investigations

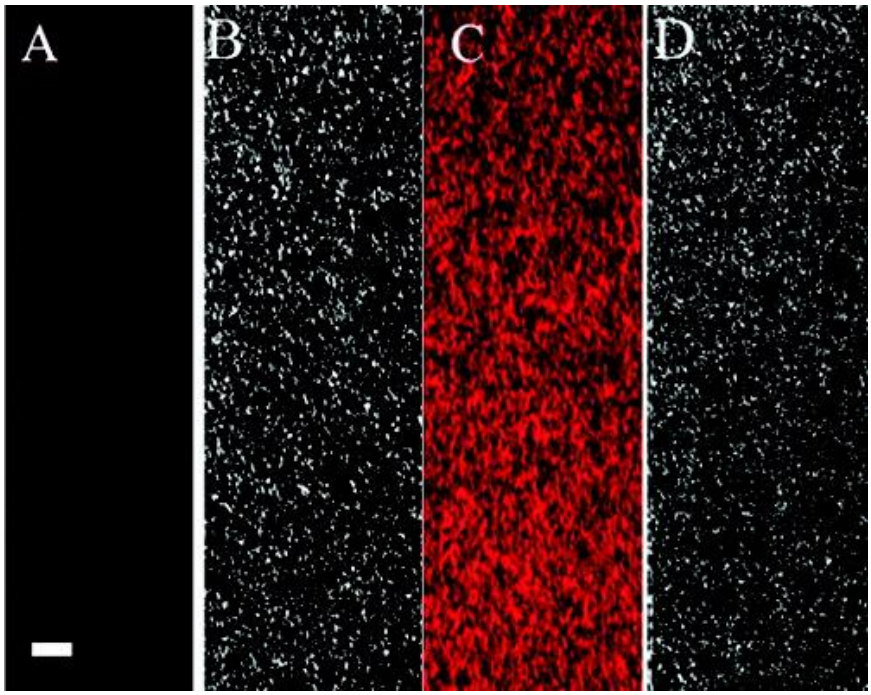

Figure 4. Typical fluorescence and second harmonic generation (SHG) images of a sample incubated with 1 mM genipin for a different amount of time. The images are taken in X-Z plane. The collagen concentration is 2.0 mg/ml. The horizontal is the X-axis, and the vertical axis is the Z-axis. Fluorescence (A and C); SHG (B and D). Control consisting of collagen only (A and B); collagen hydrogel incubated with genipin (C and D). The scale is 20 μm. The top of each image represents the actual top of the imaged gel.

revealed an increase in the fiber density and a decrease in interfibrillar spaces when corneas were treated with genipin.[39] When collagen/chitosan scaffolds were incubated with genipin, scanning electron microscopy studies showed the change of the pores' morphologies and sizes.[40]

To our knowledge we are the first to describe genipin-induced remodeling of collagen microstructures within 3D hydrogels and to directly link these changes to the induced

fluorescence. Interestingly, during our study we additionally discovered that the 100W mercury lamp emission filtered through the bandpass filter with a band center about 365 nm and bandwidth 50 nm would induce fluorescence. Specifically, the areas of samples illuminated for several seconds with this lamp through the focusing objective, showed a strong enhancement in fluorescence intensity. However, we observed no corresponding change in the hydrogels' microstructure as detected with second harmonic generation (SHG) imaging (Supporting Information Figure S2). The induced fluorescence dissipated within about fifteen minutes. We therefore concluded that this induced spectrally overlapping fluorescence is not associated with the formation of cross-links during reaction of collagen hydrogels with a genipin compound. It is possible that the fluorescent adducts of genipin itself are generated photochemically by UV light.

Characterization of Genipin Cross-Linked Collagen Hydrogels with Transmission Electron Microscopy

We used transmission electron microscopy to determine if in addition to affecting collagen microstructures, genipin modifies nanostructures as well. The transmission electron micrographs showed that the nanostructure of negatively stained reconstituted collagen fibrils varied greatly after treatments with genipin. Only under rare conditions, we observed native-like striated collagen fibrils with D-periods in the range of 62 to 67 nm (Figure 5A). Most of collagen fibrils became modified to non-striated filaments (Figure 5B). Additionally, we observed some striated fibrils with longer D-periods (Figure 5C). The genipin cross-linking mechanism depicted in Figure 1 could explain

occurrence of non-native collagen structures in TEM images. The non-striated filaments and fibrils with non-native D-periods would form when there is a disruption of native staggered alignment of collagen molecules within fibrils. The intra- and inter-molecular cross-linking of collagen molecules by genipin likely induces this disruption.

Genipin compound is potentially an excellent natural cross-linking reagent for tissue engineering applications due to its low cytotoxicity and high cytocompatibility. For example, when Chang et al. used genipin cross-linked gelatin membrane as a wound dressing material, he found that the inflammation was less severe and the healing rate was faster compared to using a glutaraldehyde-treated gelatin membrane.[10] Yao et al.

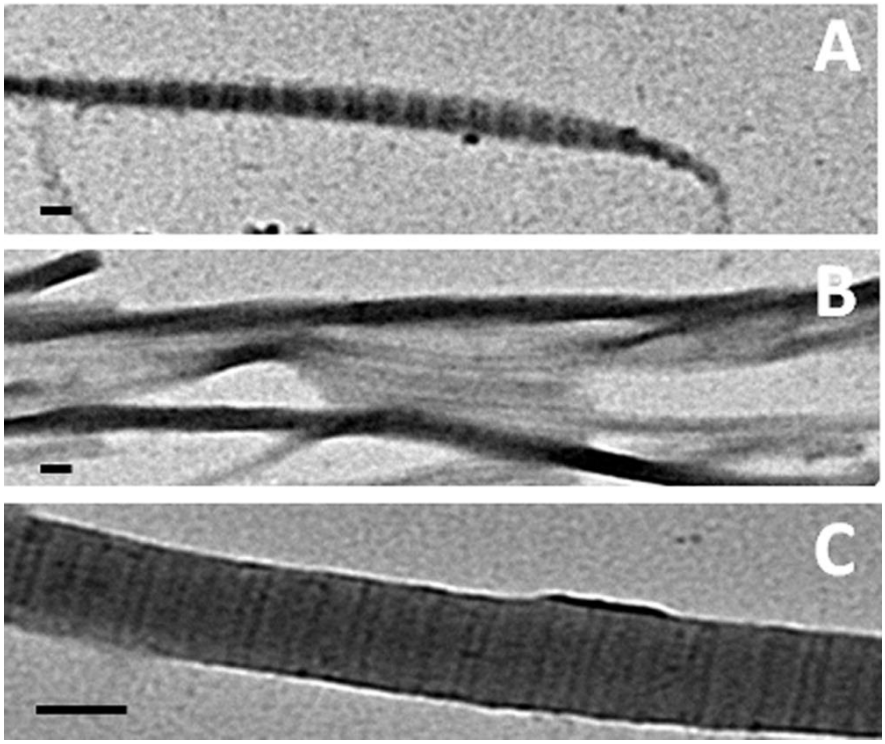

Figure 5. Transmission electron micrographs of negatively stained collagen fibrils cross-linked with genipin. (A) A typical collagen fibril with native banding. (B) The typical non-striated filaments. (C) The striated fibrils with non-native banding (longer D–period striation). The scale bar is 50 nm.

applied genipin treated materials as bone substitutes and showed that they supported growth of a new bone without inflammation.[37] Chen et al. evaluated peripheral nerve regeneration using genipin-treated gelatin and found that this material led to an adequate nerve regeneration and functional recovery.[37] Additionally, several researchers identified that genipin treated tissues and scaffolds support cellular viability, adhesion and proliferation while preserving cellular activities and function.[41],[42],[43]

The focus of this work is on describing genipin-induced modifications of collagen micro- and nano- structures within 3D collagen hydrogels while relating these changes to the induced fluorescence. However, our findings carry very broad implications. The optical methods we developed, describe cohesively the spectral properties for the reaction products between proteins and a genipin compound. In addition to aiding the development of collagen hydrogel standardization protocols for tissue engineering applications, our work can lead to a better understanding of the *in-situ* reactions between a genipin compound and proteins. It will also possibly enhance and/or move forward the applications of genipin in various fields.

Fluorescence recovery after photobleaching of cross-linked collagen hydrogels

The MPM was used to examine the generation of genipin induced fluorescence within collagen hydrogel and we then applied FRAP to confirm the induction of fluorescence. Glyceraldehyde crosslinked hydrogels were used as the comparison because the glyceraldehyde reacting with collagen generates fluorescence as well.[44] The reaction between glyceraldehyde and collagen is known as glycation which produces the

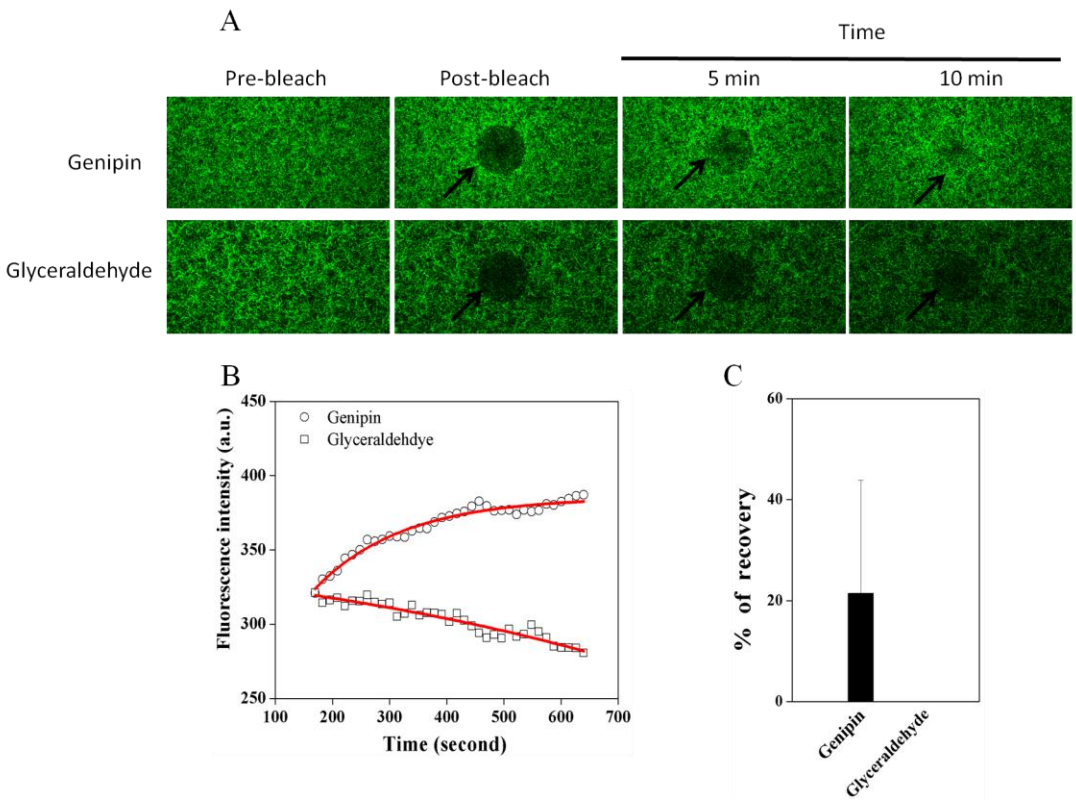

Figure 6. Fluorescence recovery after photobleaching of 3D collagen hydrogels crosslinked with genipin and glyceraldehyde. (A) A region of interest (ROI) was photobleached (arrow). Time series of images taken before, 1 min after, and 5 min, 10 min after photobleaching are presented. (B) The curves represent the first order exponential fitting from the average of 6 different areas within collagen hydrogels (C) The values represent percentages of recovery at 10 min after photobleaching of a ROI.

fluorophores called advanced glycation end-products (AGEs). FRAP images show that the genipin-induced fluorophores can be generated within the bleached spot within 3D collagen hydrogels but the AGEs are immobile (Figure 6). Within the genipin cross-linked hydrogels, the fluorescence diffused into the bleached region 5 min after the bleach. The diffusion of fluorophores stopped around 10 min after the bleach. Within glycated hydrogels, no recovery of fluorescence can be detected 10 min subsequent of the bleach event (Figure 6A). Based on the FRAP images shown in Figure 6A, the FRAP

kinetics of fluorescence recovery is plotted in Figure 6B. Figure 6C shows that the percentage of fluorescence recovery of genipin induced fluorophores is 21%.

Both genipin and glyceraldehyde modify the structure within collagen hydrogels but only the genipin induced fluorophores can diffuse within the hydrogels. This discrepancy in fluorescence recovery presumably arises from the formation of new fluorophores within genipin cross-linked hydrogels. We believe the observation of fluorescence within the photobleached region should be due to induction of fluorophores rather than diffusion. Our data shown in Figure S2 which the fluorescence is generated by UV light induction might support our assumption. The fluorophores might be formed by the self reaction of genipin molecules. The large error bar shown in Figure 6C could also be contributed from the unevenly formation of fluorophores in different area within hydrogles. The area where more fluorophores form has higher percentage of fluorescence induction and vice versa. We concluded that the induction of fluorescence is not dependent on the structural modification within collagen hydrogels.

Conclusion

We investigated the effects of genipin cross-linking on collagen hydrogels using a combination of different techniques. Specifically, we probed *in situ* one-photon fluorescence of induced photoproducts formed during cross-linking collagen hydrogels with 1 mM and separately with 10 mM genipin solutions. We then characterized the micro- and nano-structures within cross-linked hydrogels by examining second harmonic generation (SHG) and transmission electron microscopy (TEM) images respectively. We

also used fluorescence recovery after photobleaching to examine the diffusion of fluorophores within 3D collagen hydrogels. Both concentrations of genipin induced strong autofluorescence and appreciable micro- and nanostructural changes within collagen hydrogels. The ten-millimolar genipin cross-linked collagen samples generated similar final amount of fluorescence compared to those cross-linked with one-millimolar genipin. However, the ten-millimolar genipin cross-linked collagen samples were modified at a faster rate. Interestingly, the observed one-photon emission maximum was strongly dependent on the excitation wavelength. For example, the emission maximum was at 630 nm when we excited the cross-linked samples with 590 nm light. It would shift to 590 nm or 462 nm when we instead used 543 nm or 400 nm light respectively to excite the samples.

The second harmonic generation images demonstrated a remodeling of microscopic "fiber-like" structures throughout the collagen hydrogels. When the genipin cross-linking time reached 48 hours, the short 5 – 10 μm structures became modified to long, aggregated threads with lengths longer than 20 μm. The transmission electron microscopy imaging further revealed that the majority of native striated fibrils changed to non-striated filaments or fibrils with non-native striation patterns. There was no principle difference in the type of micro- or nano- structures formed upon incubating collagen gels in 1 mM versus 10 mM genipin solutions. Only the rate of cross-linking was affected. The FRAP results show that a new type of fluorophores can be induced to form within the collagen hydrogels. The knowledge obtained through this work provides us with a better

understanding how to effectively cross-link and how to monitor the extent of cross-linking of tissues and biologically derived scaffolds with a genipin reagent.

References

(1) Tibbitt, M. W.; Anseth, K. S. *Biotechnol. Bioeng.* **2009**, *103*, 655-663.

(2) Sung, H.; Huang, R.; Huang, L. H.; Tsai, C.; Chiu, C. *J. Biomed. Mater. Res.* **1998**, *42*, 560-567.

(3) Sung, H.; Liang, I.; Chen, C.; Huang, R.; Liang, H. *J. Biomed. Mater. Res.* **2001**, *55*, 538-546.

(4) Sung, H.; Chang, W.; Ma, C.; Lee, M. *J. Biomed. Mater.Res.* **2003**, *64A*, 427-438.

(5) Sung, H.; Huang, D.; Chang, W.; Huang, R.; Hsu, J. *J. Biomed. Mater. Res.* **1999**, *46*, 520-530.

(6) Lee, S.; Lim, J.; Bhoo, S.; Paik, Y.; Hahn, T. *Anal. Chim. Acta* **2003**, *480*, 267-274

(7) Almog, J.; Cohen, Y.; Azoury, M.; Hahn, T. *J. Forensic Sci.* **2004**, *49*, 255-257.

(8) Levinton-Shamuilov, G.; Cohen, Y.; Azoury, M.; Chaikovsky, A.; Almog, J. *J. Forensic Sci.* **2005**, *50*, 1367-1371.

(9) Chen, Y. S.; Chang, J. Y.; Cheng, C. Y.; Tsai, F. J.; Yao, C. H.; Liu, B. S. *Biomaterials* **2005**, *26*, 3911-3918.

(10) Chang, W.; Chang, Y.; Lai, P.; Sung, H. *J. Biomater. Sci.* **2003**, *14*, 481-495.

(11) Chen, S. C.; Wu, Y. C.; Mi, F. L.; Lin, Y. H.; Yu, L. C.; Sung, H. W. *Journal of Controlled Release* **2004**, *96*, 285-300.

(12) Yao, C. H.; Liu, B. S.; Hsu, S. H.; Chen, Y. S. *Biomaterials* **2005**, *26*, 3065-3074.

(13) Zipfel, W. R.; Williams, R. M.; Christie, R.; Nikitin, A. Y.; Hyman, B. T.; Webb, W. W. *Proc. Natl. Acad. Sci. USA* **2003**, *100*, 7075-7080.

(14) Raub, C. B.; Suresh, V.; Krasieva, T.; Lyubovitsky, J.; Mih, J. D.; Putnam, A. J.; Tormberg, B. J.; Geroge, S. C. *Biophys. J.* **2006**, *92*, 2212-2222.

(15) Brown, E.; McKee, T.; DiTomaso, E.; Pluen, A.; Seed, B.; Boucher, Y. *Nat. Med.* **2003**, *9*, 796-801.

(16) Campagnola, P. J.; Millard, A. C.; Terasaki, M.; Hoppe, P. E.; Malone, C. J.; Mohler, W. A. *Biophys. J.* **2002**, *82*, 493-508.

(17) Guo, Y.; Savage, H. E.; Liu, F.; Schantz, S. P.; Ho, P. P.; Alfano, R. R. *Proc. Natl. Acad. Sci. USA* **1999**, *96*, 10854-10856.

(18) Masters, B. R.; So, P. T. C. *Microsco. Res. Techniq.* **2004**, *63*, 3-11.

(19) Moreaux, L.; Sandre, O.; Charpack, S.; Blanchard-Desce, M.; Mertz, J. *Biophys. J.* **2001**, *80*, 1568-1574.

(20) Raub, C. B.; Suresh, V.; Krasieva, T.; Lyubovitsky, J.; Mih, J. D.; Putnam, A. J.; Tromberg, B. J.; George, S. C. *Biophys. J.* **2006**, *92*, 2212-2222.

(21) Schenke-Layland, K.; Riemann, I.; Damour, O.; Stock, U. A.; Konig, K. *Advance Drug Delivery Reviews* **2006**, *58*, 878-896.

(22) Williams, R. M.; Zipfel, W. R.; Webb, W. W. *Biophys. J.* **2005**, *88*, 1377-1386.

(23) Zipfel, W. R.; Williams, R. M.; Christie, R.; Nikitin, A. Y.; Hyman, B. T.; Webb, W. W. *Proc. Natl. Acad. Sci. USA.* **2003**, *100*, 7075-7080.

(24) Yeh, A. T.; Nassif, N.; Zoumi, A.; Tromberg, B. J. *Optics Letters* **2002**, *27*, 2082-2084.

(25) Legare, F.; Pfeffer, C.; Olsen, B. R. *Biophys. J.* **2007**, *93*, 1312-1320.

(26) Hwang, Y.; Lyubovitsky, J. G. *Anal. Methods* **2011**, *3*, 529-536.

(27) Roth, S.; Freund, I. *J.Chem.Phys.* **1979**, *70*, 1637-1643.

(28) Chen, H.; Ouyang, W.; Lawuyi, B.; Martoni, C.; Prakash, S. *J. Biomed. Mater. Res.* **2005**, *75A*, 917-927.

(29) Sundararaghavan, H. G.; Monteior, G. A.; Lapin, N. A.; Chabal, Y. J.; Miksan, J. R.; Shreiber, D. I. *J. Biomed. Mater. Res.* **2008**, *87A*, 308-320.

(30) Leddy, H. A.; Guilak, F. *Ann. Biomed. Eng.* **2003**, *31*, 753-760.

(31) Erikson, A.; Anderson, H. N.; Naess, S. N.; Sikorski, P.; Davies, C. L. *Biopolymers* **2008**, *89*, 135-143.

(32) Lelu, S.; Pluen, A. *Macromol. Symp.* **2007**, *256*, 175-188.

(33) Ramanujan, S.; Pluen, A.; McKee, T. D.; Brown, E. B.; Boucher, Y.; Jain, R. K. *Biophys. J.* **2002**, *83*, 1650-1660.

(34) Luu, D.; Martiniere, A.; Sorieul, M.; Runions, J.; Maurel, C. *The Plant J.* **2012**, *69*, 894-905.

(35) Axelrod, D.; Koppel, D. E.; Schlessinger, J.; Elson, E.; Webb, W. W. *Biophys. J.* **1976**, *16*, 1055-1069.

(36) Bultier, M. F.; Ng, Y.; Pudney, P. D. A. *J. Polym. Sci Part A: Poly. Chem.* **2003**, *41*, 3941-3953.

(37) Chen, H.; Ouyang, W.; Lawuyi, B.; Martioni, C.; Prakash, S. *J. Biomed. Mater. Res.* **2005**, *75A*, 917-927.

(38) Sisson, K.; Zhang, C.; Farach-Carson, M. C.; Chase, D. B.; Rabolt, J. F. *Biomacromolecules* **2009**, *10*, 1675-1680.

(39) Avila, M. Y.; Navis, J. L. *J. Cataract Refract Surg.* **2010**, *36*, 659-664.

(40) Yan, L., ;; Wang, Y.; Ren, L.; Wu, G.; Caridade, S. G.; Fan, J.; Wang, L.; Ji, P.; Oliverira, J. M.; Mano, J. F.; Reis, R. L. *J. Biomed. Mater. Res.* **2010**, *95A*, 465-475.

(41) Yu, X.; Liu, F.; Xu, Y.; Wang, C. *J. Mater. Sci: Mater. Med.* **2010**, *21*, 777-785.

(42) Hwang, Y.; Kolettis, N.; Yang, M.; Gillard, E. R.; Sanchez, E.; Sun, C.; Tromberg, B. J.; Krasieva, T. B.; Lyubovitsky, J. G. *Photochem. Photobiol.* **2010**, *87*, 408-417.

(43) Lau, T.; Wang, C.; Png, S.; Su, K.; Wang, D. *J. Biomed. Mater. Res.* **2011**, *96A*, 204-211.

(44) Hwang, Y.; Granelli, J.; Lyubovitsky, J. G. *Anal. Chem.* **2011**, *83*, 200-206.

Appendices

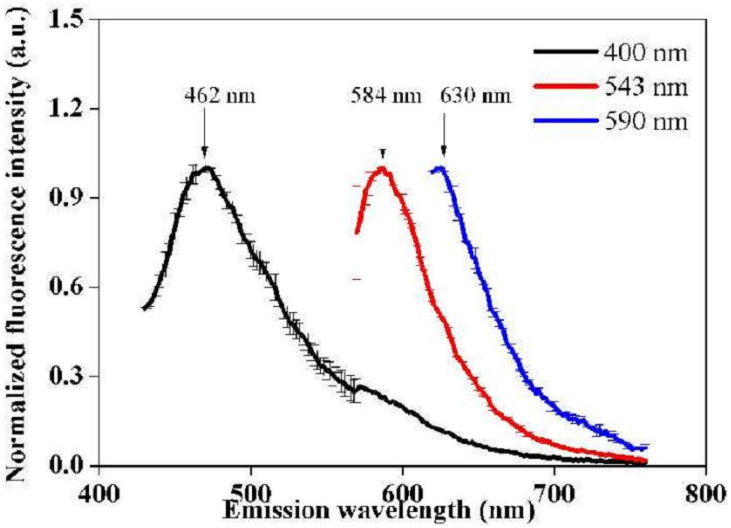

Figure S1. Fluorescence spectrum of genipin cross-linked collagen hydrogels excited with different wavelengths.

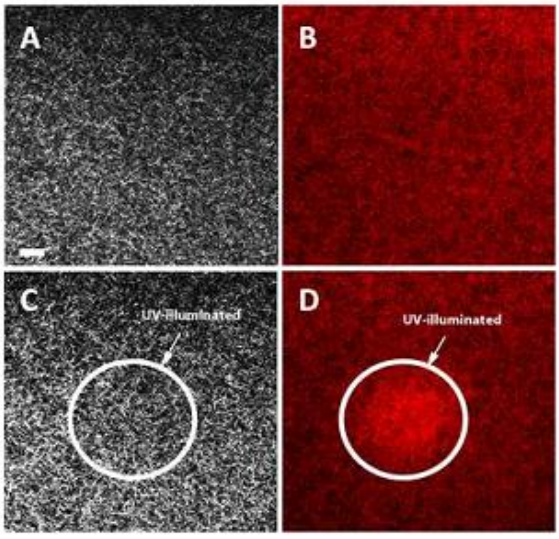

Figure S2. Ultra-violet excitation of genipin induced fluorescence. (A)SHG images before UV excitation. (B) Fluorescence image before UV excitation. (C) SHG image of the area within white circle illuminated with UV. (D) Fluorescence image of the area within white circle illuminated with UV.

CHAPTER 7

THE MICROSTRUCTURAL EFFECTS OF COLLAGEN HYDROGELS ON CELLULAR DIFFERENTIATION INTO NEURONS

Abstract

We compared the G-Olig2 embryonic stem cell and induced pluripotent stem cell (iPS) behaviors during early differentiation with retinoic acid into a neural lineage employing separately the encapsulated or topographic 3D collagen hydrogel models. For the encapsulated 3D models, the cells were polymerized within hydrogels prepared from two different initial concentrations 2 g/l and 4 g/l and differentiated *in situ*. For the topographic 3D model, the embryonic stem cells were differentiated on top of the hydrogels cross-linked with EDC, EDC/NHS (4 parts of EDC mixed with 1 part of NHS) or genipin and compared to the cells differentiated on the not cross-linked controls. In addition, two different collagen assembly factors were also examined which are initial collagen concentration (2 g/l and 4 g/l) and incubation temperature (27 ℃ and 37 ℃). The iPS cells were differentiated on top of the genipin cross-linked hydrogels and compared to the cells differentiated on the not cross-linked controls. The G-Olig2 embryonic stem cell and iPS cell differentiation was slower for the cells encapsulated within 4 g/l collagen hydrogels compared to 2 g/l once. The G-Olig2 embryonic stem cells' differentiation process on top of the 3D collagen hydrogels was affected by the cross-linking. For example, for the unmodified collagen hydrogels, the response of the differentiating ES cells consisted of cellular differentiation concomitant with cellular migration and subsequent aggregation into the clusters. The collagen of the supporting

extracellular matrix became highly aligned at the periphery of the cluster formed. The G-Olig2 differentiated stem cells remained scattered on top of the cross-linked materials. The cells were able to align collagen fibers in the materials modified with EDC while making only a clearance and no alignment of collagen fibers in the case of EDC/NHS and genipin modifications. The differentiation rate of ES cells is slower in cross-linked hydrogels. Different assembly factor also affects the differentiation process of ES cells. The differentiated cells were unable to align the collagen structure with hydrogels assembled at 4 g/l or 27 °C. The iPS cells' differentiation process on top of the cross-linked hydrogels was also affected. For example, the differentiated cells also realigned the surrounding collagen structure and no alignment was observed in genipin cross-linked hydrogels and the differentiation rate was faster in genipin cross-linked hydrogels. The data and methods developed provide an outline to monitor non-destructively *in situ* the extent of differentiating the embryonic stem cells on and within collagen-based substrates in tissue engineering applications.

Introduction

Regenerative medicine is an evolving and promising field which has a strong potential to treat the diseases which are currently incurable. The goal of regenerative medicine is to create functional tissues/organs to repair or replace the damaged ones. The main components in creating the tissue replacement are stem cells and biomaterials. In order to translate these researches from benchtop to bedside, the priority is to be able to attain the

ability to tailor the cell-material interaction and then gain control over stem cell behaviors such as migration, proliferation and differentiation[1, 2].

The main goal of our works was to attain a better understanding of the dynamic interplay between the differentiating embryonic stem cell behaviors and the collagen hydrogels' micro-environments. Our previous works identified that collagen materials assembled at different initial collagen concentrations and incubation temperatures have different structure[3] and different cross-linking reagents such as genipin and carbodiimide have different effect on the structure within collagen materials[4, 5]. These well characterized collagen hydrogels were incorporated with two types of stem cells, embryonic stem cells and induced pluripotent stem cells. Two cells seeding methods were applied, one is encapsulation and the other is topologically seeded. For all the models, retinoic acid was used to induce the neuronal differentiation of stem cells. Among the chemical factors, retinoic acid has been found to successfully induce embryonic stem cell differentiation to neuronal lineage cells[6-9].

To clearly examine the differentiating behavior of stem cell, multi-photon microscopy (MPM) was employed. MPM which is a non-linear optical imaging method can accomplish that with high contrast in 3D while having resolution comparable to the confocal imaging methods. MPM combines backscattered second harmonic generation (SHG) and two-photon fluorescence (TPF) signals suitable for obtaining structural and functional information at depth in thick living tissues [10-27]. The fluorescent contrasts

afford further opportunities to understand remodeling within biomaterials [5, 28] when biomaterials interact with cells and tissues.

The embryonic stem cell we used in this work is the mammalian embryonic G-Olig2 stem cell line. The G-Olig2 reporter system was created by the insertion of green fluorescence protein (GFP) into the locus of Olig2 thus allowing the expression of GFP to indicate the expression of the endogenous gene[29]. The Olig2 is one of the basic helix-loop-helix transcriptional factors which play a significant role in neuronal differentiation pathway of embryonic stem cells especially in the development of motor neurons and oligodendrocytes [30-32]. The development of these two cell types requires the expression of Olig2 in the spinal cord[33, 34]. In the mouse spinal cord, Olig2 first expresses in the progenitor cells[33]. The expression of Olig2 continues when the progenitor cells differentiate to oligodendrocytes; however, the Olig2 expression is down-regulated when the progenitor cells give rise to the motor neurons[35].

In addition to G-Olig2 stem cell lines, induced pluripotent stem cells (iPS) a7.wt cell line was also used. iPS cell was first generated by retroviral introducing genes encoding four transcription factors to mouse embryonic and adults fibroblast[36]. iPS cells were identified to possess similar properties to embryonic stem cells such as morphology, proliferation, the expression of some ES cell marker genes and the formation of teratomas[37]. This cell type holds great potential in medical and pharmaceutical application however several obstacles needed to be resolved, such as aberrant reprogramming, and increased possibility of teratomas formation, before iPS cells could fully utilized[38].

Our studies examining the cellular interactions with these various characterized 3D hydrogels confirm that in 3D collagen hydrogels cellular differentiation is controlled by the encapsulation and not simply by the chemical induction with a retinoic acid. Second, when the G-Olig2 stem cells and iPS cells are differentiated on top of the 3D collagen hydrogels, the cellular morphologies and collagen fibers observed during the differentiation process and the differentiation process itself differs based on if the gels are stabilized with the cross-linking reagents or not. The cross-linking collagen hydrogels with zero-length cross-linker carbodiimide as opposed to non-zero cross-linker genipin affects the differentiation process in a somewhat similar manner. Considering that modification with genipin has a different effect on microstructure compared to carbodiimide, the differentiation process appears to be affected by the differences in collagen micro-structures. These results advance our understanding of how scaffold architecture can control cell fates. The ability to manipulate the structure of collagen materials and the manipulated structure can affect the stem cell behavior increase s the potential of using biomaterial and stem cells to treat the neuronal degenerative disease.

Experimental Section

Reprogramming and derivation of murine induced pluripotent stem (IPS) cell line a7,wt

Mouse embryonic fibroblast (MEF) cells were extracted from day12.5 mouse embryos. MEF cells were maintained in Dulbecco's Modified Eagle Media (DMEM) supplemented with 10% fetal bovine serum (FBS), 1 mM L-glutamine, 0.1 mM non-essential amino acid (NEAA) and 1X sodium pyruvate. MEF cells were used at passage 2 (P2) for

reprogramming by retroviral transduction using four transcription factors, OCT4, SOX2, KLF4 and CMYC as previously described[39]. On day 6, reprogrammed MEF cells were splitted and cultivated in mouse ES media (DMEM, 15% FBS, 1 mM L-glutamine, 0.1 mM NEAA, 0.1 mM BME, beta mercaptoethanol and 1000U/ml LIF, leukemia inhibitory factor) to facilitate IPSC derivation. Media were changed daily. On day 28, individual mouse IPS cell colonies were picked, transferred to feeder layers on 0.1% gelatin-coated dishes and expanded in mouse ES media. Established mouse IPSC clones were splitted 1:5 every 3 days using 0.25% trypsin/EDTA and subcultivated on fresh layers of feeder layers. The creation of this iPS cell line was done by Dr. Duncan Liew.

Murine embryonic stem cell and murine induced pluripotent stem (IPS) cell culture

Cells of the embryonic stem cell line G-Olig2 (ATCC, SCRC-1037) and IPS cell line a7,wt (UCR stem cell core facility) were cultured on mouse embryonic fibroblast (ATCC, CCL163) in Advanced DMEM (Dulbecco's Modified Eagle Medium, 12491) with 0.1 mM β-mercaptoethanol (Sigma) and Leukemia Inhibitory Factor (LIF) at a concentration of 1000 U/ml. Medium was changed daily. The phase contrast images were obtained daily with an inverted tissue culture microscope (Tissue Culture Microscopes http://www.tissueculturemicroscopes.com/). The phase contrast images were collected with a 20x objective (0.4 NA).

Three-dimensional encapsulated cellular differentiation model

The final collagen concentrations applied here were 2.0 mg/ml and 4.0 mg/ml. An ice-cold collagen mix was prepared consisting of 6.5 parts of collagen type I (BD

Biosciences, 354249), 1 parts of reconstitution buffer (10×) and 2 parts of DMEM growth medium (Gibco Cat. No. 12800-058, 5×). For the 6.5 parts of collagen solution, 3.0 mg/ml was used for the final concentration of 2.0 mg/ml and 6.2 mg/ml was used for the final concentration of 4.0 mg/ml. The 3.0 mg/ml and 6.2 mg/ml collagen solution was corrected from the 8.58 mg/ml collagen stock. The 10× reconstitution buffer was prepared by combining 2.2 g of $NaHCO_3$ (tissue culture grade) and 4.77 g HEPES (tissue culture grade, Gibco Cat. No 845-1344) in a 100 mL medium bottle, adding 75 mL of 0.05 N NaOH added to a 95 mL doubly distilled, deionized water to the sodium bicarbonate and HEPES powder, mixing well to dissolve and bringing the solution to the final volume of 100 mL with 0.05 *N* NaOH. The buffer was filter sterilized with 0.22 μm filter into a sterile medium bottle and stored at 4℃. After three components were mixed and pH was adjusted to neutral, cells in 0.5 parts of 1X PBS buffer were added to the mixture. The mixture was pipetted into each well of 8-well chambered slide and incubated at 37 ℃ until the gels were formed. After the gels were formed, the stock solution of retinoic acid was diluted with Advanced DMEM to bring the concentration to 2×10^{-6} M and then pipetted to each gel. The retinoic acid was changed daily. The number of cell in each gel was 3×10^4 cells.

Three-dimensional topographic cellular differentiation model

Soluble rat-tail type I collagen, 8.58 mg/ml (BD Biosciences, 354249) was in 0.02 N acetic acid. The stock solution was diluted with 0.02 N acetic acid to obtain the 2X collagen aliquots. 2X initiation buffers were prepared from NaCl and phosphate buffer.

The concentration of mono-and dibasic phosphate in the buffer at pH=7.4 were calculated with Henderson-Hasselbalch equation. The pH was adjusted drop-wise with 1N NaOH or HCl. Ionic strength was adjusted with NaCl. The initiation buffer had the following components: 6.40 g/l K_2HPO_4; 3.16 g/l KH_2PO_4; 38.55 g/l NaCl (ionic strength = 0.6 M). After the pH was adjusted to a desired value, the initiation buffer was filtered with a 0.22 μm filter (Millipore, Millex GV Filter, Cat # SLGV003RS) and stored at 4℃. Material formation was initiated by mixing 2X collagen aliquot with 2X initiation buffer on ice at 1:1 ratio, verifying the pH to be 7.4±0.1. The mixture was pipetted into each well of 8-well chambered slide (MP Biomedical) and then incubated at 37 ℃ for 24 hours. The final collagen concentration of the materials is 2.0 mg/ml. 1mM Genipin, 0.1M EDC and 0.1 M EDC/.025 M NHS solutions were prepared by dissolving genipin (Sigma) in 1X PBS buffer (Invitrogen, Dulbecco's Phosphate-Buffered Saline, 14190) and adjusting pH to 7.4 with 1N NaOH. The cross-linking solutions were sterilized with a 0.22 μm filter (Millipore, Millex GV Filter, Cat # SLGV003RS) and stored at 4℃. The cross-linking reagents were added to each polymerized collagen-containing well. The materials were incubated at 37 ℃ for 24 hour. After 1 day of collagen incubation with cross-linking reagents, the materials were rinsed with 1X PBS buffer, refilled and incubated with PBS for 20 min. This was repeated for 3 times at room temperature. PBS buffer was removed and Advanced DMEM was pipetted to each well and then incubated at 37 ℃ for 24 hour to equilibrate the gels with medium. All procedures were performed under the hood and using sterile techniques. The stock solution of retinoic acid at the concentration of 2×10^{-5} M was prepared by dissolving retinoic acid (Sigma, R2625) in DMSO (Sigma, D2650).

The stock solution was filtered with 0.20 μm nylon filters (Corning, 431224) and then stored at -80 ℃. For seeding on collagen gels, 3×10^4 cells were pipetted to each gel and then incubated at 37 ℃ for 3 hours. When the cells attached to the gels, the stock solution of retinoic acid was diluted with Advanced DMEM to bring the concentration to 2×10^{-6} M and added to each gel. The retinoic acid was refreshed daily.

Multiphoton microscopy (MPM) imaging

The inverted multiphoton laser scanning microscope used in this work was the Zeiss LSM 510 NLO Meta microscopy system. It is based on an Axiovert 200M inverted microscope equipped with standard illumination systems for transmitted light and epi-fluorescence detection. It was also equipped with an NLO interface for a femtosecond titanium: sapphire laser excitation source (Chameleon-Ultra, Coherent, Incorporated, Santa Clara, CA) for multiphoton excitation. The Chameleon laser provided femtosecond pulses at a repetition rate of about 80 MHz, with the center frequency tunable from 690 to 1040 nm. A long working distance objective (Zeiss, 40x water, N.A. 0.8) was used to acquire images shown in this work. The signals from the samples were epi-collected and discriminated by long pass 650 nm dichroic beamsplitter. The SHG images were collected with the 390-405 nm band-pass filter (λ_{ex} = 800 nm). The NADH fluorescent images were collected with the 390-465 nm band-pass filter and FAD^+ fluorescent images were collected with 530-590 nm band-pass filter (λ_{ex} = 770 nm). Each image presented in this work is 12 bit, 512 x 512 pixels representing 225 μm x 225 μm

field of view. All the images were repeated on different days for two times and two samples were imaged on each day.

Results and Discussion

For all of our 3D stem cell models we added the retinoic acid (RA) at the concentration of 2×10^{-6} M starting from day 0. Retinoic acid (RA) is a biologically active form of vitamin A, and plays an important role in the development of central nervous system. It had been found to induce the differentiation of embryonic stem (ES) cells into the neural lineage cells in a concentration- and culture time-dependent manner *in vitro*. Higher concentration of RA (2×10^{-6} M) increases the expression level of markers of neural differentiation, such as postmitotic neurons (βIII-tubulin-positive), astrocytes (GFAP-positive) and neuronal progenitors (Ngn2-positive) and modulate Olig2 expression.[9] Olig2 is expressed at day 2 and down regulated by day 4 post induction indicating low numbers of the undifferentiated neural progenitor cells by day 4 time point. Applying the RA to ES cells between day 0 to day 2 leads to the highest percentage of neurogenesis.[40]

Embryonic stem cells

Three-dimensional encapsulated cellular differentiation model

The encapsulation or embedding of stem cells in collagen hydrogels during the differentiation can potentially be an effective method to deliver them to the injured areas. To determine the effect of different microstructure on the extent of differentiation of stem cells into neuronal lineage cells we encapsulated them in hydrogels prepared separately at

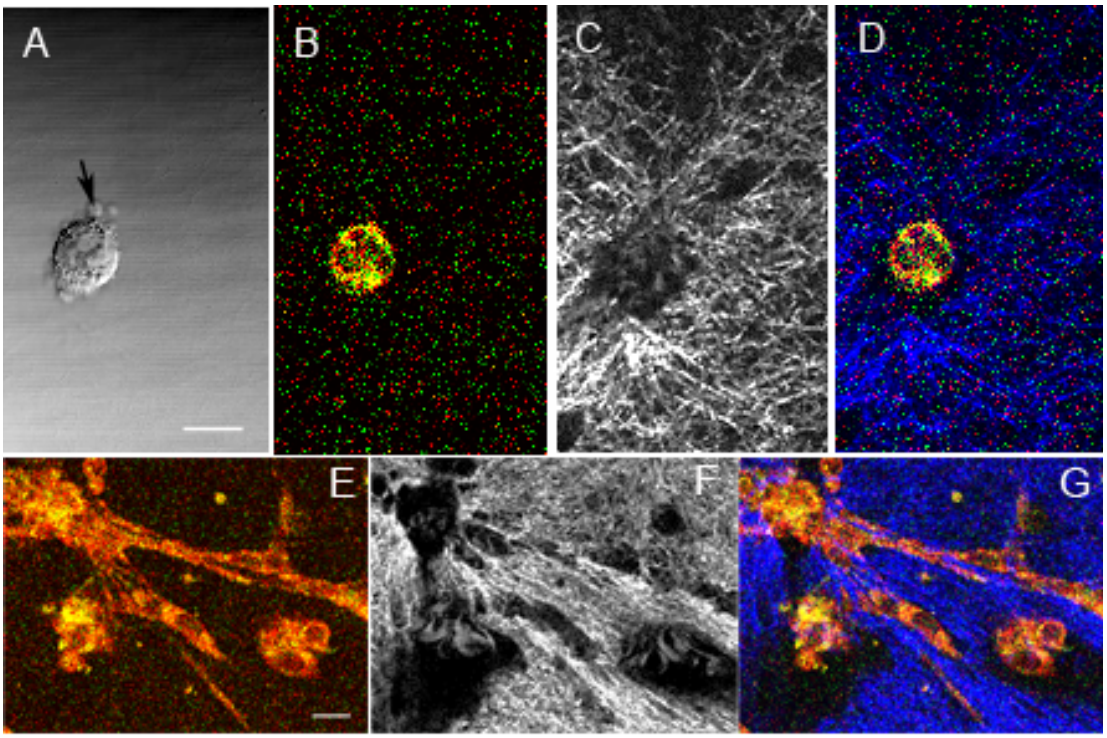

Figure 1. Multi-photon optical signals from the 3D models with G-Olig2 cell stem cells embedded in 4g/l (A-D) and 2 g/l (E-G) collagen hydrogels. Day 6 post induction of differentiation with the retinoic acid. (A)True-focus transmitted image showing overall arrangement of the stem cells during recording. The arrow points to a ~5 μm bleb we observe in the undifferentiated stem cell; (B) and (E) The multiphoton ratiometric redox fluorometry imaging of the G-Olig2 stem cells in the 3D stem cell model. λex = 770 nm. Red, NADH; green, FAD. The two colors are superimposed. (C) and (F) Second harmonic generation signal of surrounding collagen matrix. λex = 800 nm; (D) and (G) Images in (B) and (C) are superimposed and (E) and (F) are superimposed. Focusing objective (Zeiss; 40x water immersion; NA is 0.8) was used to collect 250 μm × 250 μm images. Scale bar is 25 μm.

2 g/l and 4g/l initial collagen concentrations. Different packing of collagen 'fiber-like' structures exists within the collagen hydrogels when they are polymerized from these two different initial concentrations [3] resulting in different rigidity. In Figure 1 we show that the stem cell differentiation is controlled by the encapsulating collagen microstructure and not simply by a chemical induction with a retinoic acid employed. G-Olig2 stem cell morphologies for cells embedded in 4 g/l (A-D) as opposed to 2 g/l (E-G) collagen

hydrogels as imaged at day 6 post induction are very different. Specifically, the embryonic stem cells that have been embedded in the 4 g/l collagen hydrogels remain largely undifferentiated at this time point (Figure 1A, true focus image) while the stem cells embedded in 2 g/l hydrogels had fully differentiated and migrated to make the connections with the nearby cells (Figure 1E). The highly processed extracellular matrix (ECM) can also be noted in the second harmonic generation images (Figure 1F) with intricate invaginations formed at the point of contact of cells with the ECM.

These observations and implications are important within the context of preparation of 3D cell-laden tissue engineered materials to be used as vehicles in regenerative medicine applications[41]. We have changed an initial concentration of collagen molecules from which the hydrogel was prepared, which in turn altered the micro- structural packing of the materials. The hydrogels prepared from higher initial concentration slowed down the RA induced differentiation of embryonic stem cell. The mechanism for this delayed differentiation is not clear. Cellular ability to translocate the fibers during migration, materials' stiffness and to a lesser extent a pore size could all play some role. For example, Miron-Mendoza et al.[42] had previously established that upon migration, fibroblasts translocate the collagen fibrils toward the cells in the collagen hydroges prepared at low concentration (1 g/l) while fibrils stayed stationary for the matrices prepared at higher (4 g/l) concentration. For the 2 g/l collagen hydrogel that we used in our work, the pore size was determined from the scanning electron microscopy (SEM) images as ~ 2 μm^2 while for the 4 g/l it decreases to ~1 μm^2. Stiffness (storage modulus)

of the matrices using an oscillating rheometer was 20 Pa for 2 g/l hydrogels and 62 Pa for the 4 g/l hydrogels.

Three-dimensional topographic cellular differentiation model

To determine the effect of differentiating stem cells on top of collagen hydrogels when cells are presented with different topographic information as opposed to encapsulated cells, we seeded G-Olig2 stem cells on top of collagen hydrogels prepared at 2 g/l. In one set of differentiation experiments, the cells were seeded and differentiated directly on top of the pre-formed hydrogels. In another set of experiments the cells were seeded and differentiated on the pre-formed collagen hydrogels that were cross-linked separately with non-toxic reagents 100 mM carbodiimide, 100 mM carbodiimide/NHS and 1 mM

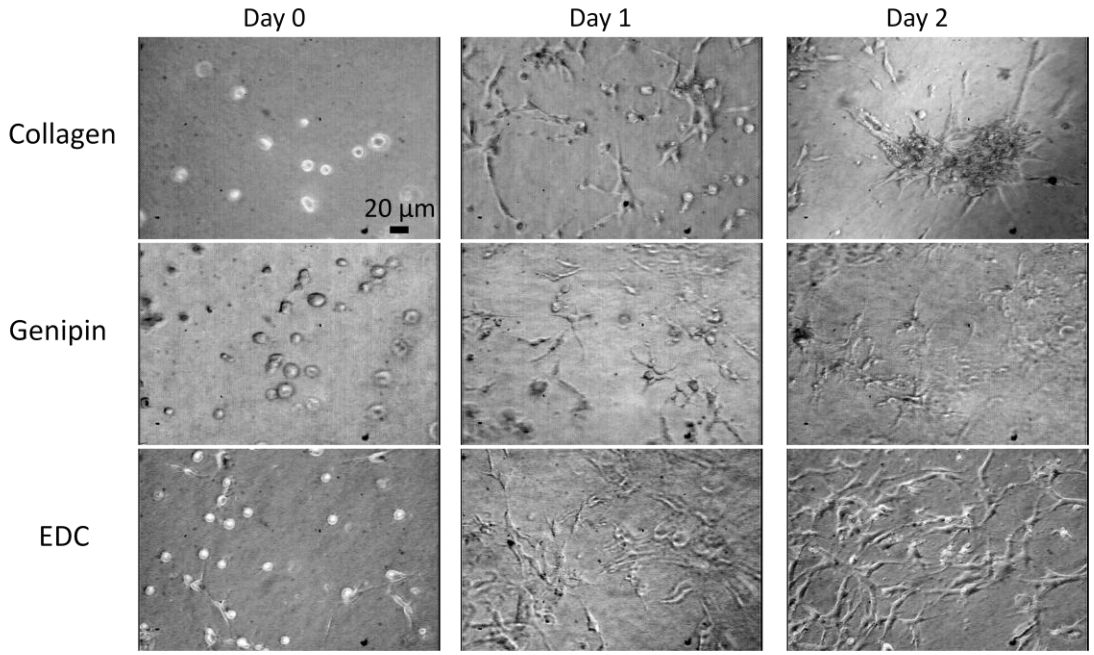

Figure 2. Phase contrast images of the G-Olig2 stem cell differentiated on top of not cross-linked and cross-linked 2 g/l collagen hydrogels. Day 0, day 1 and day 2 post induction of differentiation with the retinoic acid is shown for different cross-linking reagents. Scale bar is 20 µm

genipin. Figure 2 summarized the extent of differentiation within the first few days. For the collagen hydrogels, the response of the differentiating stem cells consisted of cellular differentiation concomitant with cellular migration and subsequent aggregation into the clusters seen in Figure 2 top panels. The differentiation took place prior to the cluster formation for the G-Olig2 stem cell line. On the EDC (Figure 2, bottom panels), EDC/NHS (not shown) and genipin (Figure 2, middle panels) strengthened collagen hydrogels, there was no clustering observed, however, the differentiating G-Olig2 stem cells appeared more slender on the genipin stabilized materials as compared to those strengthened with EDC or EDC/NHS. The differentiation rate is around the same for the cells seeded on non-crosslinked and EDC or EDC/NHS cross-linked gels but the rate is slower for the cells seeded on genipin cross-linked gels.

Figure 3 shows the multiphoton images of differentiated cells seeded on non-crosslinked and genipin-crosslinked gels 5 days post induction. The true-focused images show that the differentiating cells formed a cluster on top of the non-crosslinked gels and the stem cells differentiating on the genipin-modified collagen hydrogels remained scattered on the top of hydrogels as well and only a few cells were able to migrate into the genipin cross-linked materials (Figure 3A and 3E). We then examined the collagen of the supporting extracellular matrix, which as seen in Figure 3C became highly aligned at the periphery of the cluster and removed in the area directly under where the cluster resided comparing to the structures before the cells are seeded (Figure 3D). Moreover, the alignment of collagen fiber amplified the SHG signals. The materials themselves exhibited low second harmonic generation signals due to the genipin modification[43] and

the fibers induced as a result of collagen modification with genipin were largely

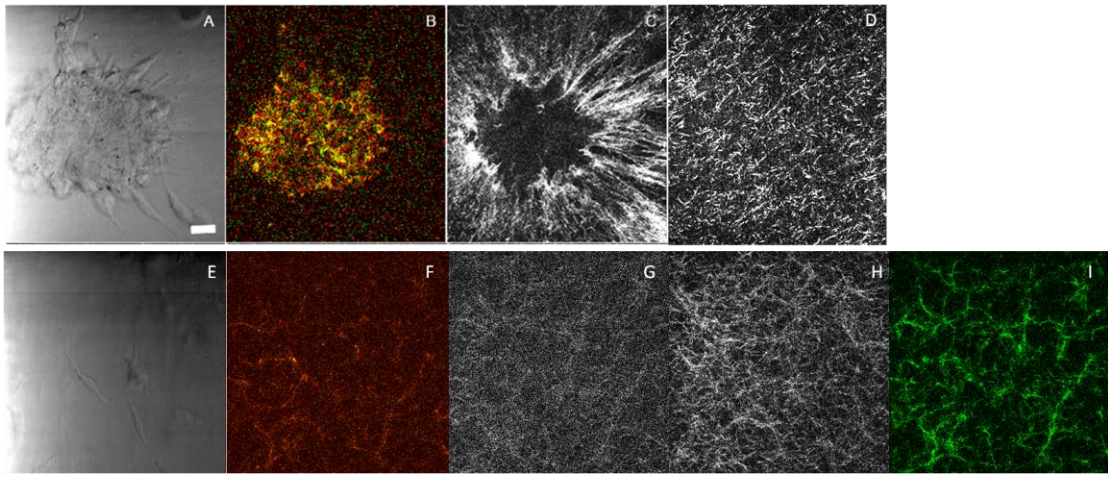

Figure 3. Multi-photon optical signals from the 3D models with G-Olig2 stem cells differentiated on top of not cross-linked (A- D) and genipin cross-linked (E-I) 2 g/l collagen hydrogels. Day 5 post induction of differentiation with the retinoic acid (A) and (E) True-focus image of a typical differentiating cellular cluster that forms when cells are cultured on top of collagen hydrogels; (B) and (F) The multiphoton ratiometric redox fluorometry imaging of the G-Olig2 stem cells in the 3D stem cell model. λex = 770 nm. Red, NADH; green, FAD. The two colors are superimposed. (C) and (G) Second harmonic generation signal of surrounding collagen matrix after cells were seeded. λex = 800 nm; (D) and (H) Second harmonic generation signal of surrounding collagen matrix before cells were seeded. λex = 800 nm; (I) Fluorescence of fibers induced as a result of cross-linking collagen with genipin. Focusing objective (Zeiss; 40x water immersion; NA is 0.8) was used to collect 250 μm × 250 μm images. Scale bar is 25 μm.

unaffected by the cells (Figure 3G). The NADH and FAD spectral signatures were uncharacteristically weak for this culture (Figure 2F) as observed through the 390 – 465 nm (NADH) and 535-590 nm (FAD) bandpass filters, 770 nm excitation, indicating a possible change in the excitation/emission characteristics of these two fluorescent species comparing to the cells seeded on the non-crosslinked gels (Figure 3B). The genipin induced fluorescence was shown in Figure 3I.

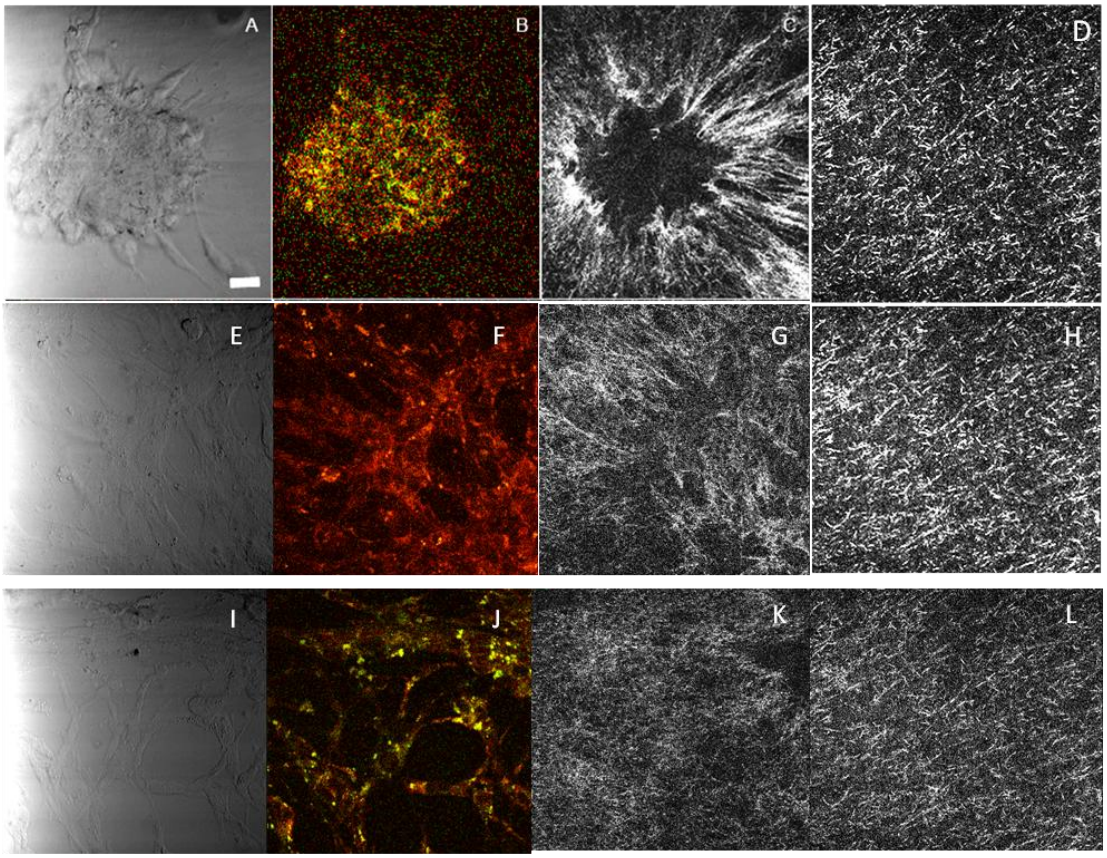

Figure 4. Multi-photon optical signals from the 3D models with G-Olig2 stem cells differentiated on top of not cross-linked (A- D), EDC cross-linked (E-H) and EDC/NHS cross-linked (I-L) 2 g/l collagen hydrogels. Day 5 post induction of differentiation with the retinoic acid (A) ,(E) and (I) True-focus image of a typical differentiating cellular cluster that forms when cells are cultured on top of collagen hydrogels; (B), (F) and (J) The multiphoton ratiometric redox fluorometry imaging of the G-Olig2 stem cells in the 3D stem cell model. λex = 770 nm. Red, NADH; green, FAD. The two colors are superimposed. (C), (G) and (K) Second harmonic generation signal of surrounding collagen matrix after cells were seeded. λex = 800 nm; (D), (H) and (L) Second harmonic generation signal of surrounding collagen matrix before cells were seeded. λex = 800 nm. Focusing objective (Zeiss; 40x water immersion; NA is 0.8) was used to collect 250 μm × 250 μm images. Scale bar is 25 μm.

The stem cells differentiating on the EDC and EDC/NHS-modified collagen hydrogels remained scattered on top with cells being able to align collagen fibers in the materials modified with EDC (Figure 4G) while making a clearance and no alignment of collagen fibers in the case EDC/NHS modification (Figure 4K). Despite the alignment of collagen

fiber in EDC cross-linked hydrogels, the SHG signal was not amplified as seen in the non-crosslinked gels (Figure 4C). The cells remained scattered on the surfaces of the hydrogels. The NADH and FAD spectral signatures (Figure 4F and 4J) were as strong as the one seen in the non-crosslinked gels (Figure 4B). The true-focused images showed the differentiated cells on the EDC or EDC/NHS crosslinked gels (Figure 4E and 4I) remained as single cell.

The somewhat similar cellular behaviors had been previously observed for the 3T3 fibroblasts that formed tissue-like aggregates when plated on soft substrates[44] consisting of collagen coated polyacrylamide while rigid substrates were found to produce high traction forces and promoted scattering of cells.[45] Our EDC, EDC/NHS and genipin-crosslinked collagen hydrogels are more rigid compared to not cross-linked collagen substrates and lead to differentiating stem cells distribution on top of the materials with only limited (about 50 μm) cellular migration into the cross-linked materials as observed with multi-photon microscopy signals.

The observations of this study were conducted on the biocompatible collagen hydrogels of the known micro- (and nano [5]) structure as opposed to extracellular matrix (ECM) coated polyacrylamide, glass or plastic substrates. The latter substrates that have been a major focus of studies aimed at understanding cellular interactions with environments did not carry molecular flexibility for the cells to re-organize micro-structure and/or understand the newly established mechanics associated with that process.

In addition to the structural modifying effect of cross-linking reagents, different collagen assembly factors also change the structure within collagen hydrogels. We test two assembly factors which are initial collagen concentration and incubation temperatures. Collagen hydrogels are assembled in two initial collagen concentrations, 2 g/l and 4 g/l and G-Olig2 stem cells are seeded on top of them. As shown in the phase contrast images (Figure 5), the differentiation rate is faster for the cells seeded on 2 g/l (Figure 5, top panels) then for the cells seeded on 4 g/l gels (Figure 5, bottom panels). On day 0, the cells remained undifferentiated, and then the cells seeded on 2 g/l gels already undifferentiated. On day 2, the differentiated cells seeded on 2 g/l gels formed a cluster but the cells seeded on 4 g/l gels were either undifferentiated or started to differentiate.

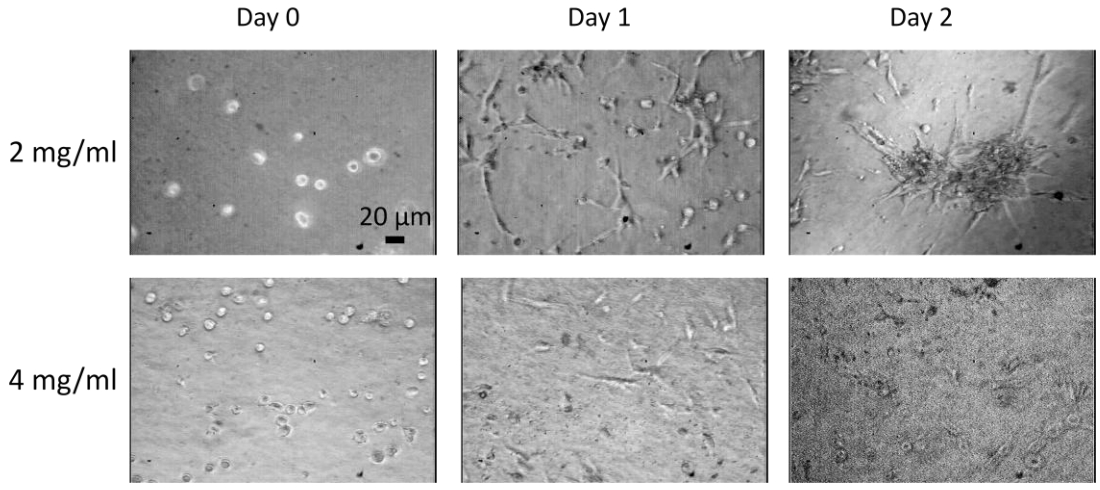

Figure 5. Phase contrast images of the G-Olig2 stem cell differentiated on top of collagen hydrogels assembled at 2 g/l and 4 g/l. Day 0, day 1 and day 2 post induction of differentiation with the retinoic acid is shown for both collagen concentrations. Scale bar is 20 μm

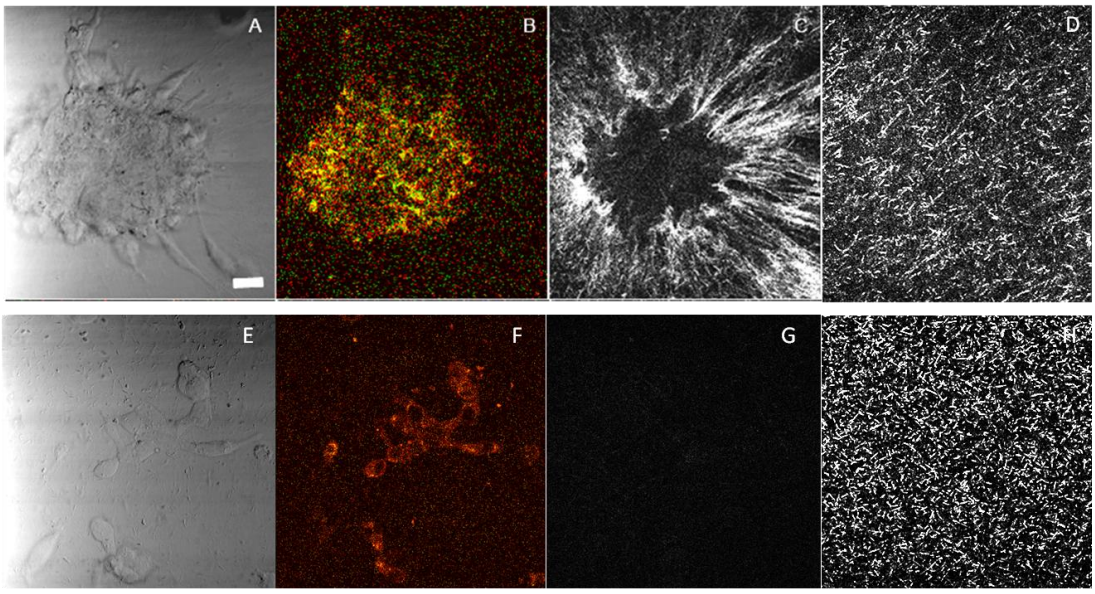

Figure 6. Multi-photon optical signals from the 3D models with G-Olig2 stem cells differentiated on top of collagen hydrogels assembled at 2 g/l (A- D) and 4 g/l (E-H). Day 5 post induction of differentiation with the retinoic acid (A) and (E) True-focus image of a typical differentiating cellular cluster that forms when cells are cultured on top of collagen hydrogels; (B) and (F) The multiphoton ratiometric redox fluorometry imaging of the G-Olig2 stem cells in the 3D stem cell model. λex = 770 nm. Red, NADH; green, FAD. The two colors are superimposed. (C) and (G) Second harmonic generation signal of surrounding collagen matrix after cells were seeded. λex = 800 nm; (D) and (H) Second harmonic generation signal of surrounding collagen matrix before cells were seeded. λex = 800 nm. Focusing objective (Zeiss; 40x water immersion; NA is 0.8) was used to collect 250 μm × 250 μm images. Scale bar is 25 μm.

The multiphoton images obtained on day 5 post induction (Figure 6) indicate that the cells seeded on 4 g/l gels still on the early stage of differentiation (Figure 6E). The NADH and FAD spectral signatures of cells seeded on 4 g/l (Figure 6F) were weaker comparing to the cells seeded on 2 g/l (Figure 6B). The cells seeded on 4 g/l were unable to realign the surrounding collagen fibers, instead they weakened the SHG signal intensity (Figure 6G). Despite the loss of SHG signal, the collagen structure was found to remain intact when a higher laser power was used (data not shown). The difference in the differentiation rate and the ability to remodel the collagen structure for the stem cells

seeded on 2 g/l and 4 g/l might be due to the similar reason which was described for the embedded model. Cellular ability to translocate the fibers during migration, materials' stiffness and to a lesser extent a pore size could all play some role.

Two different temperatures which are 27 ℃ and 37 ℃ are used to assemble the collagen hydrogels. The phase-contrast images shows that the stem cells seeded on hydrogels assembled at 27 ℃ (Figure 7, bottom panels) started the differentiation early but took longer time to form a cluster than the cells seeded on hydrogels assembled at 37 ℃ (Figure 7, top panels). On day 0, the ES cells seeded on hydrogels assembled at 27 ℃ started to differentiate while the cells seeded on hydrogels assembled at 37 ℃ remained undifferentiated. On day 2, the differentiated cells seeded on hydrogels assembled at 37 ℃ formed a cluster but the differentiated cells seeded on hydrogels assembled at 27 ℃ remained as single cells. The multiphoton images collected on day 5 post induction

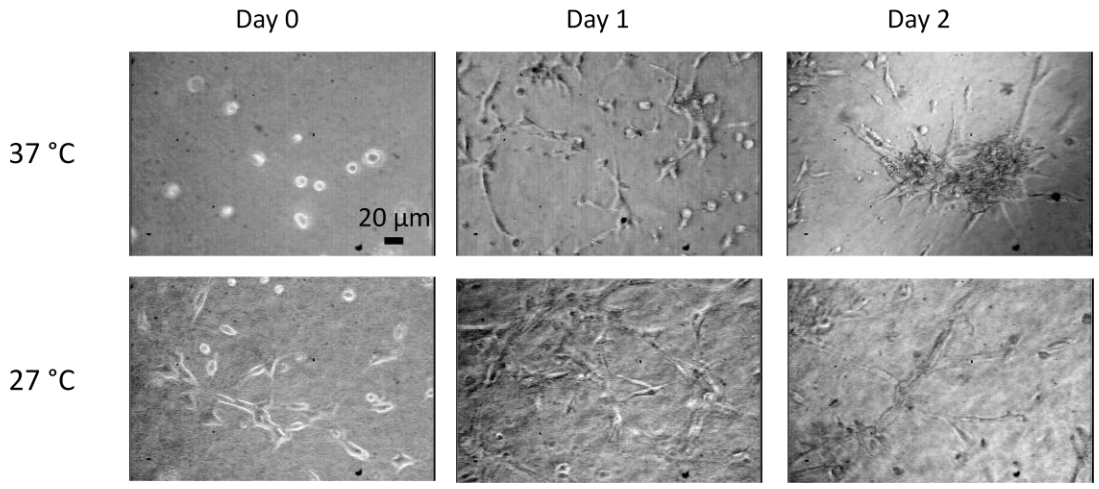

Figure 7. Phase contrast images of the G-Olig2 stem cell differentiated on top of 2 g/l collagen hydrogels assembled at 27℃ and 37℃. Day 0, day 1 and day 2 post induction of differentiation with the retinoic acid is shown for both collagen concentrations. Scale bar is 20 μm

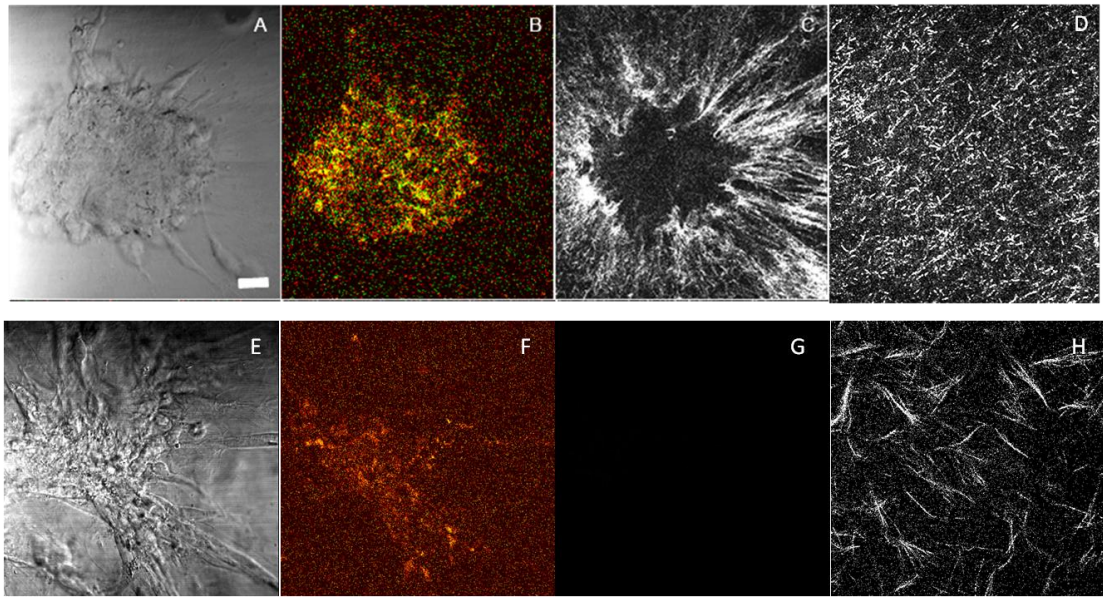

Figure 8. Multi-photon optical signals from the 3D models with G-Olig2 stem cells differentiated on top of 2 g/l collagen hydrogels assembled at 37℃ (A- D) and 27℃ (E-H). Day 5 post induction of differentiation with the retinoic acid (A) and (E) True-focus images of a typical differentiating cellular cluster that forms when cells are cultured on top of collagen hydrogels; (B) and (F) The multiphoton ratiometric redox fluorometry imaging of the G-Olig2 stem cells in the 3D stem cell model. λex = 770 nm. Red, NADH; green, FAD. The two colors are superimposed. (C) and (G) Second harmonic generation signal of surrounding collagen matrix after cells were seeded. λex = 800 nm; (D) and (H) Second harmonic generation signal of surrounding collagen matrix before cells were seeded. λex = 800 nm. Focusing objective (Zeiss; 40x water immersion; NA is 0.8) was used to collect 250 μm × 250 μm images. Scale bar is 25 μm.

shows that the differentiated cells seeded on hydrogels assembled at 27 ℃ formed a cluster (Figure 8E). The NADH and FAD spectral signatures of differentiated cells seeded on hydrogels assembled at 27 ℃ (Figure 8F)is weaker than those cells seeded on hydrogels assembled at 37 ℃ (Figure 8B). The differentiated cells seeded on hydrogels assembled at 27 °C didn't realign the surrounding collagen structures; instead they weakened the SHG signal intensity (Figure 8G). Despite the loss of SHG signal, the collagen structure was found to remain intact when a higher laser power was used (data

not shown). The possible reason which the differentiated cells seeded on hydrogels assembled at 27 °C can't realign the collagen structure might be due to the large collagen fiber assembled at 27 ℃ (Figure 8H). Compared to the small fibers assembled at 37 ℃ (Figure 8D), the differentiated cells are unable to translocate the large fibers assembled at 27 ℃, thus the differentiated cells could only weaken the SHG signal intensity.

Induced pluripotent stem cells

The schematic description of reprogramming and derivation of iPS cell line was shown in Figure 9 and the immuncytochemistry was performed to show that the cells are pluripotent.

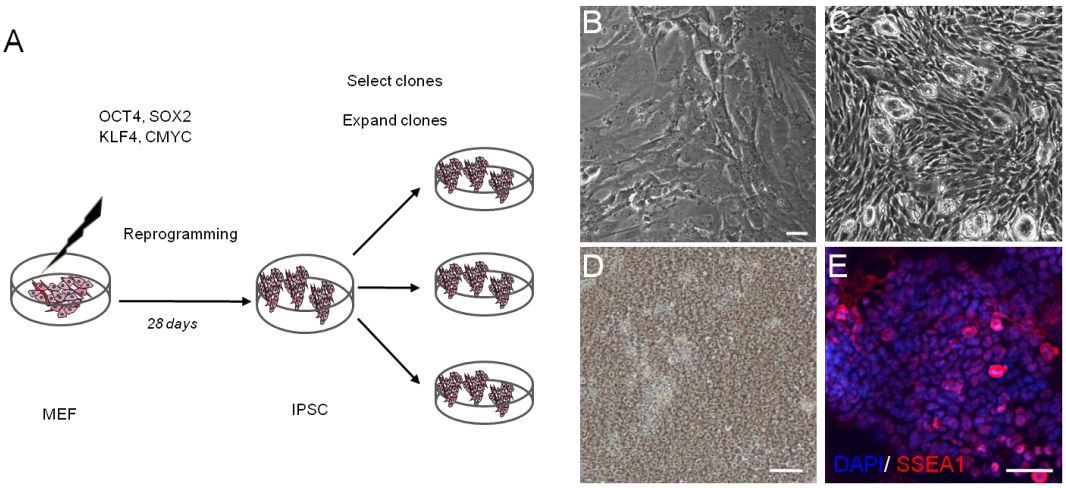

Figure 9. (A) Schematic of mouse IPS cell derivation. a7.wt mouse IPS cell clone 1 was selected and used in this study. (B) Morphology of mouse embryonic fibroblast (MEF) cells prior to reprogramming. (C) Mouse IPS cells formed compacted, dome-shaped and three dimensional colonies, a morphology typical of mouse ES cells. (D) Individual mouse IPS cells exhibited high nuclear: cytoplasm ratio with the presence of multiple nucleoli in the cell nuclei. (E) Immunocytochemistry analysis of stage specific embryonic antigen-1 (SSEA1) expression. Scale bars, 50um. This figure was made by Dr. Duncan Liew.

Three-dimensional encapsulated cellular differentiation model

To determine the effect of different microstructure on the extent of differentiation of iPS cells into neuronal lineage cells we encapsulated them in hydrogels prepared separately at 2 g/l and 4g/l initial collagen concentrations. The phase contrast images first show that the differentiation rate of iPS cells embedded in 2 g/l hydrogels (Figure 10, top panels) is faster than the cells embedded in 4 g/l hydrogels (Figure 10, bottom panels). On day 0, the cells embedded in both concentrations of hydrogels remained undifferentiated as a single cell. On day 1, the cells embedded in 2 g/l hydrogels form undifferentiated colony while the cells embedded in 4 g/l hydrogels remained undifferentiated single cell. On day 3, the cells embedded in 2 g/l hydrogels started to differentiate but the cells embedded in 4 g/l hydrogels still remained undifferentiated. Until day 7, most cells embedded in 2 g/l hydrogels differentiated and the cells embedded in 4 g/l finally differentiated as well. The multiphoton images obtained on day 10 post induction shows that the differentiated cells embedded in 2 g/l hydrogels were long and stretched (Figure 11A) and the differentiated cells embedded in 4 g/l hydrogels were small (Figure 11E). The NADH and FAD spectral signatures of differentiated cells embedded in hydrogels assembled at both concentrations were similar (Figure 11B and 11F). The differentiated cells embedded in 2 g/l hydrogels realigned the surrounding collagen structure and amplified the SHG signal intensity (Figure 11C) but the differentiated cells embedded in 4 g/l hydrogels didn't remodel the collagen structure (Figure 11G).

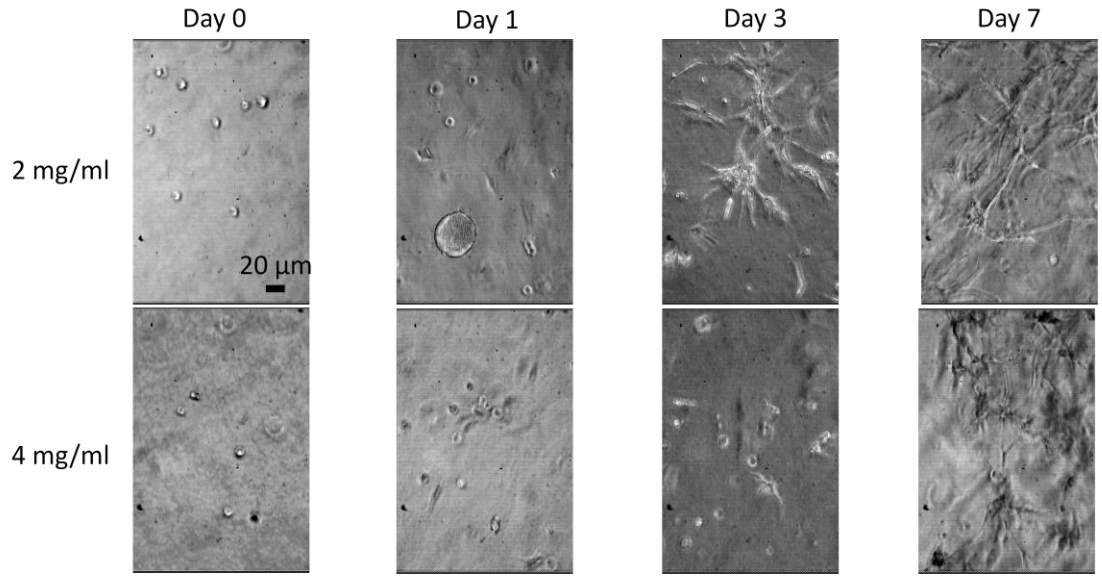

Figure 10. Phase contrast images of the iPS cells embedded in 2 g/l and 4 g/l collagen hydrogels. Day 0, day 1, day 3 and day 7 post induction of differentiation with the retinoic acid is shown for both collagen concentrations. Scale bar is 20 µm

Three-dimensional topographic cellular differentiation model

Genipin has been shown to remodel the structure within collagen hydrogels. We here examine the effect of modified structure on the differentiation of iPS cells seeded on top of genipin cross-linked hydrogels. The phase contrast images show that the differentiation rate of iPS cells initiated early on the genipin cross-linked hydrogels (Figure 12, bottom panels) then cells seeded on non-crosslinked hydrogels (Figure 12, top panels) ;the differentiated cells on non-crosslinked hydrogels stretched further than the cells on genipin cross-linked hydrogels. On day 0 and day 1, the cells seeded on both hydrogels had similar cellular behavior which the undifferentiated single cell aggregated to undifferentiated colony. The difference appeared on day 4 which the cells seeded on non-crosslinked hydrogels remained as undifferentiated colony but the cells seeded on

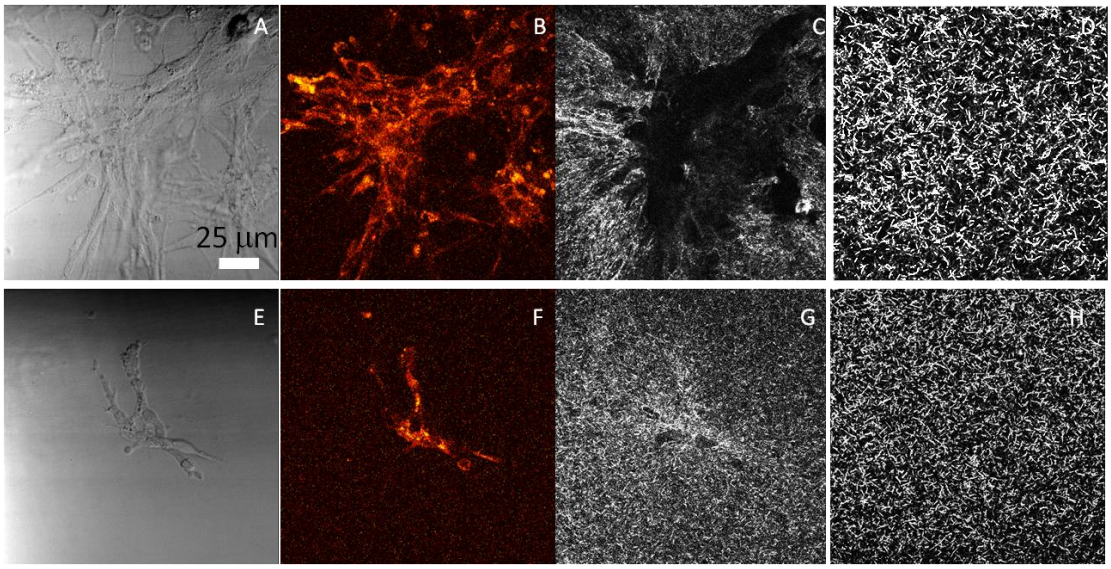

Figure 11. Multi-photon optical signals from the 3D models with iPS cells embedded in 2 g/l (A- D) and 4 g/l (E-H) collagen hydrogels. (A) and (E) True-focus image of a typical differentiating cellular cluster that forms when cells are cultured on top of collagen hydrogels; (B) and (F) The multiphoton ratiometric redox fluorometry imaging of the G-Olig2 stem cells in the 3D stem cell model. λex = 770 nm. Red, NADH; green, FAD. The two colors are superimposed. (C) and (G) Second harmonic generation signal of surrounding collagen matrix after cells were seeded. λex = 800 nm; (D) and (H) Second harmonic generation signal of surrounding collagen matrix before cells were seeded. λex = 800 nm; (I) Fluorescence of fibers induced as a result of cross-linking collagen with genipin. Focusing objective (Zeiss; 40x water immersion; NA is 0.8) was used to collect 250 μm × 250 μm images. Scale bar is 25 μm.

genipin cross-linked hydrogels started to differentiate where the cells migrated away from the colony (Dr. Duncan Liew personal communication). On day 5 and day 6, the cells on the non-crosslinked gels still remained undifferentiated colony; more cells migrated away from the colony on the genipin cross-linked gels but these cells didn't stretch (data not shown). On day 7, the cells seeded on non-crosslinked hydrogels started to differentiate and stretch without migrating away from the colony and the cells seeded on genipin cross-linked hydrogels started to stretch. Another difference appeared on day 11 which the cells seeded on non-crosslinked hydrogels differentiated to long, stretched

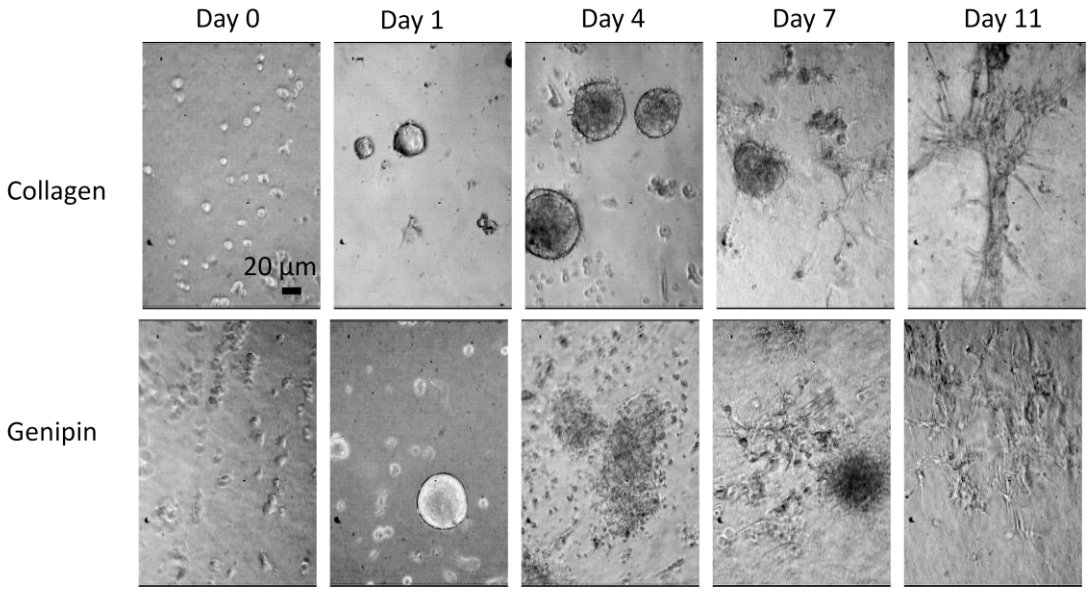

Figure 12. Phase contrast images of the G-Olig2 stem cell differentiated on top of genipin cross-linked and not cross-linked 2 g/l collagen hydrogels**.** Day 0, day 1, day 4, day 7 and day 11 post induction of differentiation with the retinoic acid is shown for different cross-linking reagents. Scale bar is 20 μm

neuronal lineage cells but the differentiated cells on genipin cross-linked hydrogels didn't stretch as much as the cells seeded on non-crosslinked hydrogels. The multiphoton images collected on day 10 post induction show that the differentiated cells on both collagen hydrogels differentiated to similar extent in true-focused images (Figure 13A and 13E) and had similar fluorescence intensity of NADH/FAD (Figure 13B and 13F). The differentiated cells on non-crosslinked hydrogels realigned the surrounding collagen structure (Figure 13C) comparing to the structure without the presence of cells (Figure 13D) but the genipin modified structure remained intact with decreased SHG intensity

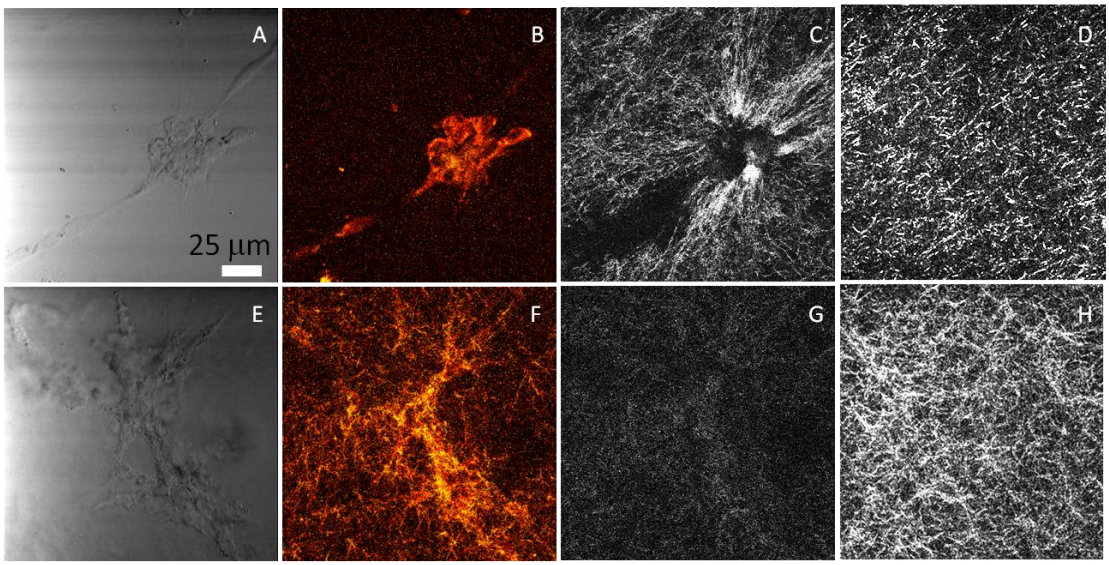

Figure 13. Multi-photon optical signals from the 3D models with iPS cells differentiated on top of a not cross-linked (A- D) and genipin cross-linked (E-H) 2 g/l collagen hydrogels Day 10 post induction of differentiation with the retinoic acid (A) and (E) True-focus images of a typical differentiating cellular cluster that forms when cells are cultured on top of collagen hydrogels; (B) and (F) The multiphoton ratiometric redox fluorometry imaging of the G-Olig2 stem cells in the 3D stem cell model. λex = 770 nm. Red, NADH; green, FAD. The two colors are superimposed. (C) and (G) Second harmonic generation signal of surrounding collagen matrix after cells were seeded. λex = 800 nm; (D) and (H) Second harmonic generation signal of surrounding collagen matrix before cells were seeded. λex = 800 nm. Focusing objective (Zeiss; 40x water immersion; NA is 0.8) was used to collect 250 μm × 250 μm images. Scale bar is 25 μm.

where the differentiated cells were located (Figure 13G) comparing the modified structure without the presence of cells (Figure 13H).

Many types of natural materials have been applied in regenerative medicine. The fibrillar collagen is one of the widely used biomaterials for the nerve guide fabrication[46] due to its prevalence in the nerves. Collagen hydrogels when employed in nerve regeneration applications have shown to give different effect based on density, concentration, viscosity and degree of cross-linking of these materials[47] implying that different interactions of cells and collagen can take place. It is recognized that the mechanical properties can drive

these differences in cellular behaviors; however, commonly there is no reference to the micro-structure that influences the behavior of stem cells. We are the first to successfully characterize the structural effect using MPM. Others studies have used hematoxylin and eosin staining to examine the neuronal differentiation of stem cell in collagen materials[48, 49], however such staining generally affects the morphology of cell and materials. MPM, a non-invasive imaging technique provides us a good opportunity to simultaneously understand the cellular behavior using the natural fluorescence from NADH and FAD and the fiber structure within collagen materials using the SHG signals.

Regenerative medicine is a promising field and it has strong potential to become an alternative treatment for patients who need transplantation. However, a lack of fully understanding on how to control cell behavior in materials remains as the obstacle which prevents the translation of this knowledge to routine clinical procedure. The properties of materials have been known to direct cell function and the ability to control the architecture of materials is critical to achieve a harmony between the materials and stem cells[2]. Many factors have been shown to determine cell response to the architecture of materials, such as material chemistry[50], biofunctionalization[51], mechanics[52], and structure [53-55]. The studies which show the structural effect on stem cell behavior demonstrate that the difference in the surface topography of materials influences the gene expression signature, proliferation and osteogenic differentiation of human bone marrow stromal cells[54, 55], and the proliferation and differentiation of mesenchymal stem cells were affected when they were seeded on the materials with different architectures[56]. Compared to these studies, our works also demonstrate that differences in surface topography and

the fiber structure surrounding cells impact the rate of stem cell neuronal differentiation and cellular modification on fiber structure. Furthermore, we illustrate the ability to consistently manipulate the structure within collagen materials by simply adjusting the collagen assembly parameters or applying different cross-linking reagents. By using these factors to tune the structural property of collagen materials, the behavior of stem cells can be well manipulated.

Conclusion

We compared the G-Olig2 embryonic stem cell and a7wt induced pluripotent cells behaviors during early differentiation with retinoic acid into a neural lineage employing separately the encapsulated or topographic 3D collagen hydrogel models. For the encapsulated 3D models, the cells were polymerized within hydrogels prepared from two different initial concentrations 2 g/l and 4 g/l and differentiated *in situ*. For the topographic 3D model, the embryonic stem cells were differentiated on top of the hydrogels cross-linked with EDC, EDC/NHS (4 parts of EDC mixed with 1 part of NHS) or genipin and compared to the cells differentiated on the not cross-linked controls. In addition, two different collagen assembly factors were also examined which are initial collagen concentration (2 g/l and 4 g/l) and incubation temperature (27 ℃ and 37 ℃). The iPS cells were differentiated on top of the genipin crosslinked hydrogels comparing to the non-crosslinked controls. The G-Olig2 embryonic stem differentiation was slower for the cells encapsulated within 4 g/l collagen hydrogels compared to 2 g/l once. The G-Olig2 embryonic stem cells' differentiation process on top of the 3D collagen hydrogels

was affected by the cross-linking. For example, for the unmodified collagen hydrogels, the response of the differentiating stem cells consisted of cellular differentiation concomitant with cellular migration and subsequent aggregation into the clusters. The collagen of the supporting extracellular matrix became highly aligned at the periphery of the cluster formed. The G-Olig2 differentiated stem cells remained scattered on top of the cross-linked materials. The cells were able to align collagen fibers in the materials modified with EDC while had no effect on the collagen fibers in the case of EDC/NHS and genipin modifications. Different assembly factor also affects the differentiation process of ES cells. The differentiated cells were unable to align the collagen structure with hydrogels assembled at 4 g/l or 27 ℃.

The differentiation rate of iPS embedded in 2 g/l hydrogels was faster than the cells embedded in 4 g/l hydrogels. The iPS cells' differentiation process on top of the cross-linked hydrogels was also affected. For example, the differentiated cells also realigned the surrounding collagen structure and no alignment was observed in genipin cross-linked hydrogels and the differentiation rate was faster in genipin cross-linked hydrogels.

These results advance our understanding of how scaffold architecture can control cell fates. The ability to manipulate the structure of collagen materials and the manipulated structure can affect the stem cell behavior increase s the potential of using biomaterial and stem cells to treat the neuronal degenerative disease.

References

(1) Sengupta, D.; Heilshorn, S. C. *Tissue Eng. : Part B* **2010**, *16*, 285-294.

(2) Stevens, M. M.; George, J. H. *Science* **2005**, *31*, 1135-1138.

(3) Hwang, Y.; Lyubovitsky, J. G. *Anal. Methods* **2011**, *3*, 529-536.

(4) Hwang, Y.; Granelli, J.; Lyubovitsky, J. *ACS Appl. Mater. Interfaces* **2011**, *4*, 261-267.

(5) Hwang, Y.; Larsen, J.; Krasieva, T. B.; Lyubovitsky, J. G. *ACS Appl. Mater. Interfaces* **2011**, *3*, 2579-2584.

(6) Bain, G.; Ray, W. J.; Yao, M.; Gottlieb, D. I. *Biochem. Bioph. Res. Co.* **1996**, *223*, 691-694.

(7) Jiang, P.; Selvaraj, V.; Deng, W. *JoVE* **2010**.

(8) Jones-Villeneuve, E. M. V.; Rudnicki, M. A.; Harris, J. F.; McBurney, M. W. *Mol. Cell Biol.* **1983**, *3*, 2271-2279.

(9) Okada, Y.; Shimazaki, T.; Sobue, G.; Okano, H. *Dev. Biol.* **2004**, *275*, 124-142.

(10) Campagnola, P. J.; Millard, A. C.; Terasaki, M.; Hoppe, P. E.; Malone, C. J.; Mohler, W. A. *Biophys. J.* **2002**, *82*, 493-508.

(11) Freund, I.; Deutsch, M.; Sprecher, A. *Biophys J.* **693**, *50*, 693-712.

(12) Guo, Y.; Savage, H. E.; Liu, F.; Schantz, S. P.; Ho, P. P.; Alfano, R. R. *Proc. Natl. Acad. Sci. USA* **1999**, *96*, 10854-10856.

(13) Han, M.; Giese, G.; Bille, J. F. *Opt. Express* **2005**, *13*, 5791-5797.

(14) Huang, S.; A., H. A.; Webb, W. W. *Biophys. J.* **2002**, *82*, 2811-2825.

(15) Laiho, L. H.; Pelet, S.; Hancewicz, T. M.; Kaplan, P.; So, P. T. C. *Journal of Biomed. Optics* **2005**, *10*, 024016.

(16) Masters, B.; So, P. T. C.; Gratton, E. *Lasers Med Sci* **1998**, *13*, 196-203.

(17) Masters, B.; So, P. T. C.; Kim, K. H.; Buehler, C.; Gratton, E. *Methods in Enzymology* **1999**, *307*, 513-536.

(18) Masters, B. R.; So, P. T. C.; Gratton, E. *Lasers Med. Sci.* **1998**, *13*, 196-203.

(19) Roth, S.; Freund, I. *J.Chem.Phys.* **1979**, *70*, 1637-1643.

(20) Roth, S.; Freund, I. *Optics Communications* **1980**, *33*, 292-296.

(21) Roth, S.; Freund, I. *Biopolymers* **1981**, *20*, 1271-1290.

(22) Stoller, P.; Kim, B. M.; Rubenchik, A. M.; Reiser, K. M.; Da Silva, L. B. *J. Biomed. Opt.* **2002**, *7*, 205-214.

(23) Strupler, M.; Pena, A. M.; Hernest, M.; Tharaux, P. L.; Martin, J. L.; Beaurepaire, E.; Schanne-Klein, M. C. *Opt. Express* **2007**, *15*, 4054-4065.

(24) Zipfel, W. R.; Williams, R. M.; Christie, R.; Nikitin, A. Y.; Hyman, B. T.; Webb, W. W. *Proc. Natl. Acad. Sci. USA.* **2003**, *100*, 7075-7080.

(25) Zipfel, W. R.; Williams, R. M.; Webb, W. W. *Nat. Biotechnol.* **2003**, *21*, 1369-1377.

(26) Zoumi, A., University of California at Irvine, Irvine, 2003.

(27) Zoumi, A.; Yeh, A.; Tromberg, B. J. *Proc. Natl. Acad. Sci. USA.* **2002**, *99*, 11014-11019.

(28) Hwang, Y.; Granelli, J.; Lyubovitsky, J. G. *Anal. Chem.* **2011**, *83*, 200-206.

(29) Xian, H.; McNichols, E.; St.Clair, A.; Gottlieb, D. I. *Stem Cells* **2003**, *21*, 41-49.

(30) Novitch, B. G.; Wichterle, H.; Jessell, T. M.; Sockanathan, S. *Neuron* **2003**, *40*, 81-95.

(31) Shin, S.; Xue, H.; Mattson, M. P.; Rao, M. S. *Stem Cells Dev.* **2007**, *16*, 131-141.

(32) Takabayashi, H.; Nabeshima, Y.; Yoshida, S.; Chisaka, O.; Ikenaka, K.; Nabeshima, Y. *Curr. Biol.* **2002**, *12*, 1157-1163.

(33) Lu, Q.; Sun, T.; Zhu, Z.; Ma, N.; Garcia, M.; Stiles, C. D.; Rowitch, D. H. *Cell* **2002**, *109*, 75-86.

(34) Zhou, Q.; Anderson, D. J. *Cell* **2002**, *109*, 61-73.

(35) Xian, H.; Gottlieb, D. I. *Glia* **2004**, *47*, 88-101.

(36) Takahashi, K.; Yamanaka, S. *Cell* **2006**, *126*, 663-676.

(37) Yamanaka, S. *Cell* **2009**, *137*, 13-17.

(38) Ronaghi, M.; Erceg, S.; Moreno-Manzano, V.; Stojkovic, M. *Stem cells* **2010**, *28*, 93-99.

(39) Torrez, L. B.; Perez, Y.; Yang, J.; zur Nieden, N. I.; Klassen, H.; Liew, C. G. *Stem Cells Inter.* **2012**, *doi:10.1155/2012/417865*.

(40) Rohwedel, J.; Guan, K.; Wobus, A. M. *Cells Tissues Organs* **1995**, *165*, 190-202.

(41) Lutolf, M. P.; Gilbert, P. M.; Blau, H. M. *Nature* **2009**, *26*, 433-441.

(42) Miron-Mendoza, M.; Seemann, J.; Grinnell, F. *Biomaterials* **2010**, *31*, 6425-6435.

(43) Hwang, Y.; Larsen, J.; Krasieva, T. B.; Lyubovitsky, J. G. *Applied Materials and Interfaces* **2011**, *3*, 2579–2584

(44) Guo, W.; Frey, M. T.; Burnham, N. A.; Wang, Y. *Biophysical Journal* **2006**, *90*, 2213–2220

(45) de Rooij, J.; Kerstens, A.; Danuser, G.; Schwartz, M. A.; Waterman-Storer, C. M. *The journal of cell biology* **2005**, *171*, 153-164.

(46) Hollinger, J. O., Ed. *An Introduction to Biomaterials*; CRC Press: Florida, 2012.

(47) Ceballos, D.; Navarro, X.; Dubey, N.; Wendelschafter-Crabb, G.; Kennedy, W. R.; Tranquillo, R. T. *Exp. Nephrol.* **1999**, *158*, 290-300.

(48) Chen, S. S.; Revoltella, R. P.; Papini, S.; Michelini, M.; Fitzgerald, W.; Zimmerberg, J.; Margolis, L. *Stem Cells* **2003**, *21*, 281-295.

(49) Michelini, M.; Franceschini, V.; Chen, S. S.; Papini, S.; Rosellini, A.; Ciani, F.; Margolis, L.; Revoltella, R. P. *Cell Profli.* **2006**, *39*, 217-229.

(50) Benoit, D. S.; Schwartz, M. P.; Durney, A. R.; Anseth, K. S. *Nat. Mater.* **2008**, *7*, 816-823.

(51) Petrie, T. A.; Raynor, J. E.; Dumbauld, D. W.; Lee, T. T.; Jagtap, S.; Templeman, K. L.; Collard, D. M.; Garcia, A. J. *Sci. Transl. Med.* **2010**, *2*, 45-60.

(52) Engler, A. J.; Sen, S.; Sweeney, H. L.; Discher, D. E. *Cell* **2006**, *126*.

(53) Dalby, M. J.; Gadegaard, N.; Tare, R.; Andar, A.; Riehle, M. O.; Herzyk, P.; Wilkinson, C. D.; Oreffo, R. O. *Nat. Mater.* **2007**, *6*, 997-1003.

(54) Kumar, G.; Tison, C. K.; Chatterjee, K.; Pine, P. S.; McDaniel, J. H.; Salit, M. L.; Young, M. F.; C.G., S. J. *Biomaterials* **2011**, *32*, 9188-9196.

(55) Kumar, G.; Waters, M. S.; Farooque, T. M.; Young, M. F.; C.G., S. J. *Biomaterials* **2012**, *33*, 4022-4030.

(56) Yilgor, P.; Sousa, R. A.; Reis, R. L.; Hasirci, N.; Hasirci, V. *Macromol. Sy.* **2008**, *268*, 92-99.

CHAPTER 8
CONCLUSION

Introduction

My thesis work established new multiscale dimensional and time approaches for characterizing collagen hydrogels. A clear pattern that the behavior of the differentiating embryonic stem cells is controlled by the structure within the collagen materials had emerged as well.

Specifically, the fundamental collagen hydrogel systems I developed delivered the following results:

1. Characterization of collagen hydrogels
    - Initial collagen concentration and incubation temperature have dramatic effects on the properties of hydrogels such as assembly kinetics, nano-structure and micro-structure
    - Manipulation of structural levels at the molecular, micro- and nano-scale is achieved when different cross-linking reagents are used to stabilize the hydrogels
    - Multiphoton microscopy that combines two-photon fluorescence and second harmonic generation signal is a powerful tool to simultaneously examine the fluorescent and structural properties of collagen hydrogels

2. Stem cell differentiation and microstructure of collagen hydrogels
    - The differentiation rate of embryonic stem cells and degradation of collagen hydrogels can be controlled with a micro- structural adjustment within hydrogels
    - The differentiated neuronal-lineage cells can realign the surrounding collagen fibers when embryonic stem cells are seeded onto the collagen material or EDC crosslinked material

The primary goal of regenerative medicine is to create the functional engineered tissue/organ to replace/repair the damaged one. The key to fulfill this goal is to obtain the ability to tailor the interaction between cell and material in order to control the cell behavior. However, the correlation between cellular behaviors and collagen hydrogels requires further investigation. Moreover, most of current embryonic stem cell research only focuses on the signaling pathways which govern the fate of embryonic stem cells. These investigations applied the common techniques such as immunocytochemstriy, microarray and PCR-based techniques to obtain the gene expression profiles, used to identify the role of each gene in regulating the cell division and differentiation of embryonic stem cells. Such information surely enhances our understanding on the genetic controls of behaviors of embryonic stem cells which leads to better comprehension on how undifferentiated stem cells differentiate to form tissues and organs. However, the information obtained isn’t sufficient for the development of engineered tissues/organs.

My thesis work fills the gap by presenting a detailed understanding on the interaction between embryonic stem cells and hydrogels. In addition, my work also demonstrates how multiphoton microscopy could be useful to the stem cell researches. Development of the non-destructive detection methods capable of sensing the interactions between stem cells and materials is critical to the fabrication of engineered tissue/organ. Multiphoton microscopy, a non-linear optical technique, can accomplish it by combing the second harmonic generation and two-photon fluorescence signals to obtain the micro-structure of collagen hydrogels as well as the cellular metabolism.

The advantage of the multiphoton microscopy not only allows the detection of cell-hydrogel interaction but also provides information on cell-cell communication. More understanding on cell-cell communication will be useful to facilitate the comprehension on cell signaling and differentiation in hydrogels. Second harmonic generation imaging not only entails the acquisition of microstructure of hydrogel but also can be used to determine the porosity of hydrogels. Porosity is an important factor in making the artificial tissue/organ because the pore size influences the growth and migration of seeded cells. The second harmonic generation images obtained in my thesis work are valuable. Most importantly, second harmonic generation images show that the manipulation of microstructure of hydrogel can be achieved. Based on this achievement in structural manipulation, the control of spatial and temporal organization of stem cell behaviors in tissue development can be easier.

Embryonic stem cells have tremendous promise in research and the clinic. In addition to their application in regenerative medicine, embryonic stem cells can also be used in mimicking the disease model and testing new drugs. Because the detailed mechanism of some of serious medical conditions, such as cancer, remain unclear, the embryonic stem cells seeded on material can be used as a model to yield information on these complex processes and a more complete understanding can generate more information about how such diseases arise and provide new strategies for treatment. Because embryonic stem cells are pluripotent, the differentiation of stem cells to target cell type seeded onto the materials can be used to test the safety and effectiveness of new medications. In order to enhance the efficacy of embryonic stem cells in these two applications, a comprehensive understanding of interaction between stem cell and material will be required. My thesis work, which offers more information on such interaction, could accelerate the process of realizing the potential uses of embryonic stem cell.